Synthesis of Hydrogels with Various Network Architecture via Click Chemistry and Their Characterization

Takuya Murakami

February 2018

Synthesis of Hydrogels with Various Network Architecture via Click Chemistry and Their Characterization

Takuya Murakami

Doctoral Program in Chemistry

Submitted to the Graduate School of

Pure and Applied Sciences

in Partial Fulfillment of the Requirements

for the Degree of Doctor of Philosophy in

Science

at the

University of Tsukuba

Acknowledgements

The studies presented in this thesis have been carried out under the direction of Prof. Craig J. Hawker at the University of California, Santa Barbara during September 2013 – August 2015 and Prof. Kazuya Saito at the University of Tsukuba during April 2017 – February 2018. The studies are concerned with "Synthesis of Hydrogels with Various Network Architecture via Click Chemistry and Their Characterization".

The author wishes to express his sincerest gratitude to Prof. Craig J. Hawker for his kind guidance throughout this work. The author is deeply grateful to Prof. Kazuya Saito for his helpful advice and warm encouragement during this work. The author would like to thank Prof. Hugh R. Brown at the University of Wollongong, Dr. Bernhard V. K. J. Schmidt at the Max Planck Institute, and Prof. Daniel Klinger at the Free University of Berlin to their valuable suggestions and discussions. The author wishes to acknowledge Dr. Takashi Kawamori, Mr. Jeffrey D. Gopez, Ms. Alaina J. McGrath, and Dr. Jimmy Lawrence for their great contribution to this work.

The author is thankful to all the members of Prof. Hawker's group and Prof. Saito's group. The author is obliged to all the staff in Materials Research Laboratory at UCSB for their assistance during the author's stay in California as a visiting scholar. This work made use of shared facilities of the UCSB MRSEC (NSF DMR 1121053), a member of the Materials Research Facilities Network (www.mrfn.org).

In addition, the author wishes to express his special thanks to Dr. Hiroaki Tokuhisa, Dr. Takashi Okada, and Mr. Hirofumi Gotou in JSR Corporation for their kind support. The author appreciates the support from an international research fellowship of JSR.

Finally, the author expresses his deep appreciation to his friends and family, especially his parents, Mr. Isao Murakami and Mrs. Satsuki Murakami for their continuous assistance and encouragement.

Takuya Murakami

February 2018

Table of Contents

Chapter 1

General Introduction

1.1 Hydrogels

Hydrogels, or water-swollen polymer networks, have attracted significant attention due to their compatibility with biological tissue and widespread use in a variety of biomedical applications,[1] including drug delivery,[2] cell encapsulation,[3] tissue engineering,[4] and regenerative medicine.[5-7] In addition to these biomedical applications, hydrogels offer a variety of promising applications, e.g., sensors, actuators, and microfluidics, which can benefit from precisely tailoring the properties of hydrogel systems.[8-9] As summarized in Table 1.1, hydrogels can be broadly classified into chemically or physically crosslinked systems. Chemically crosslinked gels or chemical gels, which are crosslinked via covalent bonds, tend to have better mechanical properties than their physically crosslinked counterparts. In an effort to improve the mechanical properties of chemical gels, novel hydrogels with various network architecture, e.g., double network gels[10] and slide-ring gels,[11] have been developed over the last decade. They are attracting many researchers because of their unique and superior properties. In contrast, physically crosslinked gels or physical gels, which are crosslinked via non-covalent bonds, have unique behaviors and functions due to the reversible nature of the non-covalent crosslinking.[1] A number of advantages arise from the reversibility when compared to purely covalent systems, including self-healing[12] and stimuli responsive properties.[13-14] While the properties of hydrogels can be tuned from mechanically robust to soft hydrogels by simply changing crosslinking densities, all of these systems are strongly influenced by the topologies of the polymer networks and the nature of the crosslinks.[15]

Table 1.1. Crosslinking systems in chemical and physical hydrogels.

	Crosslinking systems	Examples
Chemical hydrogels	Covalent bonds	Stable: typical chemical crosslinkers Labile: dynamic covalent chemistry[16]
	Topological entanglements	Interpenetrating polymer networks, crosslinked polyrotaxanes,[11] etc.
Physical hydrogels (homogeneous)	Ionic bonding	Mixtures of polycations and polyanions[17-18]
	Hydrogen bonding	2-Ureido-4[1H]-pyrimidinone[19]
	Hydrophobic effect	Amphiphilic block copolymers[20]
	Host-guest interaction	Inclusion complexes of cyclodextrin[21]
	Stereo-complexation	Enantiomeric mixtures of poly(lactide)[22]
	others	charge-transfer, π-π interaction, etc.
Physical hydrogels (heterogeneous)	Crystallization or aggregation	Agarose, gelatin, poly(vinyl alcohol), etc. Self-assembled low-MW gelators
	Nanocomposites	Fibers, particles, and sheets

1.2 Network Architecture

Interpenetrating polymer network (IPN) gels are composed of the two independent polymer networks that are interpenetrated and entangled with each other. Some studies have reported about mechanically robust IPN gels prepared through effective strategies to strengthen hydrogels.[15, 23] One of the well-known and promising examples of mechanically robust IPN gels is double network (DN) gels which contain a tightly crosslinked and brittle polyelectrolyte network and a loosely crosslinked and ductile neutral polymer network.

Generally, the preparation of IPN gels requires multiple and sequential processing steps including a time-consuming immersion process in which monomers for the second network are introduced into the primary gel. Due to the multiple steps, it is difficult to mold IPN gels into arbitrary sizes and shapes as the primary gel swells significantly during this immersion process and may become brittle. A one-pot and single-step approach could enable the fabrication of robust IPN gels with arbitrary sizes and shapes. This challenge is worthy to be done for future application. One

possible way to implement it is to use natural polymers such as agarose, gelatin, and alginate that can form self-assembled networks with limited tunability. Another way is to exploit a pair of orthogonal reactions, each of which is independent of another, enabling fine control over each network independently obtainable from readily available synthetic monomers or polymers.

Slide-ring (SR) gels were first introduced by Ito and coworkers[11] following theoretical predictions by P.-G. de Gennes.[24] SR gels can be considered as topologically crosslinked polymer networks with no covalent crosslinking between chains. To realize the sliding crosslinks that are topologically interlocked non-covalent crosslinks and can slide along the threaded polymer backbones, the supramolecular chemistry of cyclodextrin (CD) and rotaxane formation were utilized. Ito and coworkers have identified a range of fundamental and industrially important properties of SR gels such as extreme softness, low modulus, increased stretchability, and high swellability. Despite their promising properties, the synthesis of SR gels is somewhat complicated and requires three steps: formation of the *pseudo*-polyrotaxane, end-capping of the axial chain, and final crosslinking between threaded CDs.

Well-established strategies involving supramolecular-based crosslinking can be effectively employed for hydrogels with homogeneous polymer networks, in contrast to those based on aggregates or nanocomposites. There are various kinds of intermolecular interactions ranging from weak to relatively strong ones, e.g., hydrophobic effect, hydrogen bonding, and ionic bonding. Therefore, by taking advantage of the combination of crosslinking systems and polymer backbones, we can design network architecture including both random networks and regulated or structured networks to tune their properties.[15]

In hydrogel systems, there is a diverse range of selection of the polymer backbone from synthetic and natural polymers. Among water-soluble polymers, polyethers such as polyethylene glycol (PEG) and its derivatives have outstanding controllability over monomer sequence, molecular weight, and its distribution and thus have been used as the polymer backbone of well-characterized hydrogels. Furthermore, PEG-based hydrogels are hopeful candidates for biomedical applications because of their

biocompatibilities.[20] One of the drawbacks of conventional polyethers is difficulty of further functionalization, and another is that the variety of commercially available monomers is insufficient. C. J. Hawker et al. have studied functional polyethers synthesized via anion ring-opening polymerization, and demonstrated that the functional polyethers can be a versatile platform for biocompatible tailor-made polymers.[25] In this thesis, we employed polyether platforms as polymer backbones, and focused on the introduction of functionalities at the chain-ends and at the side-chains; the synthetic accessibility was examined using the two types.

1.3 Click Chemistry

Click chemistry is a new synthetic strategy for design of complicated molecules from simple or small subunits using a set of rapid, selective, and reliable reactions, first proposed by K. B. Sharpless et al. in 2001.[26] According to their definition, the reactions must be modular, wide in scope, give excellent yields without offensive by-products, and be stereospecific. Nowadays, various kinds of useful click reactions are available thanks to many researchers who have reviewed and developed bond formation reactions to expand the available click chemistry. Typical click reactions are mainly classified in the following three groups; cycloaddition, radical addition, and nucleophilic addition, as shown in Figure 1.1.

1,3-dipolar cycloaddition ([3+2] cycloaddition) between azides and alkynes has been the most successful click reaction and employed in many fields. In addition to the traditional copper-catalyzed azide-alkyne cycloaddition, strain-promoted azide-alkyne cycloaddition has facilitated a wide range of applications due to the absence of poisonous copper, such as chemical ligation in living systems.[27] Diels-Alder reactions ([4+2] cycloaddition) are also regarded as click reactions and have been used in the synthesis of materials and bioconjugates.[28] One of the interesting features of Diels-Alder reactions is thermal reversibility, which can provide self-healing properties.[29]

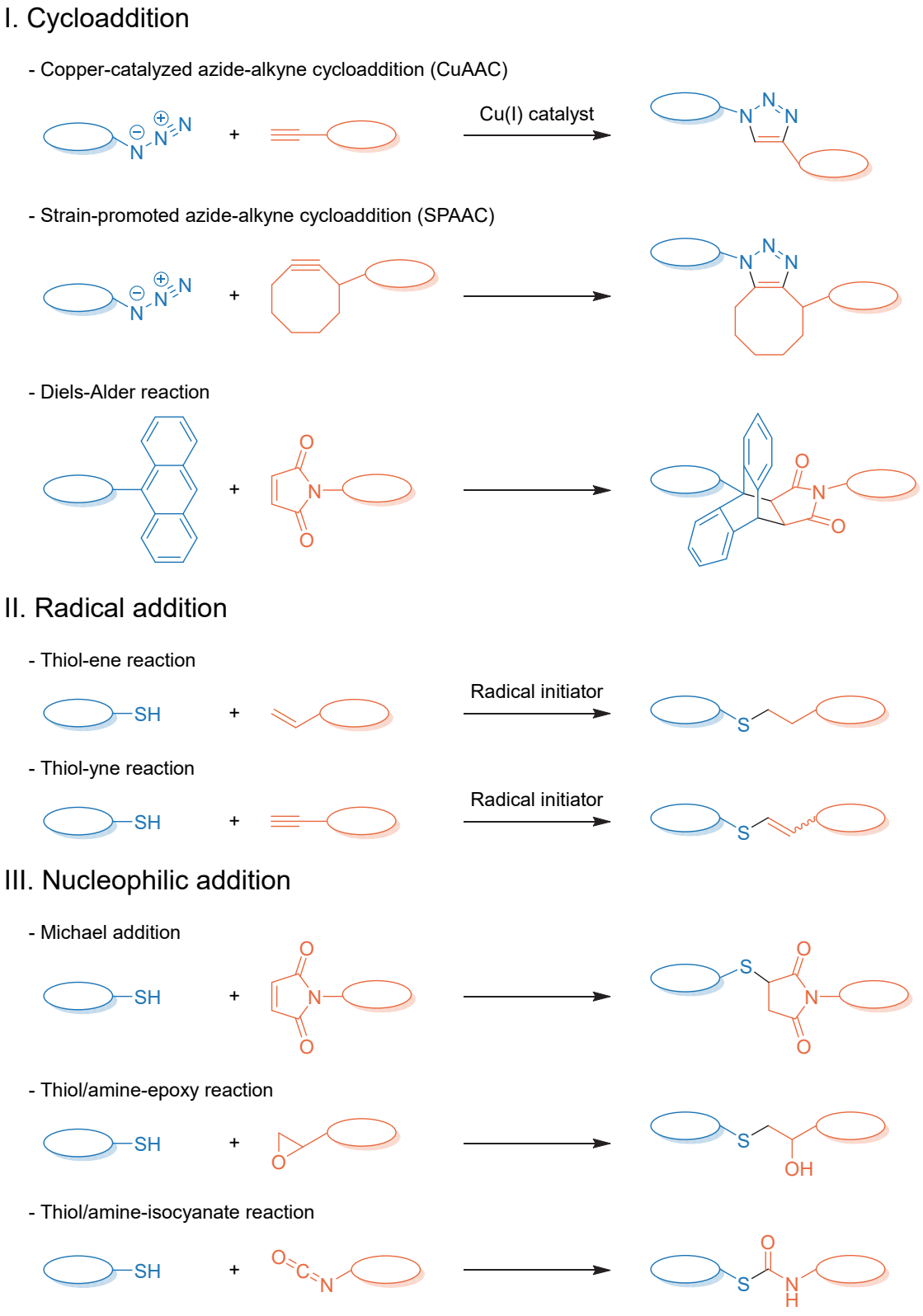

Figure 1.1. Examples of click reactions.[26, 30]

Thiol-based chemistry including radical addition and nucleophilic addition is another prominent example of click reactions.[30] In particular, the thiol-ene reaction has attracted much attention due to its robust, efficient, and orthogonal characteristics. Although this reaction has long been known for the vulcanization of rubbers with sulfur, discovered by C. Goodyear in the 19th century, it has recently been reinvented and employed in the synthesis of well-defined materials. In the presence of thermal or photo radical initiators, the reaction of unactivated alkenes and thiols proceeds in nearly quantitative yields in practical environments including neat and aqueous conditions, and shows the good orthogonality against various functional groups.

Taking advantage of the concept of click chemistry, we can efficiently design and synthesize soft materials, especially hydrogels, where ordinal chemical reactions often do not work because of limited fluidity in the matrix and restriction of using the activated reagents that cannot tolerate water and reactive functional groups.

1.4 Objective and Structure of This Thesis

Architecture of polymer networks in hydrogels plays an important role in their functions and properties. As stated above, reported or conventional methods for the fabrication of hydrogels with novel network architecture often require the laborious and time-consuming procedures with synthetic difficulties, which have hampered their practical applications. Demands of fabricating advanced hydrogel materials with engineered properties in an efficient or industrial way have been growing with expanding their applications. On the other hand, click chemistry can bring about significant facilitation of the complex functionalization in soft materials.[30] Compared to common chemical reactions, click reactions have several unique features; rapid, orthogonal, reliable, atom-economical, and applicable to aqueous and biological environments, which is suitable for construction and functionalization of polymer networks in hydrogels. In this thesis, we aimed at synthesis of hydrogels with various network architecture with precisely controlled topologies and crosslinking systems via click chemistry, and their characterization in details to provide deeper insights for the structure-property relationships in hydrogel systems. Graphical abstracts are shown

in Figure 1.2.

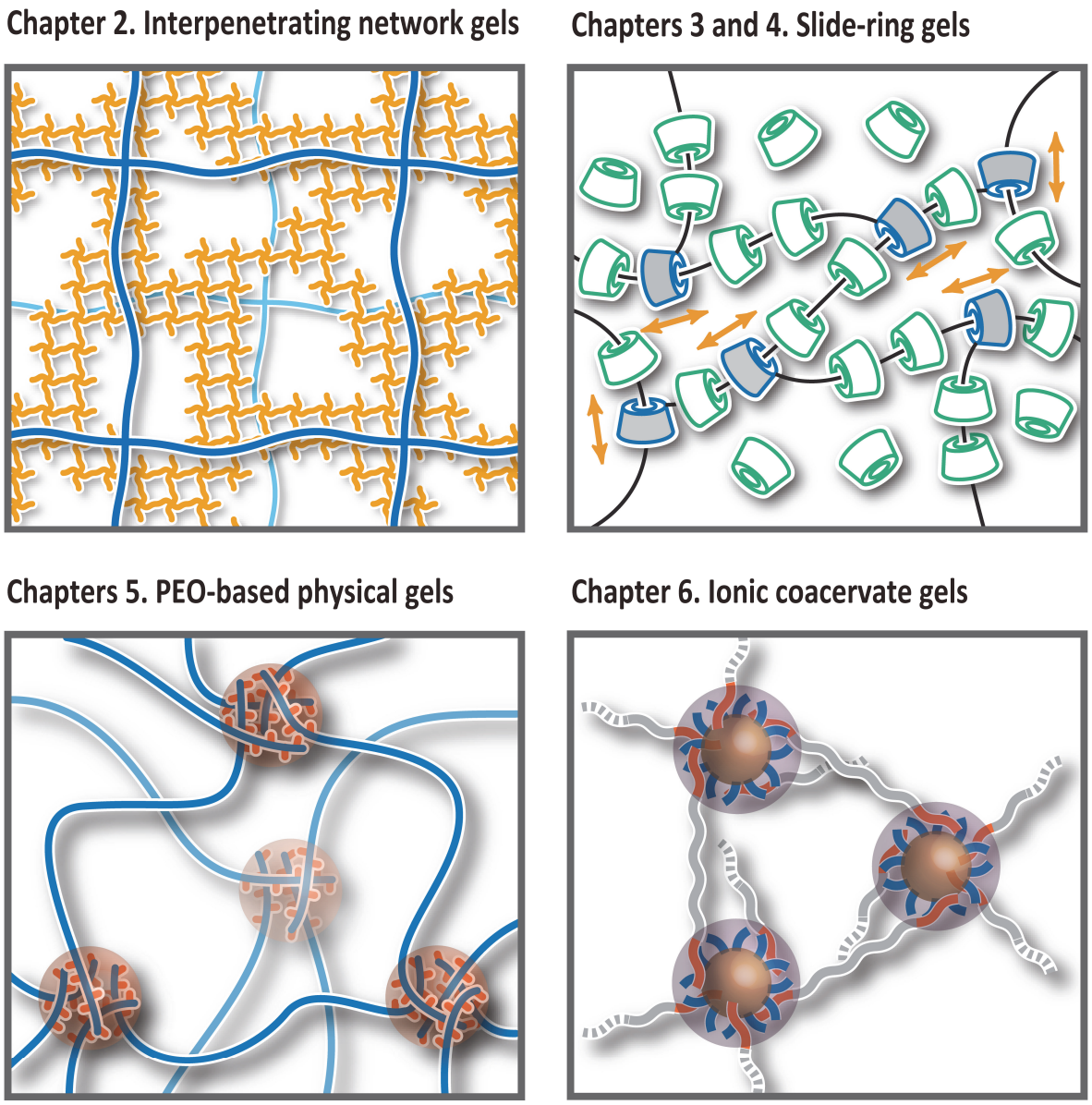

Figure 1.2. Various network architecture of hydrogels investigated in this thesis.

In Chapter 2, we present one-pot fabrication of robust IPN gels with tight and loose networks via orthogonal double click reactions. Both the crosslinked networks are simultaneously constructed in water from the bio-compatible PEG-based macromonomers. The crosslinking density of each network was finely tuned by the

macromonomer structure, permitting control of network molecular weights between crosslinks of the final gels. The mechanical properties of the obtained gels were evaluated through compression testing as well as tensile testing thoroughly.

In Chapter 3, we demonstrate a modular and robust one-pot "click" fabrication of SR gels with little or no unwanted covalent crosslinking. Formation and crosslinking of polyrotaxanes were simultaneously carried out by the combination of thiol-ene chemistry and supramolecular chemistry. The present one-pot strategy requires only sonication before curing; therefore, tedious isolation and purification processes can be omitted.

In Chapter 4, we propose a one-pot strategy for the fabrication of novel SR gels with cyclodextrin-derived crosslinks and additional free cyclodextrin ring spacers co-threaded onto the polymer backbones, following the previous chapter. The free CD units that are threaded but not linked to any other units have an effect on properties such as entropy-driven elasticity derived from the alignment entropy of threaded macrocycles. To clarify the effect of threaded macrocycles in SR networks, we deliberately added free CD units into the system to act as a spacer on the chain without adding further crosslinks to the system. The present procedure allows the sliding crosslinks and free spacers to be introduced into the SR networks simultaneously with the product ratio being controlled by the feed ratio via thiol-yne reaction.

In Chapter 5, we describe a library of physical gels comprised of PEO-based triblock copolymers with highly tunable viscoelastic properties. Their aqueous solutions exhibit a glass state at low concentrations, with stress relaxations being systematically controlled depending on the length of the side-chains (*n*-hexyl to *n*-dodecyl). A major challenge in physical gel systems is tailoring of rheological properties, with future applications being enabled by the development of a robust strategy for tuning viscoelasticity in a wide range.

In Chapter 6, we demonstrate ionic coacervate gels with hydrophobic cores derived from polyelectrolyte having a poly(propylene oxide) segment. Ionic coacervate gels are one of the tough physical hydrogels formed via ionic coacervation of polyelectrolytes, which are typically a pair of positively and negatively charged

triblock copolymers.[18] It was revealed that the ionic coacervate gels showed high storage moduli and formed regularly ordered structures of coacervate domains. Following the previous study, we introduced a hydrophobic core into the coacervate domain to construct the novel core-shell structure in ionic coacervate gels that can greatly contribute to their thermoresponsive properties.

1.5 References

1. Peppas, N. A.; Hilt, J. Z.; Khademhosseini, A.; Langer, R. *Adv. Mater.* **2006**, *18*, 1345-1360.
2. Hoare, T. R.; Kohane, D. S. *Polymer* **2008**, *49*, 1993-2007.
3. Wang, C.; Varshney, R. R.; Wang, D.-A. *Adv. Drug Deliv. Rev.* **2010**, *62*, 699-710.
4. Zhu, J.; Marchant, R. E. *Expert Rev. Med. Devices* **2011**, *8*, 607-626.
5. Annabi, N.; Tamayol, A.; Uquillas, J. A.; Akbari, M.; Bertassoni, L. E.; Cha, C.; Camci-Unal, G.; Dokmeci, M. R.; Peppas, N. A.; Khademhosseini, A. *Adv. Mater.* **2014**, *26*, 85-124.
6. Slaughter, B. V.; Khurshid, S. S.; Fisher, O. Z.; Khademhosseini, A.; Peppas, N. A. *Adv. Mater.* **2009**, *21*, 3307-3329.
7. Khademhosseini, A.; Langer, R.; Borenstein, J.; Vacanti, J. P. *P. Natl. Acad. Sci. USA* **2006**, *103*, 2480-2487.
8. Bauer, S.; Bauer-Gogonea, S.; Graz, I.; Kaltenbrunner, M.; Keplinger, C.; Schwödiauer, R. *Adv. Mater.* **2014**, *26*, 149-162.
9. Quake, S. R.; Scherer, A. *Science* **2000**, *290*, 1536-1540.
10. Gong, J. P.; Katsuyama, Y.; Kurokawa, T.; Osada, Y. *Adv. Mater.* **2003**, *15*, 1155-1158.
11. Okumura, Y.; Ito, K. *Adv. Mater.* **2001**, *13*, 485-487.
12. Garcia, S. J. *Eur. Polym. J.* **2014**, *53*, 118-125.
13. Jeong, B.; Kim, S. W.; Bae, Y. H. *Adv. Drug Deliv. Rev.* **2012**, *64*, 154-162.
14. Roy, D.; Brooks, W. L. A.; Sumerlin, B. S. *Chem. Soc. Rev.* **2013**, *42*, 7214-7243.
15. Creton, C. *Macromolecules* **2017**, *50*, 8297-8316.
16. Rowan, S. J.; Cantrill, S. J.; Cousins, G. R.; Sanders, J. K.; Stoddart, J. F. *Angew. Chem. Int. Ed.* **2002**, *41*, 898-952.

17. Luo, F.; Sun, T. L.; Nakajima, T.; Kurokawa, T.; Zhao, Y.; Sato, K.; Ihsan, A. B.; Li, X.; Guo, H.; Gong, J. P. *Adv. Mater.* **2015**, *27*, 2722-2727.
18. Hunt, J. N.; Feldman, K. E.; Lynd, N. A.; Deek, J.; Campos, L. M.; Spruell, J. M.; Hernandez, B. M.; Kramer, E. J.; Hawker, C. J. *Adv. Mater.* **2011**, *23*, 2327-31.
19. Guo, M.; Pitet, L. M.; Wyss, H. M.; Vos, M.; Dankers, P. Y. W.; Meijer, E. W. *J. Am. Chem. Soc.* **2014**, *136*, 6969-6977.
20. Alexandridis, P.; Alan Hatton, T. *Colloids Surf. A Physicochem. Eng. Asp.* **1995**, *96*, 1-46.
21. Nakahata, M.; Takashima, Y.; Yamaguchi, H.; Harada, A. *Nat. Commun.* **2011**, *2*, 511.
22. Fujiwara, T.; Mukose, T.; Yamaoka, T.; Yamane, H.; Sakurai, S.; Kimura, Y. *Macromol. Biosci.* **2001**, *1*, 204-208.
23. Johnson, J. A.; Turro, N. J.; Koberstein, J. T.; Mark, J. E. *Prog. Polym. Sci.* **2010**, *35*, 332-337.
24. de Gennes, P.-G. *Physica A Stat. Mech. Appl.* **1999**, *271*, 231-237.
25. Lee, B. F.; Kade, M. J.; Chute, J. A.; Gupta, N.; Campos, L. M.; Fredrickson, G. H.; Kramer, E. J.; Lynd, N. A.; Hawker, C. J. *J. Polym. Sci., Part A: Polym. Chem.* **2011**, *49*, 4498-4504.
26. Kolb, H. C.; Finn, M.; Sharpless, K. B. *Angew. Chem. Int. Ed.* **2001**, *40*, 2004-2021.
27. Lutz, J.-F. *Angew. Chem. Int. Ed.* **2008**, *47*, 2182-2184.
28. Tasdelen, M. A. *Polym. Chem.* **2011**, *2*, 2133-2145.
29. Zeng, C.; Seino, H.; Ren, J.; Hatanaka, K.; Yoshie, N. *Macromolecules* **2013**, *46*, 1794-1802.
30. Iha, R. K.; Wooley, K. L.; Nystrom, A. M.; Burke, D. J.; Kade, M. J.; Hawker, C. J. *Chem. Rev.* **2009**, *109*, 5620-5686.

Chapter 2

One-Pot Fabrication of Robust Interpenetrating Hydrogels via Orthogonal Click Reactions

2.1 Introduction

Hydrogels have attracted much attention in the pharmaceutical and biomedical fields as key materials for various applications based on properties such as permeability and biocompatibility, e.g., drug delivery systems,[1,2] therapeutic materials such as hydrogel wound dressing,[3] tissue engineering such as cell culture scaffolds and artificial cartilage.[4-7] However, conventional hydrogels lack the mechanical strength required for practical use. Therefore, much effort has been devoted to improving the mechanical properties of hydrogels.[8,9] For example, double network (DN) gels,[10-12] nanocomposite hydrogels,[13,14] slide-ring gels,[15,16] and ionic coacervate hydrogels[17] have been developed and reported over the last two decades. As a prime example, DN gels, first reported by Gong et al. in 2003,[10] have outstanding toughness[18] and are a unique type of interpenetrating polymer network (IPN), composed of two independent polymer networks: a tightly crosslinked brittle polyelectrolyte network (a minor component) and a loosely crosslinked ductile neutral polymer network (a major component). Apart from DN gels, mechanically robust IPN gels have also been reported and in select cases are also an effective strategy to strengthen hydrogels.[19,20] However, the preparation of DN/IPN gels requires multiple, sequential processing steps including a time-consuming immersion process in which monomers for the second network are introduced into the primary gel. These multiple steps make it difficult to mold DN/IPN gels into a certain size or complex shape as the primary gel swells significantly during this immersion process and may become brittle, both challenges for future applications.

To address these challenges, a one-pot, one-step approach could allow robust

DN/IPN gels to be fabricated with arbitrary size and shape. One possible way to do so is using natural polymers that can form self-assembled networks such as alginate, gelatin, and agarose.[7,21,22] A second strategy is to exploit orthogonal reactions that are independent of each other, enabling fine control over each network independently from readily available synthetic monomers/polymers. Tang et al. utilized Michael addition and UV-initiated radical polymerization of vinyl monomers to fabricate polyester-based IPN gels with the one-pot method. However, the gels did not have an ideal IPN structure because the networks were randomly crosslinked with each other. Most recently, Dove reported a very promising method for the one-pot fabrication of DN gels through a simultaneous orthogonal dual-click approach.[23] In this study, the authors utilized a nucleophilic thiol-yne click reaction and inverse electron-demand Diels-Alder addition with the tightly crosslinked network being the major component, and the loosely crosslinked network, the minor component. This is the opposite network topology to that for Gong-style DN gels.[18,24]

We report herein the rapid, one-pot fabrication of robust IPN gels via orthogonal double click reactions with the tight and loose networks being formed at approximately the same time leading to a covalently crosslinked IPN structure (Scheme 2.1). For this work, the same polymer backbone was selected for both networks with the weight fraction and crosslinking density tuned according to prior DN studies. This degree of control allows the relationship between mechanical properties and topology of the IPN gels to be studied.

Copper catalyzed azide-alkyne cycloaddition (CuAAC) and epoxy-amine reaction were selected as an orthogonal pair with poly(ethylene glycol) (PEG) chosen as a bio-compatible backbone. Furthermore, 4-arm telechelic macromonomers with narrow polydispersity were employed to obtain a range of network molecular weights between crosslinks (M_c) with the crosslinking density of each network being tuned to allow direct comparison between single and double, interpenetrating networks.

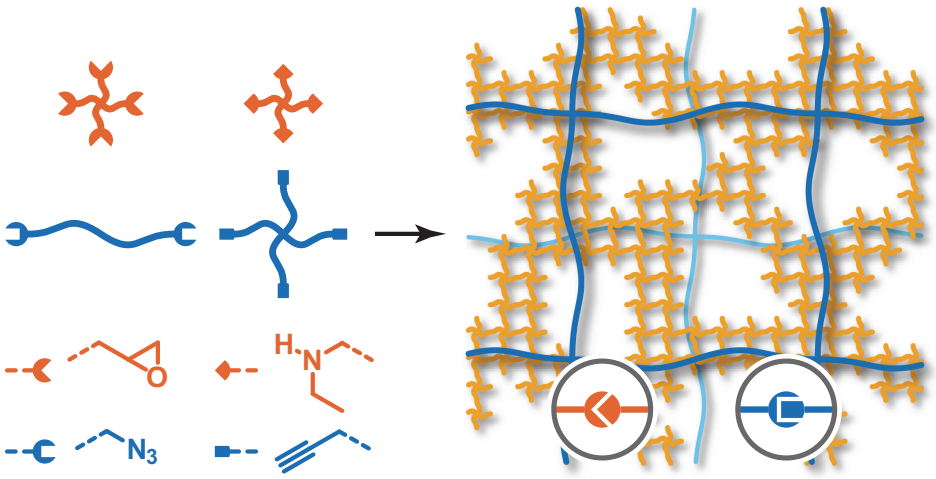

Scheme 2.1. Schematic illustration for the formation of interpenetrating networks via orthogonal double click reactions.

2.2 Experimental Section

Materials. All chemicals were used as received from Sigma-Aldrich unless otherwise specified. Hydroxy terminated linear PEG and 4-arm PEG were purchased from Sigma-Aldrich and Jenkem Technology (Beijing, China) respectively, and dried *in vacuo* prior to use. Tetrahydrofuran (THF), dichloromethane (DCM), and N,N-dimethylformamide (DMF) were collected from a dry solvent system, and used immediately thereafter.

Characterization. ^{1}H NMR spectra were recorded on a Varian VNMRS 600 spectrometer (600 MHz). Chemical shifts are reported relative to residual solvent peaks (δ 7.26 for $CDCl_3$, 2.50 for DMSO-d_6, and 4.79 for D_2O). The number-average molecular weights (M_n) and the degree of substitution (DS) for the macromonomers were calculated from integral ratios between protons corresponding to the terminal functional groups, the pentaerythritol cores, and the PEG backbones. Gel permeation chromatography (GPC) was performed on a Waters 2695 separation module equipped with a Waters 2410 differential refractometer and a Waters 2998 photodiode array detector. Chloroform with 0.25% of triethylamine was used as an eluent at a flow rate of 1 mL/min. Molecular weight and polydispersity index (PDI) were calculated relative

to linear polystyrene standards. Dynamic light scattering (DLS) analysis was performed on a Wyatt Technology DynaPro NanoStar instrument. Reported values are averages of 100 acquisitions.

Rheological experiments were performed on a TA Instruments ARES-LS1 rheometer with parallel-plate geometry (diameter: 25 or 50 mm). Frequency sweeps were performed at a strain of 1%, and strain sweeps were performed at a frequency of 1 Hz. Compression tests were carried out on a mechanical testing machine equipped with an Eaton Corporation 3108-10 load cell with a capacity of 44.48 N or an MTS 661.18A-01 load cell with a capacity of 1 kN equipped with an Electronic Instrument Research LE-01 laser extensometer using a compression rate of 20% per min. Cylindrical shape samples with a diameter of 5 mm and a length of 4 mm were used. The compression plates were mirror-polished and a small amount of water was applied on the plate in order to ensure that the gels slipped well. Tensile tests were conducted on the same mechanical testing machine using an extension rate of 200% per min. Samples were cut into rectangular shapes with dimensions of 5 mm by 25 mm by 0.5 mm and clamped with pieces of sand paper to avoid grip slippage or breakage. Swelling tests were performed at room temperature. Samples were immersed in deionized water for a week to reach an equilibrium swollen state. The weight fractions of the resulting swollen gels were determined by weight measurements of the swollen and freeze-dried samples.

Synthesis of epoxy functionalized 4-arm PEG 1. 4-arm PEG with M_n 2 kDa (10.0 g, 5.0 mmol) was dissolved in THF (50 mL) under a dry argon atmosphere. Sodium hydride (0.76 g, 30 mmol, 1.5 equiv to hydroxy groups) was added to the solution, and vigorously stirred for an hour at room temperature. Epichlorohydrin (4.7 mL, 60 mmol, 3.0 equiv) was added with a syringe to the mixture, and stirred for three days at room temperature. The reaction mixture was filtered through a silica gel pad, condensed, and poured into hexane. The precipitated liquid was collected by centrifugation, washed with hexane repeatedly, and dried *in vacuo*. The product was obtained as a pale yellow viscous liquid.

1. ^{1}H NMR (600 MHz, $CDCl_3$) δ 3.79-3.37 (m, 206H, C-(CH_2(OCH_2CH_2)$_{11.8}$$CH_2$CH(O)$CH_2$)$_4$), 3.13 (m, 4H, (~$CH_2CH(O)CH_2$)$_4$), 2.77 (m, 4H,

(~$CH_2CH(O)CH_2$)$_4$), 2.58 (m, 4H, (~$CH_2CH(O)CH_2$)$_4$). M_n 2.45 kDa. DS 97%. PDI 1.10.

Synthesis of mesylated 4-arm/linear PEG. Mesylation of PEG was carried out using an improved method[25] according to the following procedure, where synthesis of the mesylated 4-arm PEG was described as a representative. To 4-arm PEG with M_n 2 kDa (10.0 g, 5.0 mmol) was added DCM (100 mL) and triethylamine (21 mL, 0.15 mol, 7.5 equiv to hydroxy groups) under a dry argon atmosphere. After the solution was cooled to 0 °C with an ice-water bath, trimethylamine hydrochloride (1.91 g, 20 mmol, 1.0 equiv) was added to the solution. Methanesulfonyl chloride (11.5 g, 0.10 mol, 5.0 equiv) was added dropwise to the mixture. After completion of the addition, the reaction mixture was allowed to warm to room temperature and was stirred for 24 h. The reaction mixture was concentrated, diluted with ethyl acetate, and filtered to remove inorganic salts. The resulting filtrate was washed with 1 N hydrochloric acid, sodium bicarbonate, and brine, dried over magnesium sulfate, and concentrated *in vacuo*. The product was obtained as a brown viscous liquid after being dried under a high vacuum.

Mesylated 4-arm PEG (2 kDa). ^{1}H NMR (600 MHz, $CDCl_3$) δ 4.37 (t, J = 4.5 Hz, 8H, (~OCH_2CH_2OMs)$_4$), 3.76 (t, J = 4.5 Hz, 8H, (~OCH_2CH_2OMs)$_4$), 3.72-3.49 (m, 170H, (~(OCH_2CH_2)$_{10.6}$~)$_4$), 3.40 (m, 8H, C-(CH_2O~)$_4$), 3.07 (s, 12H, (~OSO_2CH_3)$_2$). M_n 2.41 kDa. DS 98%.

Mesylated PEG 10 kDa. ^{1}H NMR (600 MHz, $CDCl_3$) δ 4.36 (t, J = 4.5 Hz, 4H, (~$CH_2OSO_2CH_3$)$_2$), 3.76-3.49 (m, 904H, ~(OCH_2CH_2)$_{226}$~), 3.07 (s, 6H, (~$CH_2OSO_2CH_3$)$_2$). M_n 10.2 kDa. DS 93%.

Mesylated PEG 35 kDa. ^{1}H NMR (600 MHz, $CDCl_3$) δ 4.36 (t, J = 4.5 Hz, 4H, (~$CH_2OSO_2CH_3$)$_2$), 3.76-3.49 (m, 3173H, ~(OCH_2CH_2)$_{793}$~), 3.07 (s, 6H, (~$CH_2OSO_2CH_3$)$_2$). M_n 35.2 kDa. DS 100%.

Synthesis of amine functionalized 4-arm PEG 2. Ethylamine hydrochloride (25.0 g, 306 mmol, 25.5 equiv to mesyl groups) was dissolved in water (60 mL), and cooled to 0 °C. Sodium hydroxide (12.0 g, 300 mmol, 25 equiv) was dissolved in water (60 mL), and added dropwise to the former solution to obtain an ethylamine solution. Mesylated 4-arm PEG with M_n 2 kDa (6.0 g, 3.0 mmol) was added to the ethylamine solution at 0 °C, allowed to warm to room temperature, and stirred for two days in the dark. The reaction mixture was filtered, and was extracted with DCM three times. The

combined organic phase was washed with brine, dried over sodium sulfate, and concentrated in vacuo. The product was obtained as a pale brown liquid after being dried under a high vacuum.

2. ^{1}H NMR (600 MHz, $CDCl_3$) δ 3.67-3.49 (m, 183H, (~(OCH_2CH_2)$_{10.9}$CH_2~)$_4$), 3.39 (m, 8H, C-(CH_2O~)$_4$), 2.77 (t, J = 5.2 Hz, 8H, (~CH_2NHCH$_2$CH$_3$)$_4$), 2.64 (q, J = 7.1 Hz, 8H, (~NHCH_2CH$_3$)$_4$), 1.09 (t, J = 7.2 Hz, 12H, (~NHCH$_2$CH_3)$_4$). M_n 2.41 kDa. DS 98%. PDI 1.09.

Synthesis of azide functionalized 4-arm PEG 3a. Mesylated 4-arm PEG with M_n 2 kDa (6.0 g, 3.0 mmol) and sodium azide (3.90 g, 60.0 mmol, 5.0 equiv) were dissolved in DMF (60 mL) under a dry argon atmosphere. The reaction mixture was stirred at 80 °C for 20 h. After being cooled to room temperature, the mixture was filtered, and concentrated *in vacuo*. The obtained liquid was re-dissolved in DCM, washed with brine, dried over magnesium sulfate, and concentrated in vacuo. The product was obtained as a pale brown viscous liquid after being dried under a high vacuum.

3a. ^{1}H NMR (600 MHz, $CDCl_3$) δ 3.68-3.47 (m, 176H, (~(OCH_2CH_2)$_{10.5}$CH_2~)$_4$), 3.38 (s, 8H, C-(CH_2O~)$_4$), 3.35 (t, J = 5.1 Hz, 8H, (~OCH$_2$CH_2N$_3$)$_4$). M_n 2.33 kDa. DS 98%. PDI 1.07.

Synthesis of azide functionalized linear PEG 3b-c. Azides **3b-c** were prepared from the mesylated linear PEG with M_n 10 and 20 kDa in the same manner as **3a**. The products were obtained as a pale yellow powder.

3b. ^{1}H NMR (600 MHz, $CDCl_3$) δ 3.76-3.48 (m, 904H, ~(OCH_2CH_2)$_{793}$~), 3.37 (t, J = 5.1 Hz, 4H, (~OCH$_2$CH_2N$_3$)$_2$). M_n 10.2 kDa. DS 92%. PDI 1.11.

3c. ^{1}H NMR (600 MHz, $CDCl_3$) δ 3.76-3.48 (m, 3175H, ~(OCH_2CH_2)$_{794}$~), 3.37 (t, J = 5.1 Hz, 4H, (~OCH$_2$CH_2N$_3$)$_2$). M_n 35.1 kDa. DS 100%. PDI 1.13.

Synthesis of alkyne functionalized 4-arm PEG 4a-c. Alkynes **4a-c** were prepared from 4-arm PEG with M_n 2, 10, and 20 kDa according to the following procedure, where the synthesis of **4c** was described as a representative. 4-arm PEG with M_n 20 kDa (8.0 g, 0.40 mmol) was dissolved in THF (100 mL) under a dry argon atmosphere. Sodium hydride (0.10 g, 4.0 mmol, 2.5 equiv to hydroxy groups) was added to the solution and vigorously stirred for an hour at room temperature. Propargyl bromide 80wt%

solution in toluene (1.2 g, 8.0 mmol, 5.0 equiv) was added with a syringe to the mixture, and was stirred for three days at room temperature. The reaction mixture was filtered through a silica gel pad, concentrated, and poured into ice-cold diethyl ether. The precipitated solid was collected by filtration, washed with diethyl ether repeatedly, and dried *in vacuo*. The product was obtained as a pale yellow powder.

4a. ^{1}H NMR (600 MHz, $CDCl_3$) δ 4.17 (s, 8H, (~OCH_2C≡CH)$_4$), 3.76-3.48 (m, 190H, (~(OCH_2CH_2)$_{11.9}$~)$_4$), 3.38 (m, 8H, C-(CH_2O~)$_4$), 2.42 (s, 4H, (~C≡CH)$_4$). M_n 2.38 kDa. DS 96%. PDI 1.08.

4b. ^{1}H NMR (600 MHz, $CDCl_3$) δ 4.19 (s, 8H, (~OCH_2C≡CH)$_4$), 3.76-3.49 (m, 1024H, (~(OCH_2CH_2)$_{64.0}$~)$_4$), 3.40 (s, 8H, C-(CH_2O~)$_4$), 2.43 (s, 4H, (~C≡CH)$_4$). M_n 11.6 kDa. DS 93%. PDI 1.10.

4c. ^{1}H NMR (600 MHz, $CDCl_3$) δ 4.18 (s, 8H, (~OCH_2C≡CH)$_4$), 3.76-3.48 (m, 1954H, (~(OCH_2CH_2)$_{122}$~)$_4$), 3.39 (s, 8H, C-(CH_2O~)$_4$), 2.42 (s, 4H, (~C≡CH)$_4$). M_n 21.8 kDa. DS 96%. PDI 1.09.

General procedure for preparation of SN and IPN gels. The macromonomers **1-4** were dissolved in deionized water, and combined at an equimolar ratio of functional groups. To the mixture of the macromonomers was added a stock solution of copper sulfate pentahydrate and *N*,*N*,*N*′,*N*′,*N*″-pentamethyldiethylenetriamine (PMDTA). The resulting mixture was vortexed, and degassed with sonication. After the addition of sodium ascorbate, the obtained precursor solution was transferred into molds, put in an oven at 50 °C for 8 h. The concentration of copper, ligand, and reductant in the precursor solution were 1, 10, and 10 mM respectively. Rectangular molds were made of a Teflon frame (thickness: 0.5 or 1.0 mm) clamped between a pair of glass plates. The precursor solutions were injected into the molds to fill the entire space. The filled molds were tightly clamped and placed in an isotherm oven. Cylindrical molds were made of a 1 mL all-plastic syringe (diameter: 5 mm) with a luer lock cap. The precursor solutions taken into the syringe, deaerated, and sealed. After the filled molds were cured, the narrow tip part was cut by a razor, and the obtained cylindrical gel was pushed out with a plunger.

Preparation of tight single network, SN-1k-10. 145 mg of 35wt% aqueous solution of epoxy **1**, and 141 mg of a 35wt% aqueous solution of amine **2** were placed in a vial,

diluted with 714 mg of deionized water, vortexed, and degassed with sonication. The resulting precursor mixture was transferred into molds, and cured at 50 °C for 8 h.

Preparation of loose single network, SN-46k-20. A copper stock solution was prepared from copper sulfate pentahydrate (0.100 g, 0.4 mmol, 40 mM), PMDTA (0.693 g, 4.0 mmol, 0.4 M), and water (9.2 g). 432 mg of 35wt% aqueous solution of azide **3c**, 140 mg of 35wt% aqueous solution of alkyne **4c**, and 25 mg of the copper stock solution were placed in a vial, diluted with 379 mg of deionized water, vortexed, and degassed with sonication. After the addition of 25 mg of 0.4 M aqueous solution of sodium ascorbate, the resulting precursor mixture was transferred into molds, and cured at 50 °C for 8 h.

Preparation of interpenetrating network, IPN-1k-10/46k-20. 145 mg of a 35wt% aqueous solution of epoxy **1**, 141 mg of a 35wt% aqueous solution of amine **2**, 432 mg of a 35wt% aqueous solution of azide **3c**, 140 mg of a 35wt% aqueous solution of alkyne **4c**, and 25 mg of the copper stock solution were placed in a vial, diluted with 93 mg of deionized water, vortexed, and degassed with sonication. After the addition of 25 mg of 0.4 M sodium ascorbate, the resulting precursor mixture was transferred into molds, and cured at 50 °C for 8 h.

2.3 Results and Discussion

Synthesis of Macromonomers

Tetrafunctional 4-arm PEG and bifunctional linear PEG macromonomers were synthesized with various molecular weights and chain end functional groups (azide, alkyne, epoxy, and amine) (Scheme 2.2). As representative example, epoxy functionalized 4-arm PEG with M_n 2 kDa (**1**), and alkyne functionalized 4-arm PEG with M_n 2, 12, and 22 kDa (**4a-c**) were prepared by S_N2 reactions with epichlorohydrin and propargyl bromide respectively. Similarly, amine functionalized 4-arm PEG with M_n 2 kDa (**2**), and azide functionalized 4-arm/linear PEG with M_n 2, 10, and 35 kDa (**3a-c**) were prepared from mesylated 4-arm/linear PEG by S_N2 reactions with ethyl amine and sodium azide respectively. The macromonomers were characterized by ^{1}H NMR,

GPC, and DLS analysis and all shown to have narrow PDI (1.07-1.13) and high degrees of chain end substitution (93-100%). The hydrodynamic radii R_h of the macromonomers were determined from size distributions with overall properties summarized in Table 2.1.

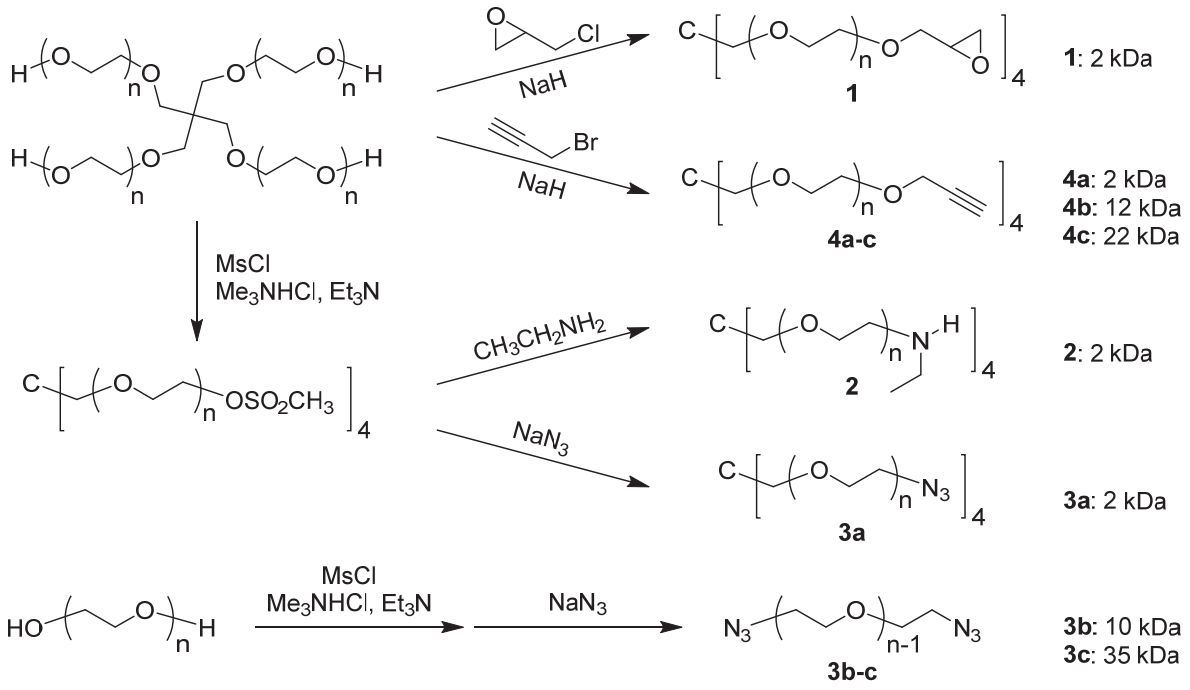

Scheme 2.2. Synthesis of telechelic PEG macromonomers.

Table 2.1. Properties of macromonomers.

Macromonomers		M_n (kDa)	PDI	R_h (nm)
4arm-PEG-epoxy	**1**	2.45	1.10	1.4
4arm-PEG-amine	**2**	2.41	1.09	1.1
4arm-PEG-azide	**3a**	2.33	1.07	1.1
Linear-PEG-azide	**3b**	10.1	1.11	3.1
	3c	35.1	1.13	5.3
4arm-PEG-alkyne	**4a**	2.38	1.08	1.1
	4b	11.6	1.10	3.1
	4c	21.8	1.09	4.2

Fabrication of IPN gels

Preliminary studies confirmed that the macromonomer pairs readily form single network (SN) gels with the SN gels being prepared according to the compositions as shown in Table 2.2. First, as a test of an epoxy-amine reaction, epoxy **1** and amine **2** were dissolved in water at an equimolar ratio of epoxy to amine, and warmed to 50 °C for 8 h to obtain SN gels with M_c of 1 kDa. As a test of CuAAC driven gelation, azides **3b,c** and alkynes **4a,c** were dissolved in water at an equimolar ratio of azide to alkyne with the copper catalyst ([$CuSO_4$]:[Sodium ascorbate]:[PMDTA] = 1:10:10 mM), and warmed to 50 °C for 8 h to obtain SN gels with M_c varying between 11 and 46 kDa. SN gels with M_c 3 kDa were made as a reference from azide **3a** and alkyne **4b** in the same way. The epoxy-amine reaction was also carried out in the presence of the copper catalyst with storage moduli of the resulting gels being plotted against the concentration of copper. It was observed that the modulus steeply decreased above 2 mM of copper which may be due to coordination of the amine to copper leading to a reduction in the nucleophilicity of amine. As a result, copper catalysts can inhibit epoxy-amine reactions, especially at a high concentration. Therefore, we used excess PMDTA as the ligand that coordinates to the copper in preference to the macromonomer, and limited the concentration of copper to 1 mM.

Following these preliminary studies, the reaction mixtures were combined and the dual network formation performed at the same time to achieve the desired one-pot fabrication of IPN gels (Scheme 2.3). Figure 2.1 shows time-sweeps of the storage moduli of representative SN and IPN gels during crosslinking. Interestingly, the CuAAC driven crosslinking was faster than the epoxy-amine reaction and slightly accelerated due to the presence of the amine macromonomer and/or an epoxy-amine adduct. The time-sweep of the IPN gel had faster and slower components corresponding to each reaction, which demonstrates that both reactions can proceed independently.

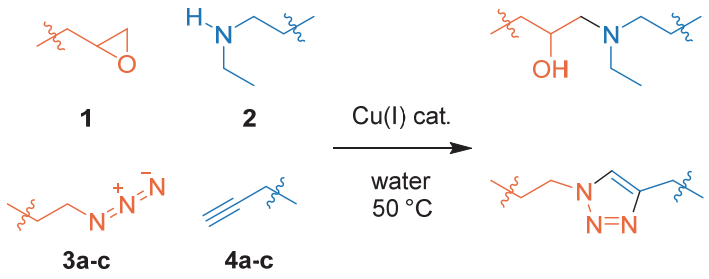

Scheme 2.3. Crosslinking reactions used in network formation.

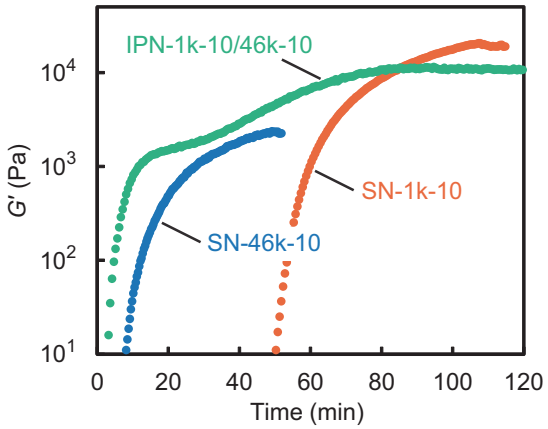

Figure 2.1. Time-sweeps of the storage moduli of the SN and IPN gels at a strain of 1% and a frequency of 1 Hz during crosslinking at 50 °C.

A library of 16 IPN gels containing both tight and loose networks were then successfully fabricated using this strategy of orthogonal click reactions with 6 SN gels prepared as reference materials. In order to evaluate the synergistic effect derived from the two different networks, we screened various compositions with varying weight fractions and crosslinking densities as a function of M_c. To refer to samples easily, we used the following sample codes: "SN-x-y" for SN gels and "IPN-x_1-y_1/x_2-y_2" for IPN gels, where the numbers x and y denote the M_c and weight concentrations of each network respectively. For example, SN-1k-10 denotes a single network (SN) gel consisting of 10wt% PEG network with M_c 1 kDa; and IPN-1k-10/46k-20 denotes an interpenetrating network (IPN) gel consisting of a 10wt% epoxy PEG network with M_c 1 kDa and 20wt% CuAAC PEG network with M_c 46 kDa.

The properties of the SN gels are summarized in Table 2.2. SN-1k is regarded as the

tight network, while SN-11k, 21k, 36k, and 46k are regarded as the loose networks in this system. For comparison, the average M_c of the IPN gels was calculated from the following equation. The average M_c of IPN-1k-10/x-20 is between 3.0 and 3.4 kDa, and nearly equal to the M_c (3.45 kDa) of the reference SN-3k. The average M_c of IPN-1k-5/x-20 is higher than SN-3k, while those of the other IPN gels are lower than SN-3k.

$$M_{c,\ average} = \left(\frac{y_1}{y_1 + y_2} \frac{1}{M_{c,1}} + \frac{y_2}{y_1 + y_2} \frac{1}{M_{c,2}} \right)^{-1} \quad (2.1)$$

Table 2.2. Compositions and properties of single networks.

		M_c (kDa)	C^*_{mix} (g/mL)	G' [a] (kPa)	G_{ph} [a] (kPa)
SN-1k	**1**+**2**	1.21	0.53	104	212
SN-3k	**3a**+**4b**	3.45	0.19	28	74
SN-11k	**3b**+**4a**	11.2	0.15	28	23
SN-21k	**3b**+**4c**	20.9	0.12	11	12
SN-36k	**3c**+**4a**	36.2	0.094	7.3	7.1
SN-46k	**3c**+**4c**	45.9	0.096	4.5	5.6

[a] Storage moduli of 20wt% PEG networks.

Homogeneity of Networks

Gong et al. reported DN gels utilizing a highly homogeneous crosslinked PEG network as a tight network with a polyelectrolyte called a "molecular stent" in order to expand the PEG network.[26] In the DN gels, the PEG network was swelled sufficiently thanks to the polyelectrolyte to reduce its crack propagation resistance and permit it to serve as a sacrificial network, while the loosely crosslinked poly(acrylamide) network sustained a large deformation. These gels showed clear yield behavior at stresses between 300 and 900 kPa and mechanical hysteresis at stresses above 200 kPa which demonstrates that the heterogeneity within the typical tight networks is not essential for the specific toughening mechanism of DN gels. However, we confirmed the heterogeneity of the tight network as well as the homogeneity of the loose networks in order to clarify the network topology of the IPN gels, because it is possible that the

heterogeneity of the tight network could affect the fracture behaviors of the IPN gels.

First, we calculated the critical overlap concentration C^* of each macromonomer from M_n and R_h, and combined them to roughly estimate mixed C^* of each single network according to the following equations:

$$C^* = (v_h)^{-1} = \left(\frac{4\pi R_h^3}{3}\frac{N_A}{M_n}\right)^{-1} \quad (2.2)$$

$$C^*_{mix} = \left(v_{h,mix}\right)^{-1} = \left(r_1 v_{h,1} + r_2 v_{h,2}\right)^{-1} = (r_1/C_1^* + r_2/C_2^*)^{-1} \quad (2.3)$$

where v_h is the specific hydrodynamic volume; and r_1 and r_2 are weight ratios of macromonomers in an equimolar mixture. If the macromonomers are crosslinked below a concentration of C^*, the resulting network has voids and a fluctuation of local density, because they cannot fill the space entirely. Considering that the C^* of the tight network (SN-1k), Table 2.2, is much higher than the actual polymer concentration (5~15wt%), the tight network must therefore be heterogeneous.

Second, we estimated theoretical storage modulus G_{ph} using a phantom network model according to the following equations, and compared it to measured storage modulus G' of SN and IPN gels.

$$G_{ph} = (\nu - \mu)k_B T = \left(1 - \frac{2}{f}\right)\nu k_B T = \left(1 - \frac{2}{f}\right)\frac{\rho N_A}{M_C}\phi\, k_B T \quad (2.4)$$

$$\phi = \frac{w_p/\rho_p}{w_p/\rho_p + (w_r - w_p)/\rho_w} \quad (2.5)$$

where ν and μ are the number densities of elastically effective chains and crosslinks respectively; f is the functionality of crosslinks; φ is the polymer volume fraction of gels; w_p is the weight of the polymers; w_r is the weight of the relaxed initial gels; ρ_p is the density of polymer (approximated by PEG 1.20 g/cm^3); and ρ_w is the density of water (1.00 g/cm^3). The estimated G_{ph} and the measured G' of the SN gels are given in Table 2.2 and plotted against M_c in Figure 2.2. G' of SN-x-20 were remarkably consistent with the theoretical curve of G_{ph}, while G' of SN-x-10 fell from G_{ph} especially at the low and high ends of M_c. These results agree with the pioneering work of Akagi

on tetra-PEG gels which showed that the elastic moduli of homogeneous crosslinked networks reached the phantom limit G_{ph} at polymer concentrations between C^* and $2C^*$.[27,28] In this work, Akagi introduced reaction efficiency p as a correction factor, where p is typically between 0.7-0.95. It is noteworthy that G' of SN-x-20 fits G_{ph} without a correction factor, suggesting that the reaction efficiency was nearly perfect, and SN-x-20 were homogeneous networks with almost no elastically ineffective defects such as loops or dangling chains. Considering SN-x-10, we assumed that the following two causes decreased G'. First, the low concentration of the chain ends at a high M_c led to an incomplete reaction. It is more likely that a chain end fails to approach a counterpart and becomes a dangling end at a higher M_c. Second, the high C^* of the network at a low M_c results in elastically ineffective crosslinking. A chain end might react with a proximate counterpart and form a loop defect at a low M_c even if the reaction efficiency were perfect. From these results, we confirmed that a slightly higher polymer concentration than C^* is needed to form a homogeneous network. The tight networks must be heterogeneous at a concentration between 5 and 15wt%, while the loose networks must be homogeneous at a concentration of 20wt%.

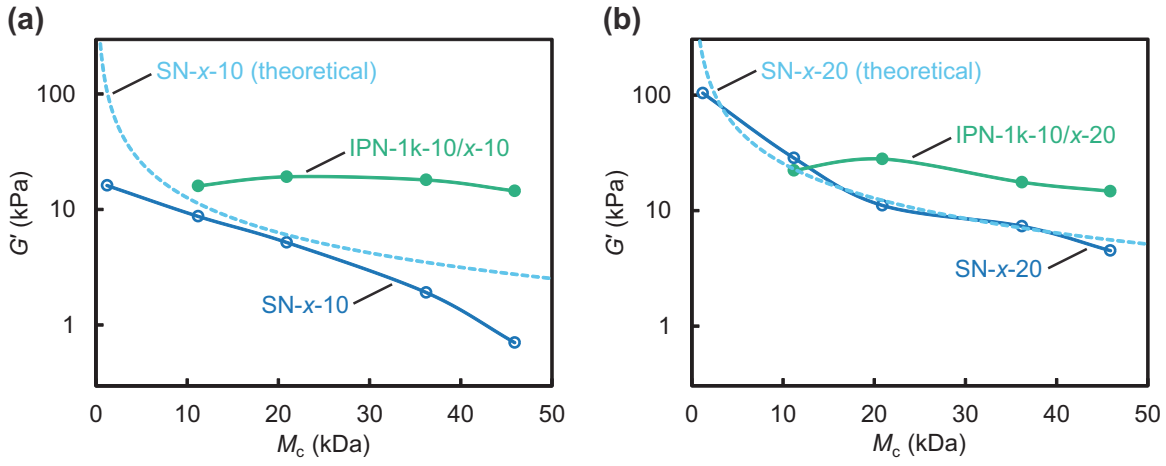

Figure 2.2. Storage moduli of the SN and IPN gels with 10wt% (a) or 20wt% (b) loose networks plotted against M_c at a strain of 1% and a frequency of 1 Hz. The solid lines indicate the experimental values of the SN and IPN gels. The dashed lines indicate the theoretical storage moduli of single networks estimated by the phantom network model.

Last, we focused on the storage modulus of the IPN gels. Compared to SN gels, *G'* of the IPN gels reflected the stiffness of the tight networks and exhibited almost the same value as that of the corresponding tight network (SN-1k-10). In other words, the *G'* of the IPN gels are nearly independent of the loose networks. For example, *G'* of SN-45k-10 was less than 1 kPa, while *G'* of IPN-1k-10/45k-10 reached up to 10 kPa.

Compression Test

To further highlight the improved properties of the interpenetrating network, uniaxial compression testing was conducted to evaluate mechanical properties. The IPN has a high stress at break even when its elastic modulus is high, while the SN has a high stress at break only when its elastic modulus is very low. In a practical point of view, the SN would be not suitable for structural materials. Initially, the IPN gels with the highest M_c (46kDa) were compared with the tight network SN-1k-*y*, the loose network SN-46k-*y*, and the reference SN-3k-*y*. Stress-strain curves of these gels under the compression test are shown in Figure 2.3a-c; and pictures of the test samples before and after compression are shown in Figure 2.4. The IPN gels were as stiff as the tight networks but they could tolerate surprisingly large deformations beyond the fracture points of the tight network. SN-1k-*y* easily crumbled at strains between 50% and 75% (Figure 2.3a). SN-46k-20 was extremely soft and easily compressed with a small amount of force. On the other hand, IPN-1k-*y*/46k-20 resisted compression and showed much higher strength than corresponding SN gels (Figure 2.3c). For example, SN-1k-10 crumbled at a strain of 55±1% and a stress of 0.19 ±0.01 MPa, while IPN-1k-10/46k-20 nearly traced the stress-strain curve of SN-1k-10, but exceeded the fracture point and reached the maximum stress (40 MPa) of the testing machine at a strain of 91%. Furthermore, IPN-1k-*y*/46k-20 required a stress over 5 MPa to be compressed to one-tenth the initial height, while SN-46k-20 was compressed to the same point at a stress of 1.5±0.1 MPa. This strengthening effect is emphasized in stress-strain curves using true stress instead of nominal stress, where true stress is calculated by dividing the force by the actual cross-sectional area based on the presumption that Poisson's ratio is 0.5. The IPN gels have almost the same elastic modulus as the tight network; nevertheless the IPN gels did not fracture below a stress of 40 MPa and significantly, did not fracture even when the strain reached beyond 90%.

The IPN gels also exhibited better performance in comparison to the reference gels. The reference SN-3k-*y* showed similar behavior to the tight network SN-1k-*y* (Figure 2.3b). IPN-1k-10/46k-20 which did not break in the test with maximum stress (40MPa) has exactly the same weight concentration and crosslinking density as SN-3k-30 that fractured at a strain of 61±4% and a stress of 0.83±0.26 MPa. Despite the fact that these two gels differ only in topology – SN or IPN – their strength is markedly different with these results clearly demonstrating the reinforcement effect of the IPN gels. In terms of fracture stress, the mechanical strengths of the IPN gels are comparable to those of conventional DN gels.

Next, we confirmed the dependences of the fracture strength of the IPN gels on M_c of the loose networks (Figure 2.3d-e). The higher M_c made the IPN gels stronger and more flexible. In other words, the IPN gels with higher M_c required higher stress and strain to break. In particular, the higher M_c was needed to keep flexibility, as the concentration of the tight network increased and the resulting IPN gels became stiffer. For example, IPN-1k-5/*x*-20 did not fracture below a stress of 40 MPa, while IPN-1k-15/*x*-20 clearly showed dependences on M_c. The fracture stresses of IPN-1k-15/*x*-20 with M_c 11, 21, 36, and 46 kDa increased as M_c increased. The highest strength (40 MPa) at the lowest strain (87%) was observed in IPN-1k-15/46k-20, where flexibility (M_c) and stiffness (weight fraction of the tight network) balanced best in compression mode.

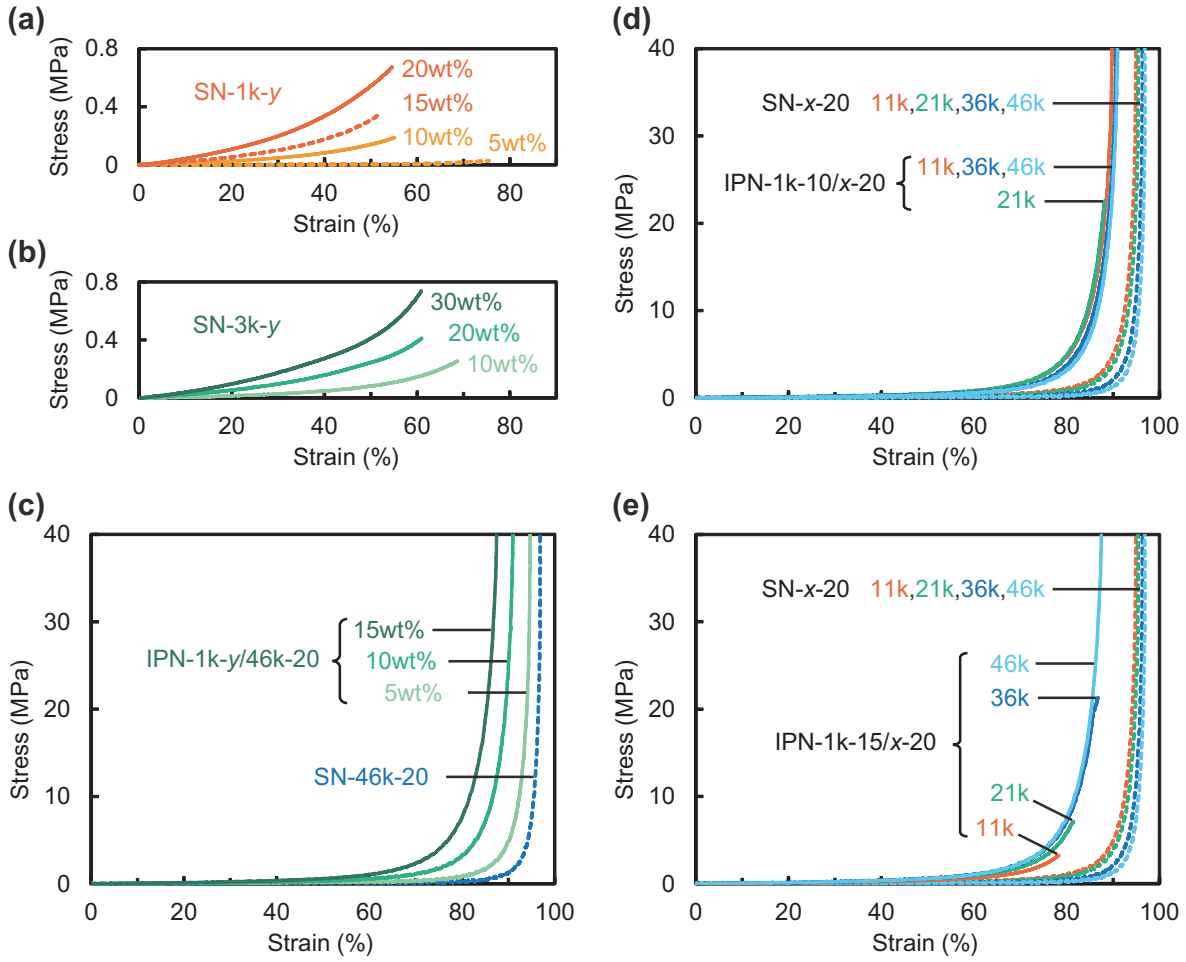

Figure 2.3. Stress-strain curves of SN-1k-*y* (a), SN-3k-*y* (b), IPN-1k-*y*/46k-20 (c), and IPN-1k-y/*x*-20 (d, e) compared with corresponding SN gels under uniaxial compression testing. The solid and dashed lines indicate the IPN and SN gels, respectively.

It is worth noting that the IPN gels showed no hysteresis or yield behavior in load/unload cycles. Compression durability was examined with a cycle test. The IPN gels recovered their shape and kept their elasticity after release from a strain over 80%. Stress-strain curves of the second and later paths could be overlapped with that of the first path. Truong et al. also observed no hysteresis behavior in their gels.[23] These results indicate that the tight networks did not damage significantly until fracture, unlike typical DN gels that damage during deformation close to and beyond the yield point. In the DN gels, chains of the tight networks are at low volume fraction and

highly extended and therefore easier to break at a low strain, so that the macroscopic crack propagation is suppressed by energy dissipation within the damage zone where the sacrificial bonds break.[18] In the IPN gels, chains of the tight networks are relaxed and not stretched in the initial state, so that the tight networks simply act as a reinforcing rigid component rather than a sacrificial component. Furthermore, the tight networks in the IPN gels tolerated large deformations repeatedly thanks to the loose network which suppressed crack propagation in them. The incorporated tight networks are remarkably more durable than the isolated tight networks despite the fact that the tight networks are heterogeneous. Thus, the superior mechanical properties of the IPN gels must be derived from the following two effects: reinforcing by stiff tight networks and suppressing the crack initiation by flexible loose networks.

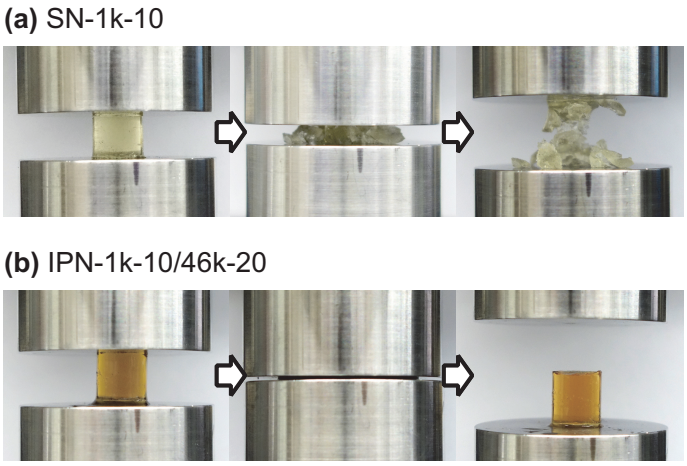

Figure 2.4. Pictures of SN-1k-10 (a) and IPN-1k-10/46k-20 (b) before and after compression. Both samples were compressed and then released (left to right direction).

Tensile Test

Uniaxial tensile testing was then carried out (Figure 2.5). Stress-strain curves of IPN-1k-*y*/46k-20 are shown in Figure 2.5c, which demonstrates that the IPN gels stretched considerably compared to the tight networks and the reference gels (Figure 2.5a,b). For example, elongation at the break of IPN-1k-10/46k-20 was 370±40%, while those of SN-1k-10 and SN-3k-30 were 36±1% and 138±6% respectively. Figure 2.5d displays the dependences of stretchability on M_c of the loose networks. Elongation at

break of both SN-*x*-20 and IPN-1k-10/*x*-20 improved with the increase of M_c. However, the elastic moduli of SN-*x*-20 decreased as M_c increased, while those of IPN-1k-10/*x*-20 were almost independent of the loose networks and dominated by the tight networks. These results are consistent with the trend of the elastic moduli under compression and the shear moduli *G'*. No yield behavior was observed under the tensile test with the highest fracture stress being close to the typical yield stress of DN gels. The advantages of the IPN gels in tensile mode are less dramatic than in compression mode, though there are positive effects from the presence of the loose network in these synthetically simple systems.

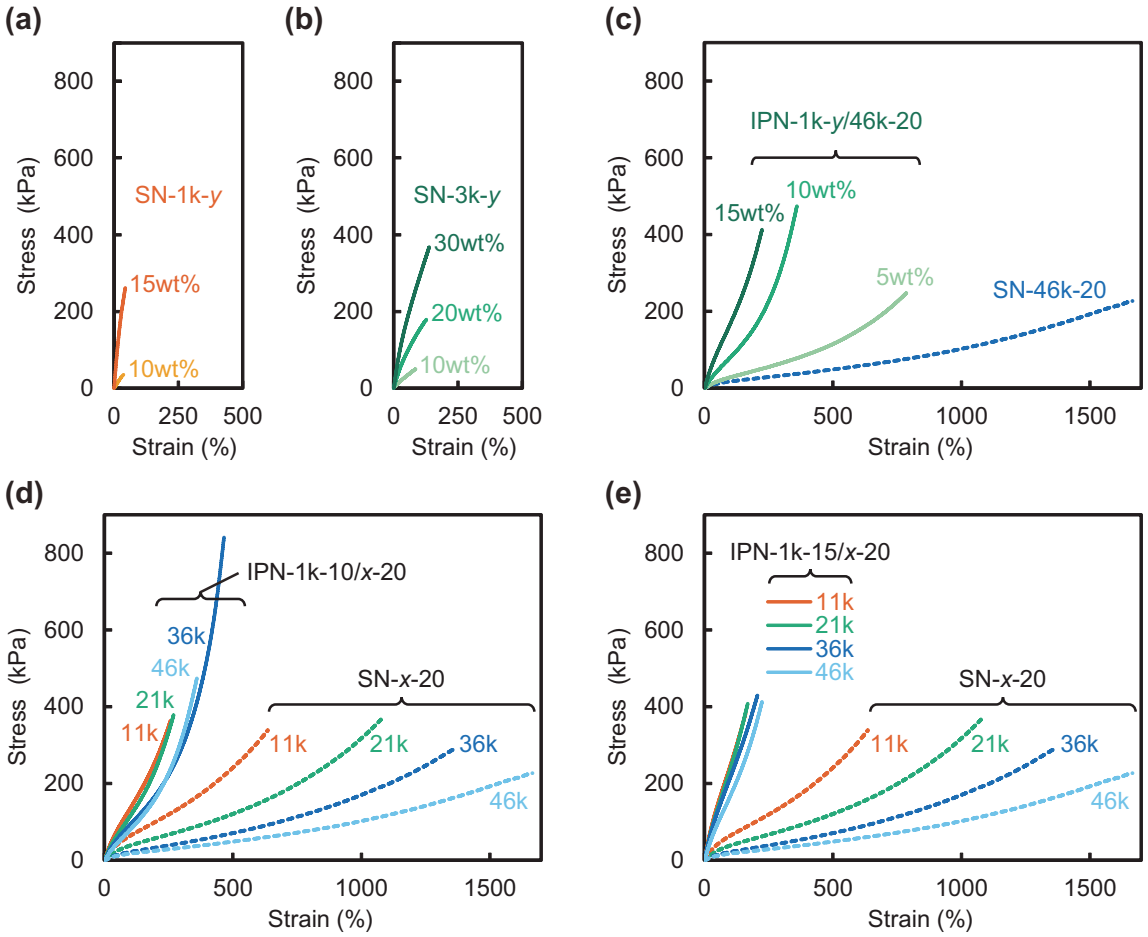

Figure 2.5. Stress-strain curves of SN-1k-y (a), SN-3k-y (b), IPN-1k-y/46k-20 (c), and IPN-1k-y/x-20 (d, e) compared with the corresponding SN gels under uniaxial tensile testing. The solid and dashed lines indicate the IPN and SN gels, respectively.

Swelling Test

Finally, equilibrium swelling tests were performed and compared swollen gels with the corresponding initial gels. The SN and IPN gels swelled up to eight times their initial weight in deionized water. The swelling degree of the IPN gels strongly depends on the weight concentration of the tight networks and M_c of the loose networks. Figure 2.6 show stress-strain curves of the swollen gels under the uniaxial compression test, where the sample codes reflect dilution during the swelling process. For example, IPN-1k-10/46k-20 swelled 5.7 times its initial weight, and its total weight concentration decreased from 30wt% to 5.3wt%. Assuming the weight ratio does not change due to both networks being covalently crosslinked and entangled, the composition of the swollen gel can be expressed by IPN-1k-1.8/46k-3.5. Interestingly, all of the IPN gels kept their elasticity in spite of dilution, and the stress-strain curves of the swollen gels were nearly identical to those for the initial gels. This may be due to the chain stretching effect cancelling the dilution effect. In addition, the limited chain extensibility made the swollen gels much more brittle than the initial gels with even the most flexible swollen IPN gel (IPN-1k-0.6/46k-2.6) fracturing at a strain of 89±1% and a stress of 4.1±0.8 MPa, while the initial gel (IPN-1k-5/46k-20) resisted a stress of 40 MPa. Improving the mechanical toughness of the swollen IPN gels is a matter for further investigation.

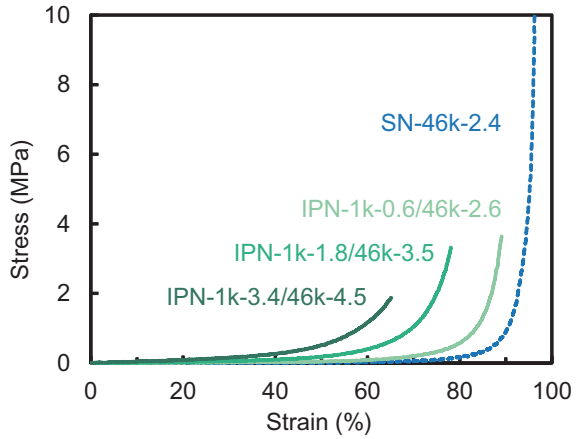

Figure 2.6. Stress-strain curves of the swollen IPN-1k-y/46k-20 and SN-46k-20 under uniaxial compression testing.

2.4 Conclusions

High performance inter-penetrating (IPN) gels were successfully fabricated via orthogonal double click reactions through a facile one-pot approach. The synthetic modularity of this strategy allows tuning the weight fraction of the tight and loose networks and the crosslinking density with various M_c ranging from 1 to 46 kDa. By combining a tight network and a loose network, nonlinear enhancement in mechanical properties was observed with the IPN gels exhibiting outstanding strength in compression. Fracture stresses reached over 40 MPa with their strength being comparable to that of conventional DN gels. Moreover, the IPN gels have high durability; they can be reversibly compressed or stretched without damage. Compared to the starting individual gels, the IPN gels were notably reinforced despite being composed of the same amount of the polymer with the same crosslinking density. It is proposed that the superior mechanical properties of the IPN gels are derived through reinforcement by the stiff, tight network and suppression of crack initiation by the flexible, loose networks. The synthetic ease and modularity of this approach paves the way for utilizing tough hydrogels for a variety of practical applications.

2.5 References

1. Qiu, Y.; Park, K. *Adv. Drug Deliv. Rev.* **2001**, *53*, 321-339.
2. Hoffman, A. S. *Adv. Drug Deliv. Rev.* **2012**, *64*, 18-23.
3. Boateng, J. S.; Matthews, K. H.; Stevens, H. N. E.; Eccleston, G. M. *J. Pharm. Sci.* **2008**, *97*, 2892-2923.
4. Lee, K. Y.; Mooney, D. J. *Chem. Rev.* **2001**, *101*, 1869-1879.
5. Ifkovits, J. L.; Burdick, J. A. *Tissue Eng.* **2007**, *13*, 2369-2385.
6. Tibbitt, M. W.; Anseth, K. S. *Biotechnol. Bioeng.* **2009**, *103*, 655-663.
7. Rennerfeldt, D. A.; Renth, A. N.; Talata, Z.; Gehrke, S. H.; Detamore, M. S. *Biomaterials* **2013**, *34*, 8241-8257.
8. Johnson, J. A.; Turro, N. J.; Koberstein, J. T.; Mark, J. E. *Prog. Polym. Sci.* **2010**, *35*, 332-337.
9. Zhao, X. *Soft Matter* **2014**, *10*, 672-687.

10. Gong, J. P.; Katsuyama, Y.; Kurokawa, T.; Osada, Y. *Adv. Mater.* **2003**, *15*, 1155-1158.
11. Haque, M. A.; Kurokawa, T.; Gong, J. P. *Polymer* **2012**, *53*, 1805-1822.
12. Chen, Q.; Chen, H.; Zhu, L.; Zheng, J. *J. Mater. Chem. B* **2015**, *3*, 3654-3676.
13. Haraguchi, K. *Curr. Opin. Solid State Mater. Sci.* **2007**, *11*, 47-54.
14. Wang, Q.; Mynar, J. L.; Yoshida, M.; Lee, E.; Lee, M.; Okuro, K.; Kinbara, K.; Aida, T. *Nature* **2010**, *463*, 339-343.
15. Ito, K. *Polym. J.* **2012**, *44*, 38-41.
16. Okumura, Y.; Ito, K. *Adv. Mater.* **2001**, *13*, 485-487.
17. Hunt, J. N.; Feldman, K. E.; Lynd, N. A.; Deek, J.; Campos, L. M.; Spruell, J. M.; Hernandez, B. M.; Kramer, E. J.; Hawker, C. J. *Adv. Mater.* **2011**, *23*, 2327-2331.
18. Gong, J. P. *Soft Matter* **2010**, *6*, 2583-2590.
19. Myung, D.; Waters, D.; Wiseman, M.; Duhamel, P. E.; Noolandi, J.; Ta, C. N.; Frank, C. W. *Polym. Adv. Technol.* **2008**, *19*, 647-657.
20. Dragan, E. S. *Chem. Eng. J.* **2014**, *243*, 572-590.
21. Hu, X.; Lu, L.; Xu, C.; Li, X. *Int. J. Biol. Macromol.* **2015**, *72*, 403-409.
22. Li, Y.; Wang, C.; Zhang, W.; Yin, Y.; Rao, Q. *J. Appl. Polym. Sci.* **2015**, *132*, 41342.
23. Truong, V. X.; Ablett, M. P.; Richardson, S. M. Hoyland, J. A.; Dove, A. P. *J. Am. Chem. Soc.* **2015**, *137*, 1618-1622.
24. Brown, H. R. *Macromolecules* **2007**, *40*, 3815-3818.
25. Yoshida, Y.; Sakakura, Y.; Aso, N.; Okada, S.; Tanabe, Y. *Tetrahedron* **1999**, *55*, 2183.
26. Nakajima, T.; Fukuda, Y.; Kurokawa, T.; Sakai, U.; Gong, J. P. *ACS Macro Lett.* **2013**, *2*, 518-521.
27. Akagi, Y.; Katashima, T.; Katsumoto, Y.; Fujii, K.; Matsunaga, T.; Chung, U.; Shibayama, M.; Sakai, T. *Macromolecules* **2011**, *44*, 5817-5821.
28. Akagi, Y.; Gong, J. P.; Chung, U.-i.; Sakai, T. *Macromolecules* **2013**, *46*, 1035-1040.

Chapter 3

One-Pot "Click" Fabrication of Slide-Ring Gels

3.1 Introduction

Hydrogels have attracted much interest in recent years with applications in the biomedical field showing significant promise,[1,2] e.g., in drug delivery,[3] tissue engineering,[4] or cell culture.[5] The introduction of supramolecular strategies for the formation of hydrogels leads to a variety of novel properties, e.g., self-healing,[6,7] or stimuli-responsive gelation,[8,9] and opens up new opportunities regarding architectural diversity and applications. A novel type of hydrogel with remarkable mechanical properties is the slide-ring (SR) gel, which contains topologically interlocked non-covalent crosslinks that can slide along a threaded polymer backbone. Theoretically predicted by de Gennes in 1999, SR gels can be considered a topologically crosslinked polymer network with no covalent crosslinking between chains.[10] Okumura et al. succeeded in synthesizing SR gels in 2001,[11] taking advantage of the supramolecular chemistry of cyclodextrin (CD) and rotaxane formation[12,13] to realize the sliding crosslink. Subsequent studies have shown the promise of CDs as a building block in supramolecular materials systems, especially for the formation of non-covalent hydrogels,[14,15] and other macromolecular architectures.[16,17] Harada et al. first reported *pseudo*-polyrotaxane[18,19] and polyrotaxane[20] using inclusion complexation between CDs and polyethers in a threading fashion, which is a prerequisite for the SR gel formation, described below. Following this work, Ito and coworkers have prepared SR gels and identified a range of fundamental and industrially important properties, for example, extreme softness, low modulus, increased stretchability, and high swellability.[21,22]

Despite their promising properties, the synthesis of SR gels is demanding, requiring three steps: formation of the *pseudo*-polyrotaxane, end-capping of the axial chain, and final crosslinking between threaded CDs. The typical procedure is

performed as follows:[11] poly(ethylene glycol) (PEG) diamine and an excess of α-CD are dissolved in hot water and then cooled to precipitate the *pseudo*-polyrotaxane. The *pseudo*-polyrotaxane is converted into the corresponding polyrotaxane in dimethylformamide with an excess of 2,4-dinitrofluorobenzene as a bulky end-capping moiety. After purification, the polyrotaxane is dissolved in sodium hydroxide solution and crosslinked via cyanuric chloride. While multi-step, this procedure is necessary to avoid synthetic limitations, e.g., the *pseudo*-polyrotaxane is insoluble in neutral water at room temperature, and good solvents cause dissociation of the complex. Similarly, the polyrotaxane must be fully dissolved during the crosslinking step to obtain homogeneous networks.

Recently, a number of approaches to solve these synthetic challenges have been described. Based on the work of Liu et al.,[23] Kato reported the use of polyrotaxanes having CDs as stoppers for the preparation of SR gels.[24] Click chemistry and atom transfer radical polymerization (ATRP)-based strategies have also been applied to SR gel formation leading to combination of covalent/slide-ring networks.[25-27] While these approaches utilizing click chemistry or ATRP are synthetically simplified from the original synthesis, the resulting gels contain both covalent and sliding crosslinks with the covalent network dominating physical and mechanical properties.

In this study, we aimed at a modular and robust one-pot "click" fabrication of SR gels with little or no unwanted covalent crosslinking (Figure 3.1). Initial complexation of monothiolated β-cyclodextrin (β-CDSH) with poly(allyl glycidyl ether)-*block*-poly(ethylene glycol)-*block*-poly(allyl glycidyl ether) (PAGE-PEG-PAGE) could be carried out in water by simple sonication. Simultaneous network formation and end-capping were then accomplished by thiol-ene chemistry. A major advantage of this strategy compared to the classical α-CD-based system is increased solubility in water of *pseudo*-polyrotaxanes formed from β-CD when compared to an equivalent amount of α-CD due to a lack of crystallinity. For example, an inclusion complex of α-CD with PEG precipitates rapidly, in less than an hour,[18] while the complex of β-CD with PEG precipitates extremely slowly thanks to its lower crystallinity, over a few days.[28] Thus, the *pseudo*-polyrotaxanes impart water solubility for extended periods and enable handling as well as curing before precipitation occurs. In addition, the present one-pot

strategy requires only sonication before curing; therefore, tedious isolation and purification processes can be omitted. The resulting one-pot process leads to strong and stretchable SR gels that do not contain covalent crosslinks, greatly expanding future applications of SR gels.

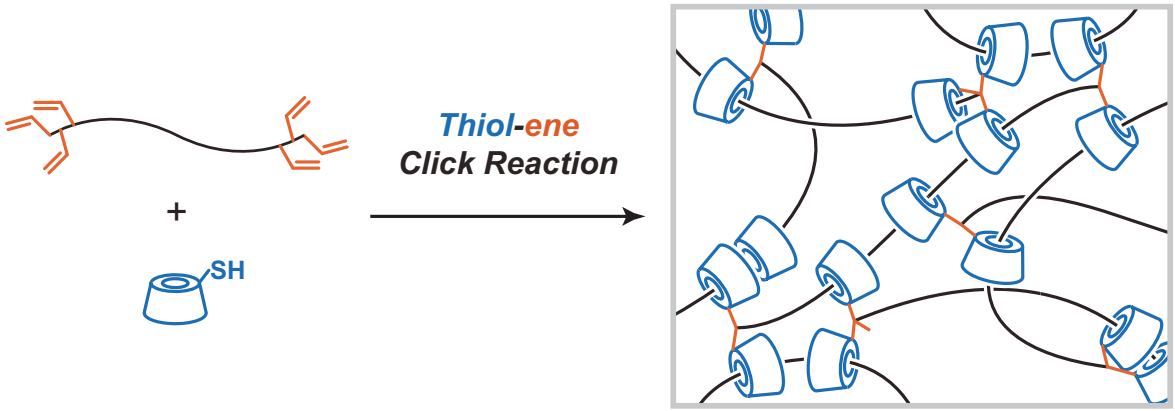

Figure 3.1. Schematic illustration of the slide-ring network formation. Possible defects in the network are also depicted; intramolecular crosslinking, and unreacted components.

3.2 Experimental Section

Materials. All chemicals were used as received from Sigma-Aldrich unless otherwise specified. Tetrahydrofuran (THF) was collected from a dry solvent system, and used immediately thereafter. Poly(ethylene glycol) (PEG) was purchased from Sigma-Aldrich, and dried *in vacuo* prior to use. Allyl glycidyl ether (AGE) was purchased from TCI America, degassed through freeze-pump-thaw cycles, and distilled from butyl magnesium chloride into a flame-dried buret for storage. Potassium naphthalenide was prepared from potassium metal and naphthalene in dry THF, and stirred with a glass-coated stir-bar for 24 hours at room temperature before use.

Characterization. ^{1}H NMR spectra were recorded on a Varian VNMRS 600 spectrometer (600 MHz). Chemical shifts are reported relative to residual solvent peaks in ^{1}H NMR (δ 7.26 for $CDCl_3$, 2.50 for DMSO-d_6, and 4.79 for D_2O). Nuclear Overhauser enhancement spectroscopy (NOESY) experiments were performed using

a mixing time of 300 ms, 256 t_1 increments, and 16 scans per t_1 increment on the same spectrometer as ^{1}H NMR. Fourier transform infrared (FTIR) spectra were acquired on a Nicolet iS10 FTIR spectrometer with an ATR accessory at a resolution of 4 cm^{-1}. Electrospray ionization time-of-flight (ESI-TOF) data were obtained on a Micromass QTOF2 quadrupole/time-of-flight tandem mass spectrometer. Gel permeation chromatography (GPC) was performed on a Waters 2695 separation module equipped with a Waters 2410 differential refractometer and a Waters 2998 photodiode array detector. Chloroform with 0.25% of triethylamine was used as an eluent at a flow rate of 1 mL/min. Molecular weight and polydispersity index (PDI) was calculated relative to linear polystyrene standards. Dynamic light scattering (DLS) analysis was performed on a Wyatt Technology DynaPro NanoStar instrument. Reported values are averages of 100 acquisitions.

Rheological experiments were performed on a TA Instruments ARES-LS1 rheometer with parallel-plate geometry (25 mm diameter except for stoichiometric study). Frequency sweeps were performed at a strain of 0.1%, and strain sweeps were performed at a frequency of 1 Hz. Tensile tests were conducted on a tensile testing machine equipped with an Eaton Corporation 3108-10 load cell (capacity 44.48 N) using a cross-head speed of 200% per min. Samples were cut into 4 mm × 16 mm and clamped with pieces of sand paper to avoid grip slippage. All experiments were performed at room temperature.

Synthesis of poly(allyl glycidyl ether)-*block*-poly(ethylene glycol)-*block*-poly(allyl glycidyl ether)] 1a-d. PAGE-PEG-PAGE **1a-d** were polymerized by anionic ring-opening polymerization of epoxides according to a previously reported method.[29] The typical procedure is as follows: dry PEG diol was dissolved in THF, and titrated with potassium naphthalenide (0.3 M in THF) at room temperature under a dry argon atmosphere in a custom reactor. AGE was added to the PEG dialkoxide macroinitiator, and allowed to polymerize for 3 days at room temperature. The polymerization was terminated with acidic methanol. The reaction mixture was filtered through a short silica gel column, and poured into hexane. The resulting precipitate was filtered, washed with hexane, and dried *in vacuo*. The number-average molecular weights (M_n) and compositions were measured by ^{1}H NMR and PDI was determined by GPC.

Synthesis of monothiolated β-cyclodextrin (β-CDSH) 2. 6A-*O*-(*p*-toluenesulfonyl)-β-cyclodextrin was prepared from β-CD according to the literature.[30] Yield 40%. 6A-Deoxy-6A-mercapto-β-cyclodextrin (β-CDSH) **2** was synthesized from the monotosylated β-CD according to the literature.[31,32] Yield 43%. ^{1}H NMR (600 MHz, DMSO-d_6) δ 5.80–5.56 (m, 14H, C2-OH and C3-OH), 4.90–4.79 (m, 7H, C1-H), 4.56–4.38 (m, 6H, C6-OH), 3.79–3.51 (m, 26H, C3-H, C5-H, and C6-H), 3.43–3.26 (m, overlaps with HDO, C2-H and C4-H), 3.01–2.94 (m, 1H, C6′-H), 2.79–2.72 (m, 1H, C6′-H), 2.05 (t, J = 8.2 Hz, 1H, C6′-SH). ESI-MS (m/z) Calcd for $C_{42}H_{70}O_{34}SNa$: 1173.34 $[M+Na]^+$, Found: 1173.38 $[M+Na]^+$.

Preparation of SR gels 3a-d. β-CDSH **2** was dissolved in 15wt% aqueous solutions of polymers **1a-d**. After sonication in a Branson 3510 sonicator for 60 min, a 0.5wt% aqueous solution of 2-hydroxy-4′-(2-hydroxyethoxy)-2-methylpropiophenone (Irgacure 2959) was added to the reaction mixture. 1.2 and 0.1 molar equivalent amounts to the allyl groups of **1a-d** were used for β-CDSH **2** and Irgacure 2959 respectively. After dilution to 15wt% by addition of deionized water, the obtained precursor solutions were degassed with a stream of argon gas, and transferred into molds, which were made of a Teflon or silicone rubber frame (0.5 or 2.0 mm thickness) clamped between a pair of glass plates. The molds were irradiated by high pressure mercury lamps (15 W, λ_{max}=365 nm) for 60 min to obtain SR gels **3a-d**.

Preparation of covalent gels 4a-d. Covalent gels **4a-d** were fabricated from polymers **1a-d** and dithiothreitol (DTT). DTT (0.5 eq.) and Irgacure 2959 (0.1 eq.) were added to aqueous solutions of **1a-d**. After dilution to 15wt%, the obtained precursor solutions were degassed with argon gas, transferred into the molds, and cured by UV irradiation.

Stoichiometric study. Storage moduli of SR gel **3a** were measured at various molar ratios of β-CDSH **2** to polymer **1a**. Precursor solutions were cured in sealed vials. Concentrations of the solutions were fixed at 10wt%. 8 mm diameter parallel-plate geometry was used for rheological experiments.

Swelling test. SR gels **3a-d** and covalent gels **4a-d** were immersed in deionized water at room temperature for a week until an equilibrium swollen state was reached. The swollen gels were dried *in vacuo*. The swelling ratio Q was calculated from $Q = w_s/w_d$,

where w_s and w_d are the weights of the equilibrium swollen gels and the dried gels respectively. The gel fraction was calculated from $w_d/(w_p + w_c)$, where w_p and w_c are the weights of the polymers (**1a-d**) and the crosslinkers (**2** or DTT) in the starting gels respectively.

Acid degradation Test. After the swelling test, the dried gels **3a-d** and **4a-d** were soaked in 1 N hydrochloric acid aqueous solution (HCl aq.) at 70°C for three days. Residual insoluble portion in the acid was filtered, and dried *in vacuo*. The gel retention was calculated from w_{deg}/w_d, where w_{deg} is the weight of the dried insoluble portion.

Alkali treatment. SR gels **3a-d** were soaked in 1 N sodium hydroxide aqueous solution (NaOH aq.) for 20 min. All the gels turned slightly yellow and transparent. The gels were weighed before and after this treatment to calculate water uptake.

3.3 Results and Discussion

Synthesis of polymers 1a-d and β-CDSH 2

Tri-block copolymers PAGE-PEG-PAGE **1a-d** were synthesized by standard anionic ring-opening polymerization. Molecular weights of the PEG mid-block were varied among 20 kDa (**1a**), 35 kDa (**1b** and **1c**), and 100 kDa (**1d**). The numbers of allyl groups per chain (N_{allyl}) were also varied with M_n, because they are critical in network formation and crosslinking density. **1a** and **1b** have similar values for N_{allyl}, differing in the M_n of the mid-blocks; while **1a**, **1c**, and **1d** have almost the same ratio of N_{allyl} to overall degree of polymerization for the backbone. The molecular weights and compositions of **1a-d** are summarized in Table 3.1. β-CDSH **2** was synthesized according to the literature.[31,32]

DLS analysis

First, *pseudo*-polyrotaxanes **1a-d/2** were prepared from PEO-based triblock copolymers **1a-d** and β-CDSH **2** with analysis DLS showing that the PAGE end-blocks did not retard β-CDSH threading. Figure 3.2 shows intensity-based size distributions of **1a**, **2**, and **1a/2** in water (2 mg/mL). Hydrodynamic radii of **1a** were calculated to be

4.6, 62, and 430 nm, and those of **2** were 0.8, 48, and 280 nm. The peaks correspond to single molecules and aggregates with the aggregation behavior of β-CD being previously described in the literature.[33] However, it should be kept in mind that intensity-based distributions exaggerate higher radius components as the intensity of scattered light is proportional to the radius to the sixth power. Before sonication the peaks of **1a/2** nearly overlapped with those of **1a** and **2**, and after sonication the peak corresponding to free β-CDSH **2** disappeared completely, which indicates that the CD was consumed by inclusion complexation. Hydrodynamic radii of **1a/2** after sonication were 4.6, 69, and 650 nm, which must be derived from the inclusion complex and its aggregates. Furthermore, we observed that the peak for **2**, was recovered after the addition of 1 N NaOH aq. to **1a/2**, which demonstrates that reversible dissociation of the complex occurred due to electrostatic repulsion of CD in the presence of the strong base.[34] Similar results were obtained for **1b/2** and **1d/2**. These results indicate efficient threading of β-CD on the triblock copolymers occurs during sonication.

Table 3.1. Molecular weights and compositions of polymers **1a-d**.

Polymer	M_n (kDa)	Degree of Polymerization	N_{allyl}	PDI
1a	0.4–20–0.4	3.7–454–3.7	7.4	1.12
1b	0.4–35–0.4	3.2–795–3.2	6.4	1.13
1c	1.1–35–1.1	9.4–795–9.4	18.8	1.08
1d	2.5–100–2.5	21.7–2270–21.7	44.2	1.41 [1)]

[1)] The PDI of **1d** was higher than the others because of a high PDI of the starting PEG (1.47).

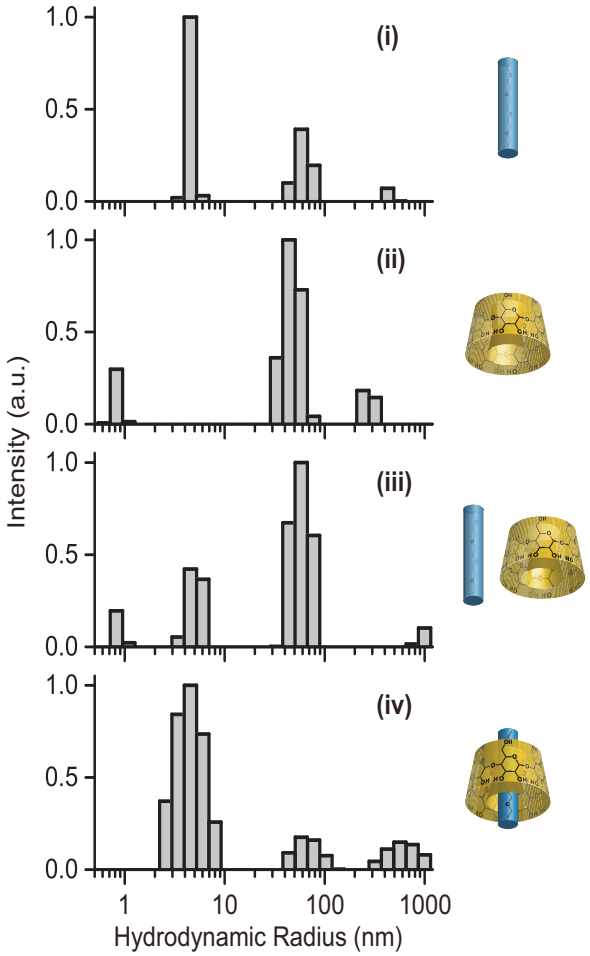

Figure 3.2. Intensity-based size distributions of **1a** (i), **2** (ii), and **1a/2** before (iii) and after (iv) sonication in water obtained via DLS.

NOESY experiments

Following DLS analysis, NOESY experiments were carried out to obtain direct evidence for complex formation. A representative NOESY spectrum of **1a/2** in D_2O is shown in Figure 3.3 with cross peaks corresponding to correlation between the CH_2 protons of PEG and the H-5 protons of β-CD clearly present. Significantly, there was no peak related to correlation between the allyl protons of the PAGE end-block and protons of CD. These results indicate that the inclusion complex of β-CDSH **2** with the polymer **1a** was formed and that the CDs were threaded primarily on the PEG mid-block. As a PEG chain is not bulky enough to fill the inner cavity of β-CD entirely, the H-5 protons on the narrow edge are more proximate to a threaded PEG chain than the

H-3 protons on the wide edge leading to increased correlation between the backbone PEG and the H-5 protons of the β-CD. These results also clearly show that β-CDs are able to thread over the PAGE end-blocks with little steric hindrance in analogy with the observed threading of *α*-CDs and location on the mid-block of poly(propylene glycol)-*block*-poly(ethylene glycol)-*block*-poly(propylene glycol).[35]

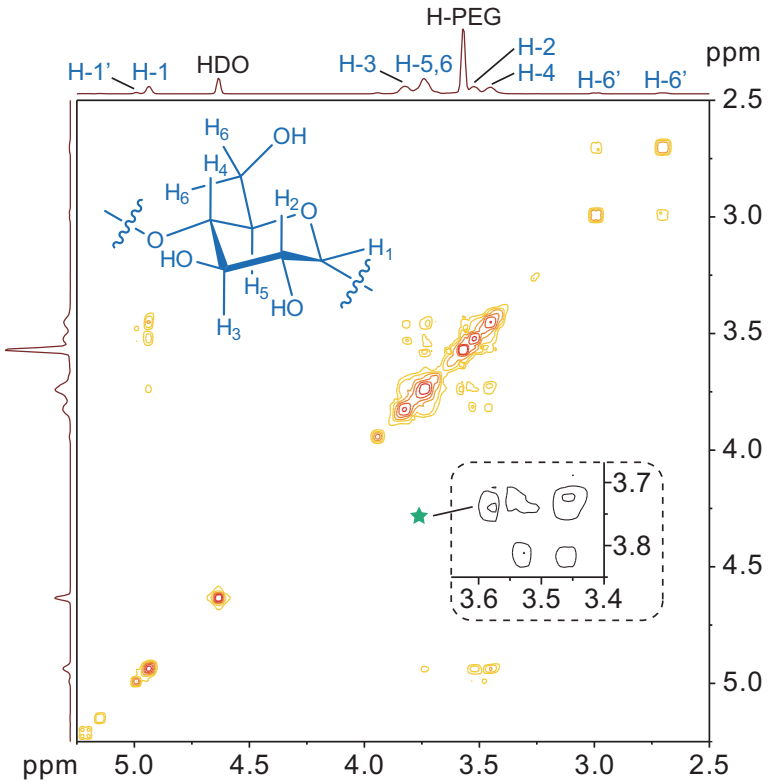

Figure 3.3. NOESY spectrum of *pseudo*-polyrotaxane **1a/2** in D_2O. The NOE cross peak was observed between the CH_2 proton of PEG at 3.57 ppm and the H-5 proton of β-CD at 3.74 ppm. The inset chemical structure shows a glucose unit of β-CD. H-3 and H-5 protons face inside the cavity of β-CD. H-1′ and H-6′ protons are located in the thiolated glucose unit of **2**.

Preparation of SR gels

SR gels **3a-d** were prepared from *pseudo*-polyrotaxane **1a-d/2** by a thiol-ene click reaction in water utilizing the water soluble photoinitiator Irgacure 2959 (Scheme 3.1). For the preparation of **3a-d**, a slight excess (1.2 eq.) of **2** was used in order to suppress

possible side-reactions, e.g., radical homo-coupling of allyl groups. In addition, the concentration of the initiator was carefully chosen to again avoid side-reactions leading to the formation of covalent crosslinks. In demonstrating the building block nature of this procedure, control reactions were performed by replacing β-CDSH **2** with a mixture of β-CD and 2-mercaptoethanol. No gelation was observed in these samples, indicating that serious side-reactions, such as crosslinking between allyl groups, do not occur under these mild conditions. The presence of CD in the SR gels was confirmed by FTIR using dried gels.

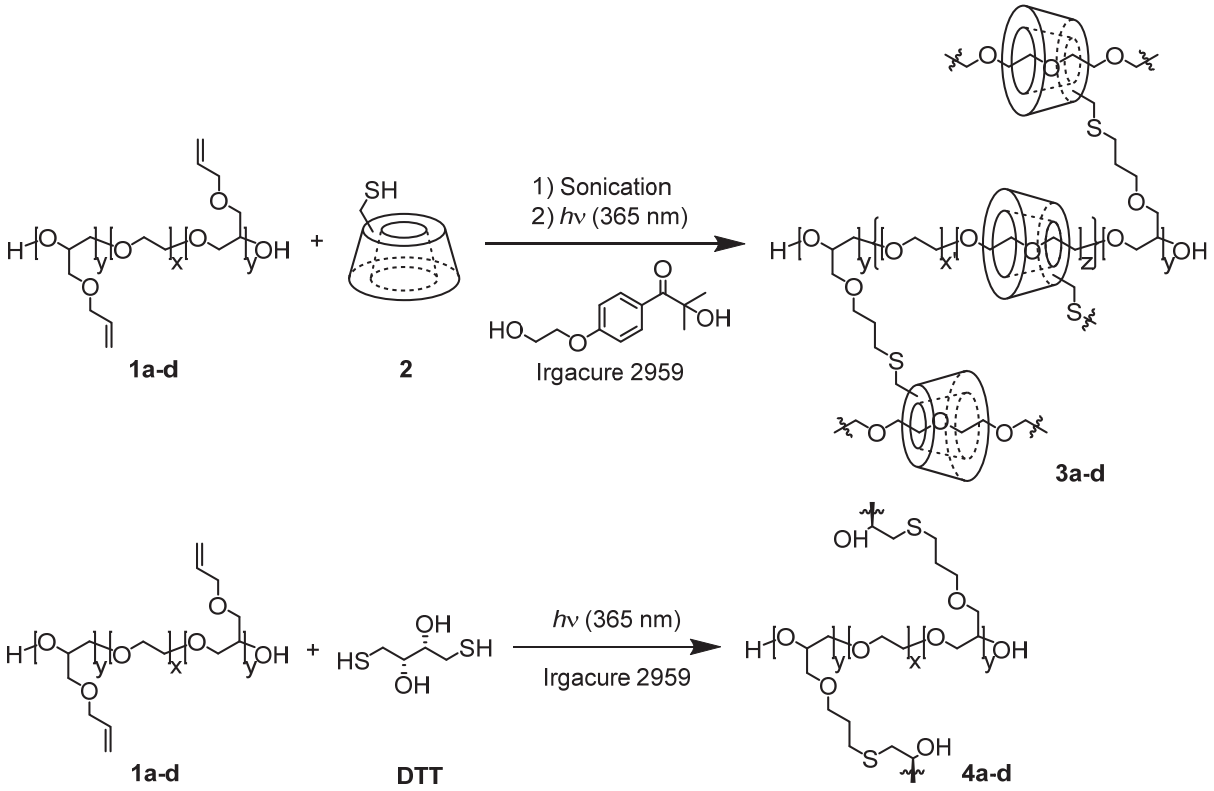

Scheme 3.1. Synthesis of SR gels **3a-d** and covalent gels **4a-d**.

Preparation of covalent gels

Covalent gels **4a-d** were prepared in order to compare the properties of topologically crosslinked gels with those for covalently crosslinked gels prepared using similar building blocks. Dithiothreitol (DTT) was utilized as a water soluble dithiol compound for crosslinking between allyl groups. Unlike topological

crosslinking, the present covalent crosslinking with DTT undergoing reaction with two adjacent allyl groups on the same chain requires two allyl groups for one crosslink. Furthermore, intramolecular crosslinking, which does not contribute to network formation, cannot be ignored. Thus, the crosslinking densities of the covalent gels are potentially less than half of those of the corresponding SR gels. Among the covalent gels, **4b** was exceptionally soft with the gel fraction of **4b** being ~60%, which is less than for other covalent gels. **4b** was incompletely crosslinked due to the low ratio of allyl groups, and judged to be inadequate for evaluation; therefore, the following discussion focuses on **4a**, **4c**, and **4d**.

Stoichiometric study

In order to study the effect of stoichiometry on network formation, storage moduli *G′* and loss moduli *G″* of SR gel **3a** were plotted against the molar fraction of **2** in a Job plot (Figure 3.4).[36] The peak value of *G′* was recorded near a molar fraction of 0.5 and demonstrates that β-CDSH **2** efficiently reacts with an equimolar amount of allyl groups contained along the backbone of polymer **1a**.

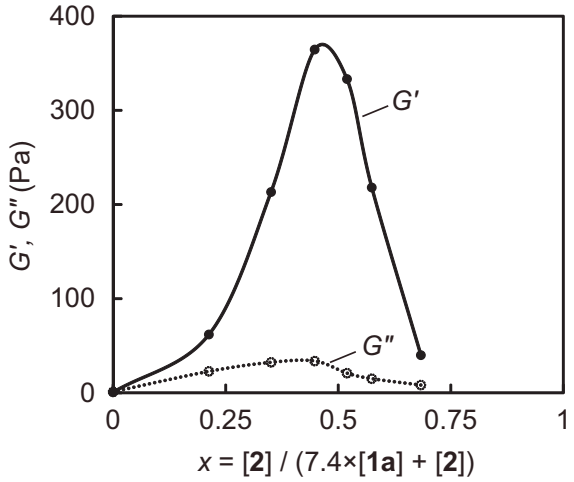

Figure 3.4. Job plot of *G′* and *G″* of **3a** against molar fraction of β-CDSH **2**. Total concentrations of **1a** and **2** were constant at 10wt%.

Rheology

The ability to prepare well-defined hydrogels with accurate structural control over

their building blocks prompted a thorough investigation of their rheology. Figure 3.5 shows frequency sweeps of G' and G'' for the range of gels studied. Significantly, the SR gels were comparable to the corresponding covalent gels in modulus with G' ranging from 3.9 to 8.9 kPa for **3a-d** and 6.2 to 11.2 kPa for **4a-4d.** In addition, G' was nearly two orders of magnitude higher than the G'' except for the high frequency region (above 10 Hz).

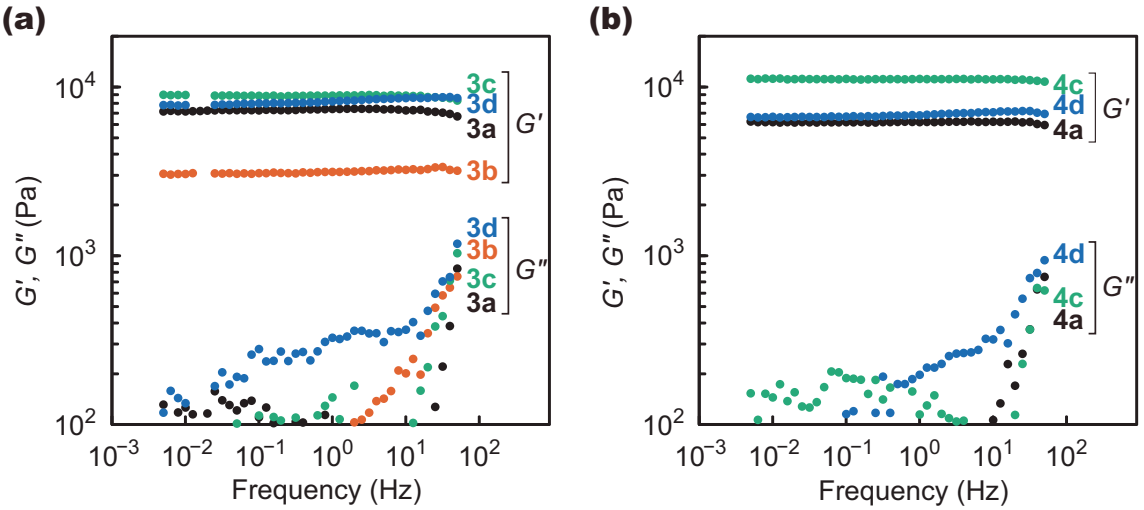

Figure 3.5. Frequency sweeps of G' and G'' of SR gels (a), and the corresponding covalent gels (b).

In order to understand these results, we considered the difference in network topology between the SR gels and the covalent gels and estimated the following key factors: the number of elastically effective sliding crosslinks per chain (N_{sc}), the functionality of the crosslink (f), and the molecular weight of polymer chains between crosslinks (M_c). The phantom network model of Gaussian chains is one of the most commonly used models for hydrogels. Equation 3.1 expresses the model for a perfect network and indicates that elastic modulus is inversely proportional to M_c. The polymer volume fraction of the relaxed initial gels (ϕ_r) was calculated according to Equations 3.2. The f of the SR gels is expressed by Equation 3.3 using $N_{sc}/2$ which is the number of sliding crosslinks at the chain terminal. In addition, the following plausible presumption was applied to this estimation: $M_c = M_{n,PEG}/(N_{sc}+1)$ for the SR gels

and $M_c = M_{n,PEG}$ for the covalent gels, where $M_{n,PEG}$ is the molecular weight of the PEG mid-block. It is natural that the SR crosslinks divide the mid-block into small segments as the cyclodextrin rings move along this block and the covalent crosslinks do not. The results of G', N_{sc}, f, and M_c are summarized in Table 3.2.

$$G = (\nu - \mu)k_BT = \left(1 - \frac{2}{f}\right)\nu k_BT = \left(1 - \frac{2}{f}\right)\frac{\rho_p N_A}{M_c}\phi_r k_BT \qquad (3.1)$$

$$\phi_r = \frac{w_p/\rho_p}{w_p/\rho_p + w_c/\rho_c + (w_r - w_p - w_c)/\rho_w} \qquad (3.2)$$

$$f = 2(N_{sc}/2) + 1 \quad \text{(for the SR gels)} \qquad (3.3)$$

Here ν and μ are the number densities of elastically effective chains and crosslinks respectively, w_r is the weight of the relaxed initial gels, ρ_p is the density of **1a-d** (approximated by PEG 1.20 g/cm^3), ρ_c is the density of **2** (approximated by β-CD 1.44 g/cm^3) or DTT (1.30 g/cm^3), and ρ_w is the density of water (1.00 g/cm^3).

The calculated N_{sc} demonstrates how many of the SR crosslinks were effectively coupled to the linear chains. The calculated N_{sc} were smaller than N_{allyl}, which indicates the presence of defects and aggregation of the SR crosslinks. The possible defects are as follows: unreacted allyl groups and CDs, unthreaded CDs, loop structures (intramolecular crosslinking), and ladder structures (multiple crosslinking between two chains). The loop-type crosslinking can occur easily due to proximity between threaded CDs and allyl groups on a chain, and the ladder-type crosslinking also may occur because threaded CDs on a chain tend to aggregate by hydrogen bonding and react with allyl groups on another chain serially. Moreover, the aggregation of the crosslinks can also cause decrease of apparent N_{sc}. As a result, N_{sc} decreased to ~N_{allyl}/4 from that for a perfect system ($N_{sc} = N_{allyl}$).

M_c and f of the covalent gels were also calculated according to Equation 3.1 and 3.2. f of **4a** was 3.0 on the assumption that M_c equals $M_{n,PEG}$, while f of **4c** and **4d** could not be determined on the same assumption. The calculated M_c of **4c** and **4d** did not match $M_{n,PEG}$ even if f became infinite. This observation implies that a polymer chain entanglement effect should be considered for **4c** and **4d**. In fact, the molecular weight

between entanglements of a 10% solution of polyethylene oxide can be estimated to be about 40 kDa. Therefore, entanglements may also be contributing to the elastic properties of **3d**.

In examining sliding elasticity in detail, Fleury et al. and Kato et al. have reported a dynamic transition between rubbery and sliding states,[37-39] which they clearly observed via the dependence of G' on frequency for conventional SR gels. SR crosslinks are potentially susceptible to frequency, because they behave as fixed links at a higher frequency, while sliding freely at a lower frequency. Furthermore, Ito and Mayumi et al. reported novel entropic elasticity derived from alignment entropy of threaded CDs.[40,41] The conventional SR gels have a large number of unreacted free CDs on a chain, which do not contribute to network formation but affect elastic properties of the gels. The elastic modulus of the conventional SR gels increases initially but then decreases inversely with increasing crosslinking density because the sliding elasticity is controlled by the alignment entropy change of the free CDs. Accordingly, the free CDs play an important role in the elasticity of the gels.

In contrast to the conventional SR gels described above, the present contribution is based on a novel type of network topology where the SR gels **3a-d** are intentionally fabricated without free CDs or dangling chain ends. This leads to the present SR gels that have only a small number of CDs per chain, all of which can contribute to network formation. In addition, the threaded CDs are less movable due to aggregation. Consequently, the sliding elasticity of these novel SR gels was minor as determined by rheological experiments. For this reason, there was little dependence of G' on frequency or strain in SR gels **3a-d**. Nevertheless, there is room for further research, i.e., to incorporate sliding elasticity into the present approach.

Tensile test

Stress-strain curves of the SR and corresponding covalent gels are shown in Figure 3.6. The elastic modulus of the gels showed a similar tendency to the shear modulus. Overall, the SR gels were more stretchable than the corresponding covalent gels in spite of their shorter M_c, especially at highly crosslinked networks (elongations at break of **3c** and **4c** were 700% and 300% respectively). Moreover, elongation at break

of all systems was 700% or higher with **3b** reaching above 1200%. When compared to conventional SR gels which exhibit a J-shaped curve without hysteresis,[21] these novel SR gels **3a-d** showed complex-shaped curves without hysteresis. In the low-strain region the curves are similar to the curve described by the fixed junction model, while in a high-strain region the tensile stress of the SR gels rapidly increases along a J-shaped curve. It is expected from these results that the SR crosslinks should start sliding in the high-strain region as the gels harden with deformation. It is probable that the initial behavior of the SR gels is derived from aggregation of the SR crosslinks, which suppresses the sliding ability of the crosslinking points.

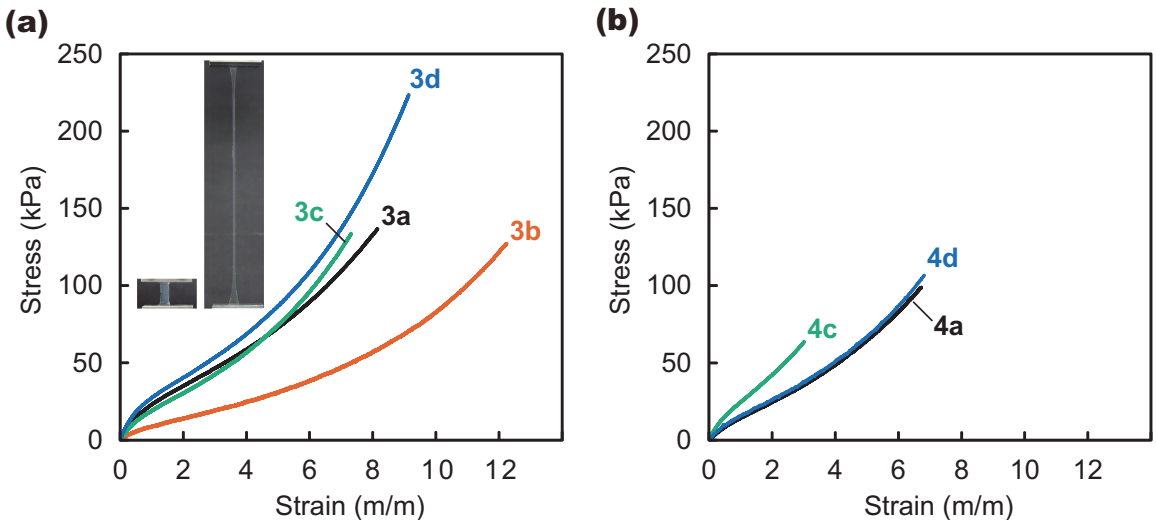

Figure 3.6. Stress-strain curves of the SR gels (a) and the covalent gels (b) under uniaxial tensile loading. The strain rate was 200% /min. The inset pictures correspond to **3a** gel before and after stretching.

Swelling behavior

Swelling/shrinking is an essential function of hydrogels and is closely correlated to the network structure. In order to study the swelling behavior, we immersed the gels in deionized water at room temperature for a week to achieve an equilibrium swollen state (Figure 3.7b). The SR gels absorbed 20 to 50 times their dry weights of water, which is similar to the corresponding covalent gels. M_c was estimated from the Flory-Rehner equation (Equation 3.4). The polymer volume fraction of the swollen gels (ϕ_s)

was calculated from Equation 3.5 using the swelling ratio Q. The results are summarized in Table 3.2.

$$-[\ln(1-\phi_s)+\phi_s+\chi\phi_s^2]=\frac{\rho_p V_1}{M_c}\left(\phi_r^{2/3}\phi_s^{1/3}-\frac{2}{f}\phi_s\right) \quad (3.4)$$

$$\phi_s=\frac{w_p/\rho_p}{w_p/\rho_p+w_c/\rho_c+(Q-1)(w_p+w_c)/\rho_w} \quad (3.5)$$

Here V_1 is the molar volume of water (18 cm^3/mol), and χ is the polymer-solvent interaction parameter (approximated by PEG-water 0.43).

In the SR gels, the M_c estimated from Q were higher than the M_c estimated from G'. In view of the equilibrium swelling theory, the Q of the SR gels can be said to be unexpectedly high. It is possible that the SR crosslinks are sliding along the chain, which lowers the stress and leads to the observed high swellability.

Acid degradation test

An acid degradation test was performed in order to clarify the difference in stability between the SR and covalent gels. Since the SR gels are formed from non-covalent CD-based crosslinks, the gels should potentially be acid degradable, in contrast to covalent gels, which are formed from stable covalent crosslinks. The acid degradability of the SR gels is derived from the acid-promoted decomposition of the CDs by hydrolysis of glycosidic bonds. The half-life of the small molecule β-CD is 15 hours in 0.2 N HCl aq. at 70 °C.[42] To ensure decomposition of the threaded CDs, the gels were immersed in 1 N HCl aq. at 70 °C for three days. After this time, all the SR gels has undergone complete degradation, while the covalent gels, with the exception of gel **4b**, were stable to degradation and remained intact (Table 3.2). These observations further confirmed the central role that non-covalent, CD-based slide-ring crosslinks play in network formation for these systems.

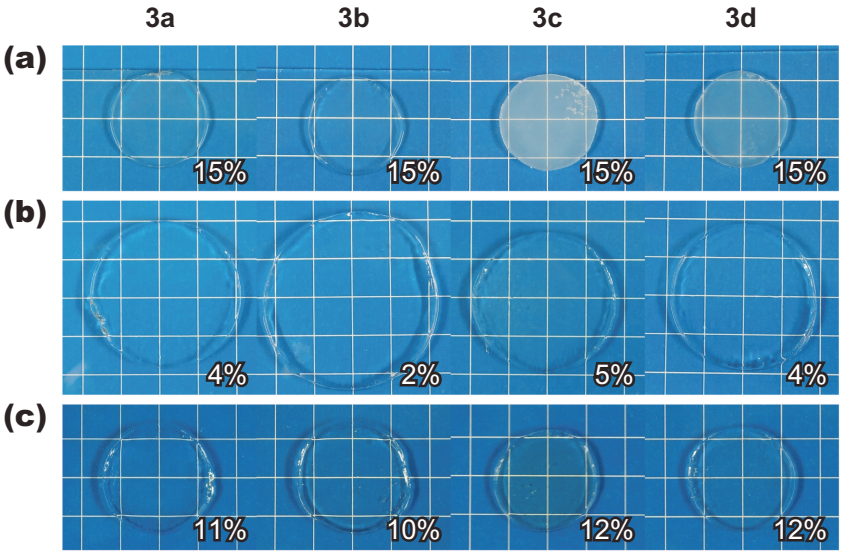

Figure 3.7. Photo images of SR gels **3a-d** in an initial state (a), an equilibrium swollen state (b), and an alkaline state (c). The numbers in the images denote weight concentrations of the gels. (a) The concentrations of the starting gels are 15wt%. (b) The gels swelled up to 1.8 times in diameter and 7.5 times in weight during the swelling test. (c) The haze of the starting gels disappeared after short time immersion in 1 N NaOH aq.

Alkali treatment

The influence of aggregation in these materials was then examined by treating the SR gels under alkaline conditions. Due to their strong hydrogen bonding, CDs are known to aggregate under neutral conditions leading to the possibility that the non-covalent SR crosslinks are partly frozen. It was therefore interesting to observe that initially white turbid SR gels gradually turned to transparent gels when soaked in 1 N NaOH aq. (Figure 3.7c). A rational explanation for this change in appearance is the hydroxyl groups of the CDs becoming partially negatively charged at alkaline pH, disrupting aggregation and undergoing dispersion along the chains due to electrostatic repulsion.[34] The polymer weight fractions of these gels also decreased from 15wt% to 10~12wt% after alkali treatment due to swelling. In spite of this dilution effect and the loss of hydrogen bonding, the SR gels retain their stiffness with the G' of **3d** slightly increasing suggesting that the breakup of CD aggregates leads to an

increase in N_{sc}.

Table 3.2. Summary of gel properties.

		3a	**3b**	**3c**	**3d**	**4a**	**4c**	**4d**
N_{allyl}		7.4	6.4	18.8	44.2	7.4	18.8	44.2
M_n of mid-block	(kDa)	20	35	35	100	20	35	100
G'	(kPa)	7.4	3.1	8.9	8.2	6.2	11.2	6.8
N_{sc} [1)]		1.6	1.4	2.4	4.4	-	-	-
f [1)]		2.6	2.4	3.4	5.4	3.0	inf [3)]	inf [3)]
M_c [1)]	(kDa)	7.8	15	10	19	20	33 [3)]	54 [3)]
Q		25	50	20	24	37	27	34
N_{sc} [2)]		0.5	-0.1 [3)]	1.4	3.3	-	-	-
f [2)]		1.5	0.9 [3)]	2.4	4.3	1.2	inf [3)]	inf [3)]
M_c [2)]	(kDa)	13	38 [3)]	15	23	20	22 [3)]	34 [3)]
Gel fraction	(wt%)	98	83	100	97	91	97	95
Gel retention after hydrolysis	(wt%)	0	0	0	0	97	100	100

[1)] estimated from G'. [2)] estimated from Q. [3)] These results were calculated to satisfy the given equations, but their validity is questionable due to ignoring some effects, such as defects and entanglement.

3.4 Conclusions

In the present contribution, slide-ring gels based solely on non-covalent, rotaxane crosslinking were successfully fabricated by a versatile and convenient one-pot, thiol-ene click chemistry approach. DLS analysis and NOESY experiments revealed the formation of a novel *pseudo*-polyrotaxane by threading of β-CDSH on the central PEG block of PAGE-PEG-PAGE triblock copolymers. Coupling of the thiol groups of the cyclodextrin units with the allyl groups present in the end blocks of the triblock copolymer allowed for formation of the SR gels. Control experiments showed no serious side reactions between triblock copolymer chains, allowing for direct

comparison with the corresponding covalent gels. This comparison showed remarkable rheological properties for the SR gels with elastic moduli up to 8.9 kPa. Furthermore, the SR gels could be stretched from 7 to 13 times in length, thanks to their non-covalent "sliding" crosslinks. Additionally, the SR gels were degradable under acidic conditions, which supports the presence of the SR crosslinks. We expect that the synthetic ease and modular nature of this one-pot fabrication method will enable a wide spectrum of researchers to study slide-ring gels for a variety of applications.

3.5 References

1. Hoffman, A. S. *Adv. Drug Deliv. Rev.* **2002**, 54, 3-12.
2. Peppas, N. A.; Hilt, J. Z.; Khademhosseini, A.; Langer, R. *Adv. Mater.* **2006**, 18, 1345-1360.
3. Qiu, Y.; Park, K. *Adv. Drug Deliv. Rev.* **2001**, 53, 321-339.
4. Lee, K. Y.; Mooney, D. J. *Chem. Rev.* **2001**, 101, 1869-1880.
5. Tibbitt, M. W.; Anseth, K. S. *Biotechnol. Bioeng.* **2009**, 103, 655-663.
6. Cui, J.; del Campo, A. *Chem. Commun.* **2012**, 48, 9302-9304.
7. Kakuta, T.; Takashima, Y.; Nakahata, M.; Otsubo, M.; Yamaguchi, H.; Harada, A. *Adv. Mater.* **2013**, 25, 2849-2853.
8. Komatsu, H.; Matsumoto, S.; Tamaru, S.; Kaneko, K.; Ikeda, M.; Hamachi, I. *J. Am. Chem. Soc.* **2009**, 131, 5580-5585.
9. Lange, R. F. M.; Van Gurp, M.; Meijer, E. W. *J. Polym. Sci. Part A: Polym. Chem.* **1999**, 37, 3657-3670.
10. de Gennes, P.-G. *Physica A* **1999**, 271, 231-237.
11. Okumura, Y.; Ito, K. *Adv. Mater.* **2001**, 13, 485-487.
12. Arunachalam, M.; Gibson, H. W. *Prog. Polym. Sci.* **2014**, 39, 1043-1073.
13. Wenz, G.; Han, B. H.; Muller, A. *Chem. Rev.* **2006**, 106, 782-817.
14. Hetzer, M.; Schmidt, B. V. K. J.; Barner-Kowollik, C.; Ritter, H. *Polym. Chem.* **2014**, 5, 2142-2152.
15. Kretschmann, O.; Choi, S. W.; Miyauchi, M.; Tomatsu, I.; Harada, A.; Ritter, H. *Angew. Chem., Int. Ed.* **2006**, 45, 4361-4365.
16. Chen, G.; Jiang, M. *Chem. Soc. Rev.* **2011**, 40, 2254-2266.

17. Schmidt, B. V. K. J.; Hetzer, M.; Ritter, H.; Barner-Kowollik, C. *Prog. Polym. Sci.* **2014**, 39, 235-249.
18. Harada, A.; Kamachi, M. *Macromolecules* **1990**, 23, 2821-2823.
19. Harada, A.; Kamachi, M. *J. Chem. Soc., Chem. Commun.* **1990**, 1322-1323.
20. Harada, A.; Li, J.; Kamachi, M. *Nature* **1992**, 356, 325-327.
21. Ito, K. *Polym. J.* **2007**, 39, 489-499.
22. Noda, Y.; Hayashi, Y.; Ito, K. *J. Appl. Polym. Sci.* **2014**, 131, 40509.
23. Liu, Y.; Yang, Y. W.; Chen, Y.; Zou, H. X. *Macromolecules* **2005**, 38, 5838-5840.
24. Kato, K.; Komatsu, H.; Ito, K. *Macromolecules* **2010**, 43, 8799-8804.
25. Cai, T.; Yang, W. J.; Zhang, Z.; Zhu, X.; Neoh, K.-G.; Kang, E.-T. *Soft Matter* **2012**, 8, 5612-5620.
26. Tan, S.; Blencowe, A.; Ladewig, K.; Qiao, G. G. *Soft Matter* **2013**, 9, 5239-5250.
27. Zhou, Y. X.; Fan, X. D.; Xue, D.; Xing, J. W.; Kong, J. *React. Funct. Polym.* **2013**, 73, 508-517.
28. Udachin, K. A.; Wilson, L. D.; Ripmeester, J. A. *J. Am. Chem. Soc.* **2000**, 122, 12375-12376.
29. Hunt, J. N.; Feldman, K. E.; Lynd, N. A.; Deek, J.; Campos, L. M.; Spruell, J. M.; Hernandez, B. M.; Kramer, E. J.; Hawker, C. J. *Adv. Mater.* **2011**, 23, 2327-2331.
30. Byun, H.-S.; Zhong, N.; Bittman, R. *Org. Synth.* **2000**, 77, 225.
31. Ihara, T.; Uemura, A.; Futamura, A.; Shimizu, M.; Baba, N.; Nishizawa, S.; Teramae, N.; Jyo, A. *J. Am. Chem. Soc.* **2009**, 131, 1386-1387.
32. Fujita, K.; Ueda, T.; Imoto, T.; Tabushi, I.; Toh, N.; Koga, T. *Bioorg. Chem.* **1982**, 11, 72-84.
33. Coleman, A. W.; Nicolis, I.; Keller, N.; Dalbiez, J. P. *J. Incl. Phenom. Macrocycl. Chem.* **1992**, 13, 139-143.
34. Karino, T.; Okumura, Y.; Ito, K.; Shibayama, M. *Macromolecules* **2004**, 37, 6177-6182.
35. Li, J.; Ni, X.; Zhou, Z.; Leong, K. W. *J. Am. Chem. Soc.* **2003**, 125, 1788-1795.
36. Gil, V. M. S.; Oliveira, N. C. *J. Chem. Educ.* **1990**, 67, 473-478.
37. Fleury, G.; Schlatter, G.; Brochon, C.; Travelet, C.; Lapp, A.; Lindner, P.; Hadziioannou, G. *Macromolecules* **2007**, 40, 535-543.
38. Kato, K.; Ito, K. *Soft Matter* **2011**, 7, 8737-8740.

39. Kato, K.; Yasuda, T.; Ito, K. *Macromolecules* **2013**, 46, 310-316.
40. Mayumi, K.; Tezuka, M.; Bando, A.; Ito, K. *Soft Matter* **2012**, 8, 8179-8183.
41. Ito, K. *Polym. J.* **2012**, 44, 38-41.
42. Schönberger, B. P.; Jansen, A. C. A.; Jansen, L. H. M. *Proceedings of the Fourth International Symposium on Cyclodextrins* **1988**, 61-63.

Chapter 4

Structural Versatility in Slide-Ring Gels: Influence of Co-threaded Cyclodextrin Spacers

4.1 Introduction

Hydrogels are water-swellable, crosslinked polymers that have a broad range of applications ranging from biomedical devices,[1] to tissue-engineering,[2] drug delivery,[3] and personal care materials.[4] While the properties of hydrogels can be tuned from mechanically robust, for example double network[5-8] or reinforced hydrogel structures,[9-11] to soft hydrogels with low crosslinking densities, all of these systems are strongly influenced by the nature of the crosslinking (physical versus covalent).[12]

Well-established strategies towards physically crosslinked hydrogels involves supramolecular-based crosslinking in water, e.g. via hydrogen bonding,[13,14] host-guest interaction,[15-19] metal coordination,[20,21] or coacervate formation.[22,23] A number of advantages arise from the reversibility of these supramolecular bonds when compared to purely covalent systems. This includes self-healing behavior and stimuli responsive properties. For example, hydrogels formed via 2-ureido-4-pyrimidone hydrogen bonding have been shown to have self-healing and shape memory properties[13,14] while cyclodextrin-ferrocene based hydrogels show macroscopic recognition/adhesion as well as redox responsive behavior.[24-26] The supramolecular properties of cyclodextrins have also been used for the preparation of hydrogels, known as slide-ring (SR) gels, which were first introduced by Ito and coworkers[27] following theoretical predictions by de Gennes.[28] In this class of supramolecular gels, the cyclodextrin units are threaded on a polymer chain without the possibility of being unthreaded (polyrotaxane formation) with crosslinking induced via CD units that can move along the chain leading to unique mechanical properties, such as softness and stretchability.[29] As entropy-driven elasticity, derived from the alignment entropy of threaded macrocycles,

is an important characteristic, free CDs that are threaded but not linked to any other units play an important role in properties such as elasticity.[30] For example, Kato et al. recently demonstrated the effect of density of the threaded macrocycles on the stress-strain behavior of SR gels with limited extensibility being observed for systems with a higher density of macrocycles threaded along the chains.[31] These effects were attributed to the entropy that prevents the macrocycles from sliding together.

Despite these promising properties, the preparation of SR gels traditionally requires tedious procedures that hamper practical applications and hinder the ability to tune the ratio of "free" versus "linked" cyclodextrin units. To solve these synthetic challenges, a number of strategies for the preparation of SR networks have been reported with most systems relying on the use of CDs as stoppers[32] with click chemistry[33,34] or radical polymerization[35,36] strategies being preferred for formation. Recently, we reported the successful fabrication of SR gels through a convenient one-pot approach using thiol-ene click chemistry.[37] *Pseudo*-polyrotaxanes of monothiolated β-cyclodextrin (CDSH) threaded on poly(allyl glycidyl ether)-*block*-poly(ethylene glycol)-*block*-poly(allyl glycidyl ether) were prepared in water and subsequently photo-crosslinked by UV irradiation. Taking advantage of this synthetic ease and to obtain a deeper insight into the effects of threaded macrocycles in SR networks, in this study, we deliberately added "free" CD units into the system to act as a spacer on the chain without adding further crosslinks to the system. (2-Hydroxypropyl)-β-cyclodextrin (HPCD) was chosen as a sliding spacer thanks to its high solubility in water and low crystallinity of its inclusion complex with polyethylene glycol (PEG) with the SR networks being formed through a thiol-yne reaction of the sliding crosslinker CDSH and polyethylene glycol α,ω-dipropargyl ether (DP-PEG) in the presence of inert HPCD (Scheme 4.1). This procedure allows the sliding crosslinks and free spacers to be introduced into the SR networks simultaneously with the product ratio being controlled by the feed ratio.

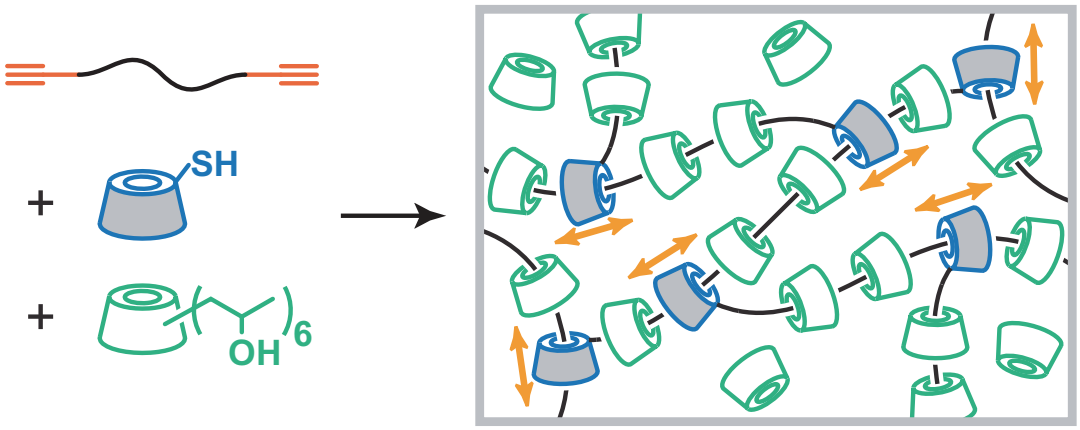

Scheme 4.1. Schematic illustration of the SR network formation in the presence of an inert CD derivative. The sliding spacers threaded on the chains (green) are depicted as well as the sliding crosslinks (blue) and the isolated CDs that are not incorporated in the network (green).

4.2 Experimental Section

Materials. All chemicals were used as received from Sigma-Aldrich unless otherwise specified. Tetrahydrofuran (THF) was collected from a dry solvent system and used immediately thereafter. Polyethylene glycol (PEG) and (2-hydroxypropyl)-β-cyclodextrin (HPCD) were purchased from Sigma-Aldrich and Tokyo Chemical Industry respectively, and dried *in vacuo* prior to use.

Characterization. ^{1}H NMR spectra were recorded at 25 °C on a Varian VNMRS 600 spectrometer (600 MHz). Chemical shifts are reported relative to residual solvent peaks in ^{1}H NMR (δ 7.26 ppm for $CDCl_3$ and 4.79 ppm for D_2O). Nuclear Overhauser enhancement spectroscopy (NOESY) experiments were performed using a mixing time of 300 ms, 400 t_1 increments, and 16 scans per t_1 increment on the same spectrometer as ^{1}H NMR. Fourier transform infrared (FT-IR) spectra were acquired on a Nicolet iS10 FTIR spectrometer with an ATR accessory at a resolution of 4 cm^{-1}. Electrospray ionization time-of-flight (ESI-ToF) data were obtained on a Micromass QTOF2 quadrupole/time-of-flight tandem mass spectrometer. Gel permeation chromatography (GPC) was performed on a Waters 2695 separation module equipped with a Waters 2410 differential refractometer and a Waters 2998 photodiode array

detector. Chloroform with 0.25% of triethylamine was used as an eluent at a flow rate of 1 mL/min. Molecular weight and the polydispersity index (PDI) were calculated relative to linear polystyrene standards. Dynamic light scattering (DLS) analysis was performed at 25 °C on a Wyatt Technology DynaPro NanoStar instrument. The refractive index increment (d*n*/d*c*) was assumed to be 0.136 mL/g for PEG in water. Reported values are averages of 100 acquisitions.

Rheological experiments were performed at 25 °C on a TA Instruments ARES-LS1 rheometer equipped with parallel-plate geometry with a diameter of 8 mm (for the stoichiometric study) or 25 mm (for the other studies). Frequency sweeps were performed at a strain of 1%, and strain sweeps were performed at a frequency of 1 Hz. Tensile tests were conducted on a mechanical testing machine equipped with an Eaton Corporation 3108-10 load cell with a capacity of 44.48 N and an Electronic Instrument Research LE-01 laser extensometer using a cross-head rate of 200% per min. Samples were cut into rectangular shapes with dimensions of 8 mm by 16 mm by 0.8 mm and clamped with pieces of sandpaper to avoid grip slippage or breakage. Samples broken at the edge of the grip were ignored. All experiments were performed at room temperature unless otherwise specified.

Synthesis of 6A-deoxy-6A-mercapto-β-cyclodextrin (CDSH). CDSH was synthesized from 6A-*O*-(*p*-toluenesulfonyl)-β-cyclodextrin according to the literature.[37-39] ^{1}H NMR (600 MHz, D_2O) δ 5.15 (br s, 1H, C1-*H*), 5.12–5.06 (m, 1H×6, C1-*H*), 4.02–3.82 (m, 2H×7+2H×6, C3-*H*, C5-*H* and C6-H_2OH), 3.72–3.55 (m, 2H×7, C2-*H* and C4-*H*), 3.15 (d, *J* = 14.2 Hz, 1H, C6-H_2SH), 2.86 (dd, *J* = 14.6, 6.8 Hz, 1H, C6-H_2SH). ESI-MS (m/z) Calcd for $C_{42}H_{70}O_{34}SNa$: 1173.34 $[M+Na]^+$, Found: 1173.38 $[M+Na]^+$.

Spectral analysis of (2-hydroxypropyl)-β-cyclodextrin (HPCD). The degree of substitution was calculated to be ~5.6 based on the integral ratio between the C1-H and methyl protons in the ^{1}H NMR spectrum. ^{1}H NMR (600 MHz, D_2O) δ 5.34–5.04 (m, 1H×7, C1-*H*), 4.15–3.35 (m, 6H×7+3H×5.55, C2-6-*H* and OCH_2C*H*(OH)CH_3), 1.30–1.10 (m, 3H×5.55, $OCH_2CH(OH)CH_3$).

Synthesis of polyethylene glycol α,ω-dipropargyl ether (DP-PEG). PEG with M_n 20 kDa (8.0 g, 0.40 mmol, 1.0 equiv) was dissolved in toluene (60 mL) with heating under

a dry argon atmosphere. Crushed KOH (0.45 g, 8.0 mmol, 20 equiv) was added to the solution and vigorously stirred for 30 min at 50 °C. Propargyl bromide (80wt% solution in toluene, 2.4 g, 16 mmol, 40 equiv) was added to the mixture using a syringe and stirring continued for four days at 50 °C. The reaction mixture was diluted with toluene, filtered through a silica gel plug, and poured into a large excess of hexane. The precipitated solid was collected by filtration, stirred in diethyl ether, and washed with diethyl ether to remove residual propargyl bromide. The product was obtained as a white powder after drying *in vacuo*. Yield 7.5 g. Degree of substitution was calculated to be 98+% from ^{1}H NMR spectrum. ^{1}H NMR (600 MHz, $CDCl_3$) δ 4.19 (d, J = 2.3 Hz, 4H, OCH_2C≡CH), 3.77–3.48 (m, 4H×454, (CH_2CH_2O)$_{454}$), 2.43 (t, J = 2.4 Hz, 2H, OCH$_2$C≡CH). M_n = 20100 g/mol. PDI = 1.19.

Synthesis of polyethylene glycol α,ω-diglycidyl ether (DG-PEG). PEG with M_n 20 kDa (6.0 g, 0.30 mmol, 1.0 equiv) was dissolved in THF (60 mL) with heating under a dry argon atmosphere. Sodium hydride (0.14 g, 6.0 mmol, 20 equiv) was added to the solution and stirring continued for 30 min. Epichlorohydrin (1.1 g, 12 mmol, 40 equiv) was added to the mixture using a syringe, and stirred for 24 h. The reaction mixture was filtered through a silica gel plug, and poured into a large excess of hexane. The precipitated solid was collected, washed with hexane, and dried *in vacuo*. The product was obtained as a white powder. Yield 4.2 g. ^{1}H NMR (600 MHz, $CDCl_3$) δ 3.77 (dd, J = 11.6, 3.1 Hz, 2H, OCH_2CH(O)CH$_2$), 3.76–3.48 (m, 4H×454, (CH_2CH_2O)$_{454}$), 3.42 (dd, J = 11.6, 5.9 Hz, 2H, OCH_2CH(O)CH$_2$), 3.16–3.13 (m, 2H, OCH$_2$CH(O)CH$_2$), 2.78 (t, J = 4.6 Hz, 2H, OCH$_2$CH(O)CH_2), 2.59 (dd, J = 5.0, 2.7 Hz, 2H, OCH$_2$CH(O)CH_2). M_n = 20100 g/mol. PDI = 1.07.

Preparation of SR gels. DP-PEG (201 mg, 10 μmol), HPCD (0 to 350 mg, 0 to 240 μmol, 0 to 24 eq), 2-hydroxy-4'-(2-hydroxyethoxy)-2-methylpropiophenone (Irgacure 2959) (1wt% aqueous solution, 201 mg, 9 μmol), and deionized water (363 to 13 mg) were placed into a small vial and vortexed to dissolve. A freshly dissolved hot aqueous solution of CDSH (8wt%, 576 mg, 40 μmol, 4 eq) was added to the reaction mixture, vortexed, and the resulting pale yellow mixture was sonicated in a Branson 3510 ultrasonic bath for 1 h, transferred into a glass mold, and subsequently exposed to UV light ($_{max}$ 365 nm, 15 W) at room temperature for 5 h. The weight concentrations of the

polymer and the photo initiator in the precursor solution were fixed at 15wt% and 0.15wt% respectively.

Stoichiometric study. Storage and loss moduli of the SR gels were measured at various feed ratios x of CDSH to DP-PEG. Aqueous solutions of DP-PEG (40wt%, 302 mg, 6 μmol), CDSH (8wt%, 129–432 mg, 9–30 μmol, 1.5–5.0 eq), Irgacure 2959 (1wt%, 121 mg, 5.4 μmol), and deionized water (453–151 mg) were mixed and sonicated for 1 h. The obtained precursor solution was cured with UV light for 5 h in a glass mold.

Characterization of SR gels. Swelling experiments were performed as follows. The pristine gels were immersed in deionized water at room temperature for a week until an equilibrium swollen state was reached; during this process, the deionized water was replaced repeatedly to remove any soluble fraction of the immersed gels. After the rheological experiments, the resulting swollen gels were dried *in vacuo* to yield the washed dry gels. The swelling ratio Q was calculated from $Q = w_s/w_d$, where w_s and w_d are the weights of the equilibrium swollen gels and the washed dry gels respectively. After FT-IR analysis, the washed dry SR gels were hydrolyzed in acidic D_2O (0.1 N sulfuric acid in deuterated water (0.8 mL), and heated in sealed vials at 70 °C for 24 h) for ^1H NMR analysis in solution. The resulting solutions were used directly for ^1H NMR analysis. The obtained ^1H NMR spectra of the washed and subsequently hydrolyzed samples in D_2O are shown in Figure 4.2. Incorporation molar ratios r_c and r_s denote the molar ratios of CDSH and HPCD to DP-PEG incorporated into SR networks respectively. r_c and r_s were estimated from the following equations:

$$\begin{cases} a_1 = 3 \times 5.55 \times r_s \\ a_2 = 4 \times 454.0 + 40 \times r_c + (42 + 3 \times 5.55) \times r_s \\ a_3 = 7 \times r_c + 7 \times r_s \end{cases} \quad (4.1)$$

, where a_1, a_2, and a_3 were NMR integral ratios of the peaks in 1.00–1.35 ppm (region I), 3.15–4.65 ppm (region II), and 4.90–5.75 ppm (region III) respectively. The gel fraction F was also calculated from $F = w_d/(w_o \times C)$, where w_o is the weight of the pristine SR gels as prepared, and C is the total weight concentration of the starting materials without free isolated CDs in the gels, and calculated from $C = 15\% \times (20100 + 1151 \times r_c + 1457 \times r_s)/20100$.

Synthesis of a polyrotaxane model compound. DG-PEG (120 mg, 6 μmol), HPCD (418 mg, 287 μmol, 48 eq), 5-aminofluorescein (50 mg, 143 μmol, 24 eq), sodium hydroxide (5.7 mg, 143 μmol, 24 eq), and deionized water (407 mg) were placed in a small vial. The reaction mixture was sonicated for 1 h, and stirred at 50 °C for 24 h under an argon atmosphere. The reaction mixture was diluted with water, filtered through a PTFE 0.25 μm membrane, and dialyzed against water for 10 days using a MWCO 6–8 kDa membrane with the water being replaced repeatedly. The resulting solution was lyophilized to yield the polyrotaxane as a fluffy solid ^{1}H NMR (600 MHz, D_2O) δ 7.70–6.60 (m, 13.53H, aromatic protons of the fluorescein moiety), 5.35–4.95 (m, 54.85H, C1-*H*), 4.25–3.15 (m, 2270.38H, (CH_2CH_2O)$_{454}$, C2-6-*H* and $OCH_2CH(OH)CH_3$), 1.35–1.00 (m, 130.36H, $OCH_2CH(OH)CH_3$).

4.3 Results and Discussion

Preparation of SR gels

Slide-ring networks were prepared through a modified one-pot strategy involving a photo-initiated thiol-yne reaction of polyethylene glycol α,ω-dipropargyl ether (DP-PEG) with monothiolated β-cyclodextrin (CDSH) as a sliding crosslinker and 2-hydroxypropyl-β-cyclodextrin (HPCD) as a sliding spacer (Scheme 4.2).[40,41] HPCD was chosen as the inert macrocyclic spacer due to its high solubility (>600 mg/ml) in water and lack of cross-reactivity during network formation.[42] A typical procedure for gel formation is as follows: DP-PEG, CDSH (x eq), HPCD (y eq), and a water-soluble photo initiator Irgacure 2959 were dissolved in water, and sonicated for 1 h. The precursor solution was then transferred into glass molds and irradiated with UV light (365 nm) for 5 h to yield SR gels SR-r_c-r_s. The polymer concentration in the gels was fixed at 15wt% with x and y denoting the feed molar ratios of CDSH and HPCD to DP-PEG respectively, while r_c and r_s denote the incorporated molar ratios. The feed ratio x of CDSH was fixed at 4 eq based on the following stoichiometric study, and the feed ratio y of HPCD was varied from 0 to 24 eq to control the final ratio of sliding spacers to crosslinking spacers.

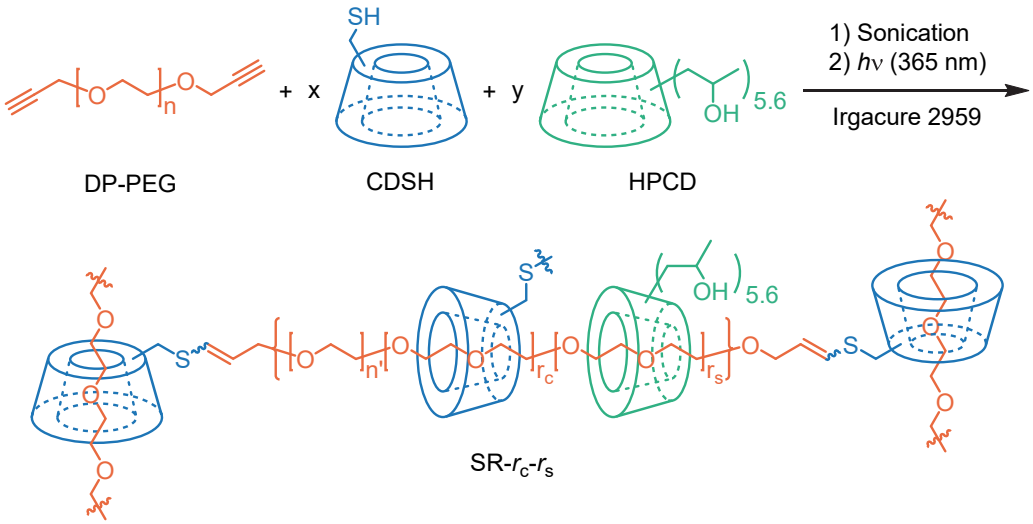

Scheme 4.2. Synthesis of SR gels SR-r_c-r_s, where x and y denote feed ratios, and r_c and r_s denote incorporation ratios of CDSH and HPCD to DP-PEG respectively.

Stoichiometric study of SR gels without spacers

To optimize the feed ratio of crosslinker for effective network formation, a stoichiometric study of SR gels without spacers was carried out. The feed ratio x of CDSH was varied between 1.5 and 5.0 eq, and the storage and loss moduli G' and G'' of the SR gels were plotted against x. G' was observed to increase rapidly with increasing feed ratio below 3.5 eq, while the resulting gels become turbid above 5 eq due to the poor solubility of the inclusion complex (Figure 4.1). As a result, the feed ratio x was fixed at 4.0 eq for all subsequent gel formation and characterization studies.

Incorporation ratios

In contrast to the previously studied SR gels that do not contain sliding CD spacer units, the proposed SR gels have a number of advantages derived from the interaction between threaded CDs. Controlling and quantifying the level of incorporation of individual cyclodextrin units (crosslinked CDSH and spacer HPCD) threaded along the PEG backbone is therefore key to tuning properties. To determine the level of incorporation, the cyclodextrin-based crosslinks present in the SR gels were hydrolyzed in D_2O-H_2SO_4 at 70 °C to obtain homogeneous solutions and the resulting samples analyzed by ^1H NMR (Figure 4.2). The incorporation ratios were calculated

from integral ratios of methyl protons specific to HPCD (~1.2 ppm) and comparison with C1-H protons for all cyclodextrin monomers and backbone resonances for the PEG main chain. From this analysis the product ratio of HPCD and CDSH was calculated and summarized in Table 4.1 and Figure 4.3. The incorporation ratio r_c of CDSH is estimated to be between 3.1 and 3.6 eq for all samples which on comparison with the constant feed ratio x of CDSH (fixed at 4 eq) demonstrates the efficient threading and/or crosslinking of CDSH. In contrast, the threading efficiency of HPCD on PEG was ~15-20% with the incorporation ratio r_s of HPCD proportionally increasing as the feed ratio y of HPCD increases. This leads to an average of ~2 sliding spacers between sliding crosslinks in SR-3.6-4.7 and a coverage ratio of ~ 5% (Table 4.1), where the coverage ratio was calculated based on the fact that each β-CD accommodates the repeating units of PEG.[43] This is in accord with the study reported by Mondjinou et al., in which HPCD-based polyrotaxanes were prepared in nonpolar solvents such as hexane and diethyl ether, instead of polar solvents due to the solvent dependence of the threading efficiency of HPCD.[44,45]

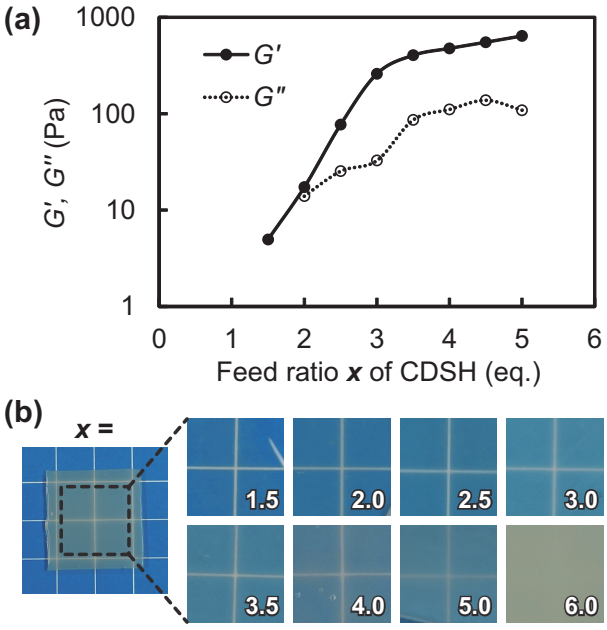

Figure 4.1. Stoichiometric study varying the feed ratio x of CDSH to DP-PEG. (a) Storage and loss moduli of the SR gels at a polymer concentration of 12wt%. (b) Photo images of the SR gels with various amounts of CDSH.

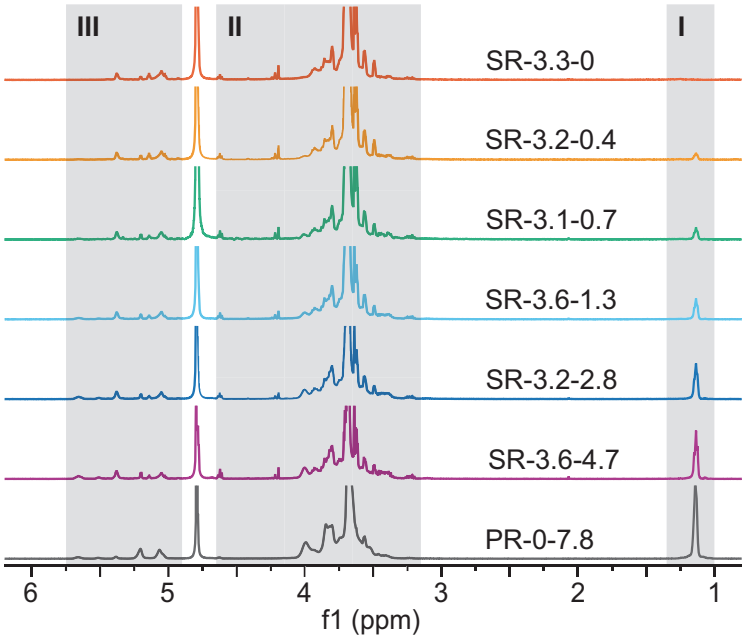

Figure 4.2. ^{1}H NMR spectra of the washed and subsequently hydrolyzed SR-r_c-r_s and the hydrolyzed polyrotaxane in D_2O. The peaks in the region I, II, and III were integrated to calculate the integral ratios a_1, a_2, and a_3 respectively.

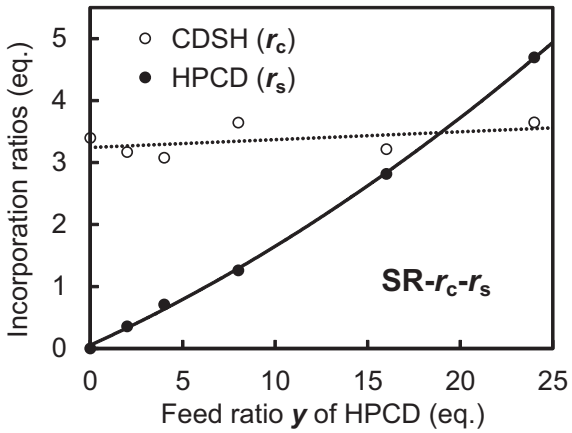

Figure 4.3. Incorporation ratios of CDSH and HPCD, plotted against the feed ratio y of HPCD.

The gel fraction F was determined by gravimetric analysis of the gels before and after swelling. Values of ~60-80% indicate the presence of unreacted or partially reacted yne groups and/or elastically ineffective intramolecular crosslinking. While each triple bond can potentially react with two thiols, a percentage of yne groups may have

reacted with less than a single CDSH on average owing to the second reaction (thiol-ene) being sterically hindered due to the bulky CD substituent. Significantly, the gel fraction was observed to increase with increasing HPCD, suggesting that the HPCD could suppress these defects by dispersion of the threaded CDSH units along the backbone, increasing the steric availability of the yne groups and decreasing intramolecular crosslinking.

Table 4.1. Summary of compositions and properties of SR gels.

	Molar ratios				Coverage ratio (%)	Gel fraction F (%)	Swelling ratio Q	φ	G' (kPa)	G_{ph} (kPa)
	x	y	r_c	r_s						
SR-3.3-0	4	0	3.3	0	2.2	63	88	0.081	1.25	12.1
SR-3.2-0.4	4	2	3.2	0.4	2.3	70	68	0.090	2.05	13.3
SR-3.1-0.7	4	4	3.1	0.7	2.5	71	62	0.092	2.92	13.7
SR-3.6-1.3	4	8	3.6	1.3	3.2	71	53	0.094	3.54	13.9
SR-3.2-2.8	4	16	3.2	2.8	4.0	79	41	0.107	5.21	16.0
SR-3.6-4.7	4	24	3.6	4.7	5.5	78	37	0.109	6.05	16.2

Coverage ratio was calculated from an equation: $3 \times (r_c + r_s)/454$. Gel fraction $F = w_d/(w_o \times C)$. Swelling ratio $Q = w_s/w_d$. φ is the elastically effective polymer volume fraction of the pristine gels. G' was obtained from the viscoelasticity measurement. G_{ph} was calculated with the phantom network model based on the assumption that all the junctions are fixed and homogeneously dispersed on the chain.

Synthesis and characterization of a polyrotaxane model compound

In order to investigate the inclusion complexation of HPCD in water, a polyrotaxane model compound PR-0-r_s was prepared (Scheme 4.3). As *pseudo*-polyrotaxane formation of HPCD with PEG is difficult to characterize due to unthreading of HPCD from the polymer chain, polyrotaxanes were prepared by initial threading of HPCD with polyethylene glycol α,ω-diglycidyl ether (DG-PEG) followed by nucleophilic addition of 5-aminofluorescein to the epoxide chain ends leads to end-capping group and rotaxane stabilization. Dialysis against water for 10 days using a

MWCO 6–8 kDa membrane then leads to the desired model systems.

The obtained polyrotaxane PR-0-7.8 was analyzed via ^{1}H NMR, nuclear Overhauser enhancement spectroscopy (NOESY), and dynamic light scattering (DLS) analysis. Comparison of the ^{1}H NMR spectra for the starting materials DG-PEG and HPCD with the purified polyrotaxane is shown in Figure 4.4 and clearly shows the presence of HPCD in the polyrotaxane. The incorporation ratio of HPCD to PEG was estimated to be ~7.8 eq from integration values with the threading efficiency being slightly lower than that for the SR gels due to the elevated reaction temperature and increased dilution. NOESY experiments were also carried out to confirm supramolecular association between the CDs units and the PEG backbone with the expected correlations being observed. To further illustrate rotaxane formation, intensity-based size distributions for aqueous solutions of DG-PEG, HPCD, a physical mixture of DG-PEG with 24 eq HPCD, and the polyrotaxane were examined via DLS at a concentration of 10 mg/mL (Figure 4.5). The cyclodextrin, HPCD, and the HPCD/PEG mixture were found to have a peak at ~1 nm, which is derived from individual, non-aggregated HPCD molecules. In contrast, the polyrotaxane derivative did not show any peaks at ~1 nm indicating that any free HPCDs was removed during the dialysis process, further supporting rotaxane formation.

Additionally, we verified the determination method of the incorporation ratios taking advantage of the polyrotaxane. The SR gels were in-situ hydrolyzed before NMR measurement due to difficulties in gel-state analysis, however, the accuracy might be questionable because C1-H proton of CD could decrease during the hydrolysis process. Accordingly, ^{1}H NMR spectra of the pristine and hydrolyzed polyrotaxane were compared. The method provided the values r_c=0.2 and r_s=7.7 for PR-0-7.8, which reasonably coincide with the actual values. As a consequence, the method was found to be accurate enough for this study, though the incorporation ratios may be slightly underestimated.

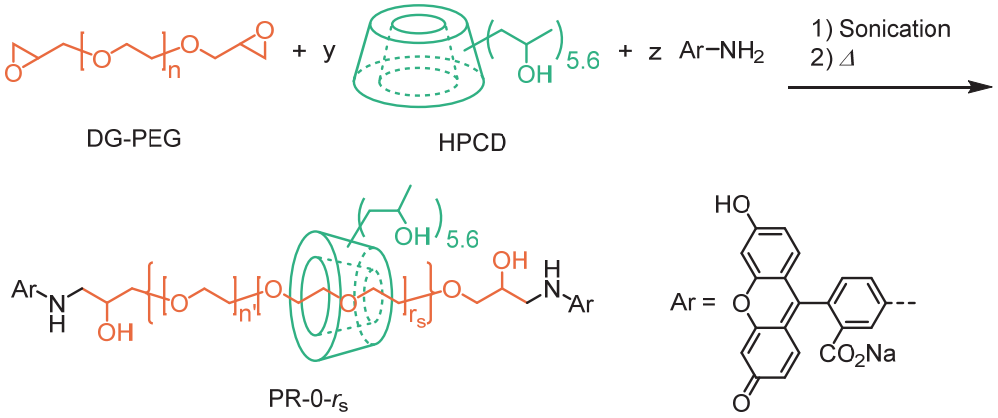

Scheme 4.3. Synthesis of polyrotaxane model compound PR-0-r_s.

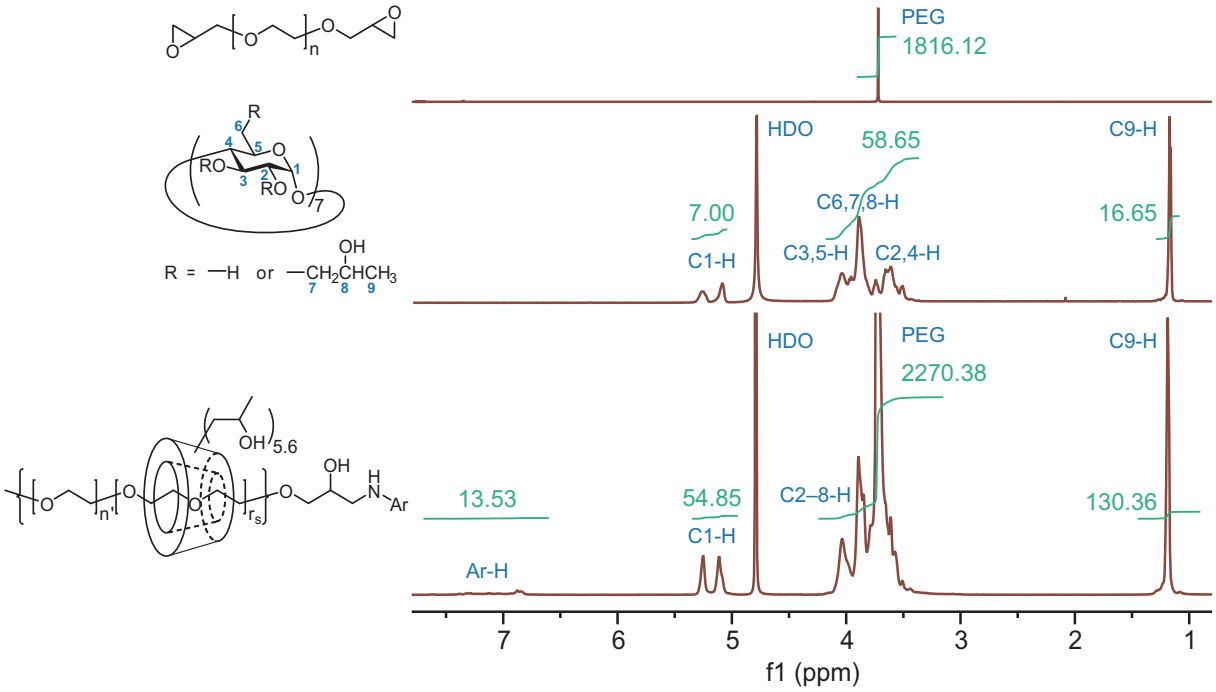

Figure 4.4. ^{1}H NMR spectra of DG-PEG (top), HPCD (middle), and polyrotaxane PR-0-7.8 (bottom) in D_2O.

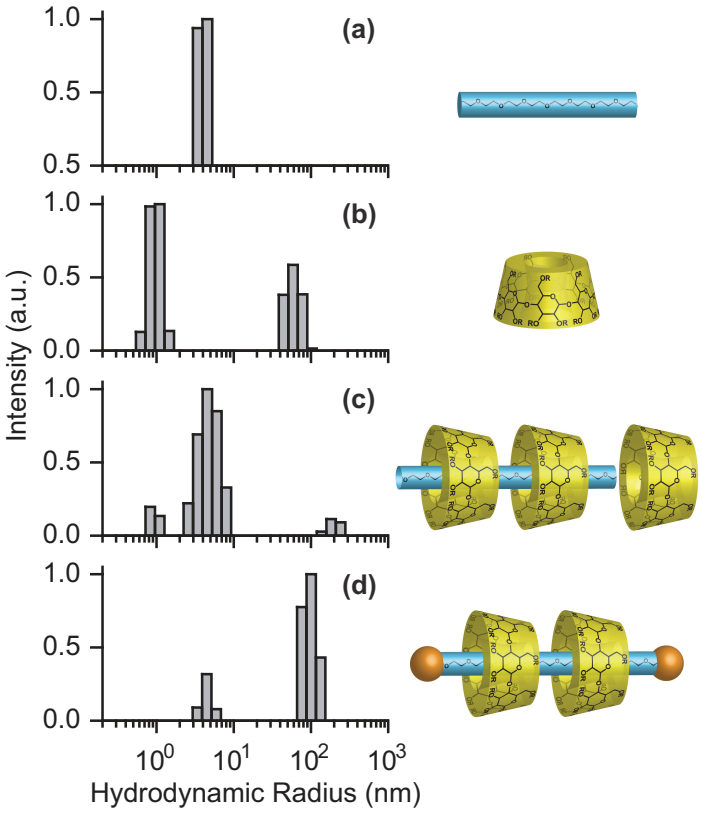

Figure 4.5. Intensity-based size distributions obtained via DLS: DG-PEG (a), HPCD (b), a mixture of DG-PEG with 24 eq HPCD (c), and the polyrotaxane PR-0-7.8 (d).

Rheological investigations of SR gels

After formation of SR gels, the rheological properties of the purified rotaxane gels were evaluated. The dynamic frequency and strain sweeps for the storage modulus G' and loss modulus G'' of the SR gels are shown in Figure 4.6 with G' plotted against the incorporation ratio of HPCD in Figure 4.7. Significantly, the SR gels were observed to have remarkably low G', with G' increasing as the incorporation of HPCD increases. For example, G' of SR-3.3-0 is 1.3 kPa at a frequency of 1 Hz and a strain of 1%, while G' for SR-3.6-4.7 reaches 6.1 kPa, ca. five times stiffer.[31] It should be stressed that HPCD supports no intermolecular crosslinking, and the polymer volume fractions are nearly constant for all of the samples. As a result, the sliding spacers can influence the sliding elasticity of the SR networks only through the sliding crosslinks, suggesting that this elasticity gain is derived from interactions between the sliding crosslinks and spacers,

illustrating that the rheological properties of the SR gels can be tuned via the introduction of sliding spacers.

It is noteworthy that there is little dependence of G' on frequency in contrast to the phase transition behavior from a sliding state to a rubbery state reported by Fleury et al. and Kato et al.[46,47] In typical SR networks, chains slide freely at a low frequency, but start stretching instead of sliding at higher frequencies. In order to investigate the rubbery state, the shear modulus G_{ph} of the phantom network model was estimated based on the assumption that each chain end forms a fixed junction with another chain according to the following equations:

$$G_{ph} = (\nu - \mu)k_BT = \left(1 - \frac{2}{f}\right)\nu k_BT = \left(1 - \frac{2}{f}\right)\frac{\rho_{PEG}N_A}{M_C}\phi\, k_BT \quad (4.2)$$

$$\phi = F \times \frac{w_{PEG}/\rho_{PEG}}{w_{PEG}/\rho_{PEG} + w_{CD}/\rho_{CD} + w_w/\rho_w} \quad (4.3)$$

where ν and μ are the number densities of elastically effective chains and crosslinks respectively; f is the functionality of crosslinks and assumed to be 3 for this study; M_c is the molecular weight between crosslinks and calculated to be $M_{n,PEG}/3$; φ is the elastically effective polymer volume fraction of the pristine gels; w_{PEG}, w_{CD}, and w_w are the weights of PEG, CDs, and water in the gels respectively; ρ_{PEG}, ρ_{CD}, and ρ_w are the densities of PEG (1.20 g/cm^3), CDs (1.44 g/cm^3), and water (1.00 g/cm^3) respectively. The calculated φ and G_{ph} are summarized in Table 4.1. Compared to G_{ph}, the observed G' are low even at the maximum coverage ratio. From these results, we can expect that the sliding state must be dominant and that crosslinks can slide along the chain over a wide range of frequency and strain.

Unusually, G' increases with strain between 0.1% and 0.8% but is otherwise independent of strain (Figure 4.6b). These modulus gaps may result from the behavior of the sliding crosslinks. On the other hand, a similar phenomenon has been also reported by Kato et al.[48] They observed strain-hardening behavior under compression on polyrotaxane-based SR gels, and concluded the behavior was originated from the counteracting entropy of the polymer chains and rings. However, it is not clear that

their discussion can apply to our work, because both works are totally different in the network structures. For example, they used polyrotaxanes of M_n 32 kDa PEG backbone with a constant coverage ratio of 25% and crosslinked randomly between rings, while we used polyrotaxanes of M_n 20 kDa PEG backbone with various coverage ratios between 2.2 and 5.5% and crosslinked precisely between chain ends and rings. Thus, the origin of the modulus gap still remains a matter for further discussion.

It should also be noted that the threaded macrocycles can hamper the sliding of chains through crosslinks by the entropic effect, which presumably contributes to sliding elasticity.[49,50] When a length of chain between sliding crosslinks contains a number of threaded macrocycles then the chains ability to slide through crosslinks is restricted as this process would shorten the length of chain and hence decrease the entropy of the sliding macrocycles. Hence the sliding spacers have a significant impact on the elasticity of the SR gels, an impact which can also be extracted from the data in this study. Indeed, the systematic variation of G' with the coverage ratio of sliding spacers shows the effect of the sliding spacers on this elastic behavior.

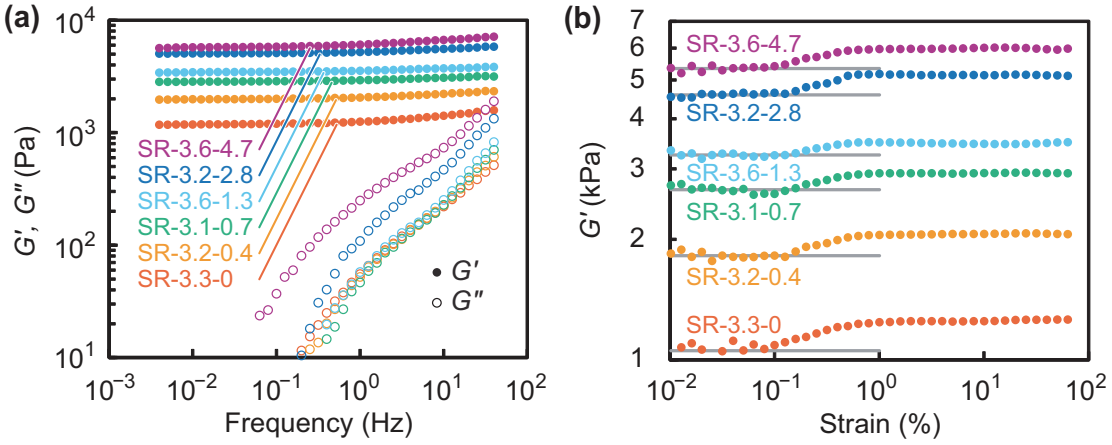

Figure 4.6. Rheological behaviors of the SR gels. (a) Dynamic frequency sweeps at a strain of 1%, and (b) dynamic strain sweeps at a frequency of 1 Hz.

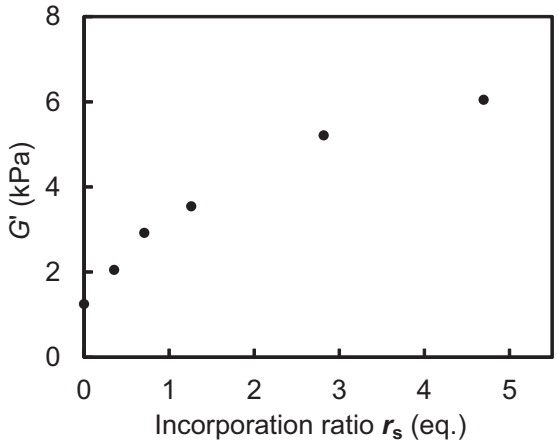

Figure 4.7. Storage moduli *G′* of the SR gels plotted against the incorporation ratio of the sliding spacer HPCD. *G′* values were recorded at a frequency of 1 Hz and a strain of 1%.

Mechanical properties of SR gels

One of the major advantages of SR gels is their remarkable extensibility. For these novel SR gels with added sliding HPCD spacers, the mechanical properties were probed through uniaxial extension in stress-strain measurements with respect to the ratios of sliding spacers (Figure 4.8). As expected, the purified SR gels were found to be soft and stretchable with the addition of sliding spacers leading to a significant change in the materials properties. Traditional covalently crosslinked gels will initially follow but gradually deviate from a curve of a neo-Hookean model because covalent crosslinks restrict moving or relaxing of chains when a certain stress is applied. This neo-Hookean model is generally accurate only at a small strain. In contrast, SR gels are expected to behave as a neo-Hookean material over a much wider strain range due to crosslinks sliding along the chain at a moderate coverage ratio.[31,51] The stress-extension relationship of incompressive neo-Hookean materials is as follows:

$$\sigma = G(\lambda - \lambda^{-2}) \quad (4.4)$$

where σ is nominal stress, and λ is extension. This model was fitted with the actual stress-strain curves for SR gels with different loadings of the HPCD spacer between λ = 1.2 and 1.7, and were overlaid on the curves in Figure 4.8. It is worth emphasizing

that the SR gels show a similar neo-Hookean shape over a wide strain range, particularly with a low coverage ratio, indicating effective chain slippage. In addition, the resulting moduli increase through increasing the incorporation of HPCD, which corresponds to the shear moduli obtained through rheological experiments.

In terms of elongation, the SR gels exhibit good stretchability independent of elastic moduli. For example, SR-3.3-0 and SR-3.6-4.7 show fracture strains of 460±50% and 530±30% respectively. Kato et al. reported that as more macrocycles are threaded on the backbone chains, a stronger "repulsion" force would make the resulting gels stiffer with a lower extension to break.[31] In the reported study, Kato et al. used dense α-CD/PEG polyrotaxanes typically with a coverage ratio of 5–25% and a polymer M_w of 35–350 kDa (for highly extensible material).[47] In contrast, we used sparse β-CD/PEG polyrotaxanes with a coverage ratio of 2–6%, suggesting that crosslinks are still able to slide along the chain fully with only minimal chain stretching. Consequently, this type of SR network exhibits nearly constant stretchability.[31,51]

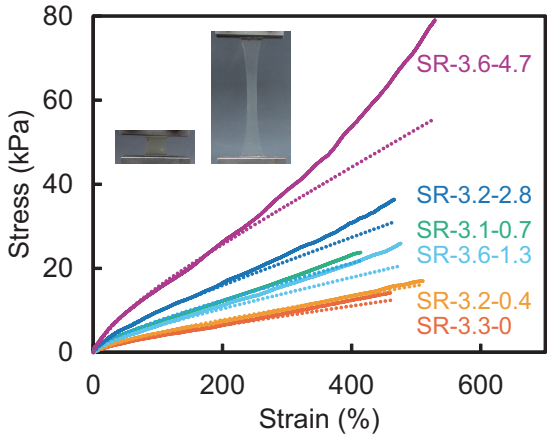

Figure 4.8. Stress-strain curves of the SR gels under uniaxial tensile loading. The strain rate is 200% min^{-1}. The dotted lines denote the fitted curves based on the neo-Hookean model.

Swelling behavior of SR gels

One reason for the increased interest in gels with sliding crosslinks is the

expectation that the crosslink sliding process may allow a higher swellability when compared to gels with similar chain lengths but fixed covalent crosslinks. Hence equilibrium swelling experiments were carried out to evaluate pure SR networks without isolated HPCD and those with HPDC sliding spacers to confirm swelling behavior. The pristine SR gels were initially immersed in water at room temperature for a week to achieve an equilibrium state. Swelling ratios *Q* were then calculated by gravimetric analysis, and are depicted in Figure 4.9 with respect to the HPCD content in the SR gels. Importantly, the incorporation of HPCD changes the swelling behavior of the SR network dramatically. SR-3.3-0 absorbs ~90 times its dry weight in water, while SR-3.6-4.7 absorbs less than half that amount with all of the gels absorbing more than 40 times their dry weights, which is higher than for other SR gels with no spacers.[37] This high swellability, which corresponds to linear extensions between 4 and 5, suggests that the crosslinks slide and that the elastic properties of the gels are heavily influenced by the sliding crosslinks. The observed decrease in swelling ratio with increasing number of sliding spacers is most likely a result of the sliding spacers counteracting the sliding of the crosslinks as is seen in the elastic behavior.

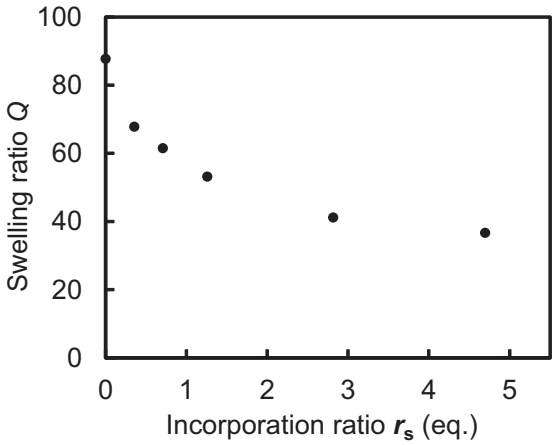

Figure 4.9. Swelling ratios *Q* of the SR gels plotted against the incorporation ratio r_s of HPCD.

Dynamic frequency sweeps of *G'* of the swollen gels are shown in Figure 4.10. Compared to the pristine gels, *G'* of the swollen gels were around 1 order of magnitude

lower due to dilution. However, the gels once again exhibit dependence on the incorporation of HPCD with minor variations being due to slight changes in polymer concentration of the gels (~15wt%×$C^{-1}Q^{-1}$). It should be noted that the swollen gels were composed of only pure SR networks without any non-threaded HPCD, further illustrating that the sliding spacers play an important role in both elasticity and swelling behavior.

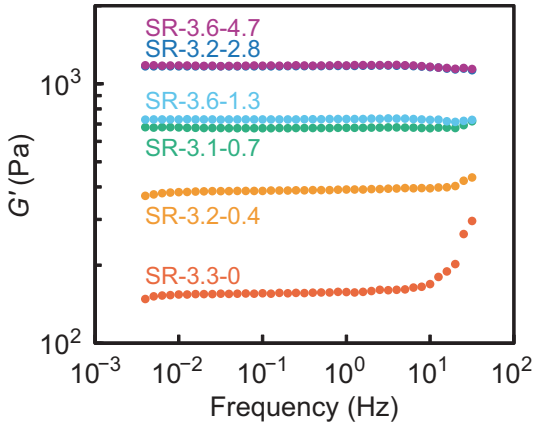

Figure 4.10. Dynamic frequency sweeps of the swollen SR gels (SR-3.2-2.8 overlaps with SR-3.6-4.7 almost entirely).

4.4 Conclusions

In this study, a one-pot strategy for the fabrication of novel slide-ring (SR) gel containing sliding spacers in addition to sliding crosslinks is reported. Thiol-yne click chemistry is utilized for the photo-initiated crosslinking reaction of the *pseudo*-polyrotaxanes that are prepared *in situ* from monothiolated-β-cyclodextrin (CDSH), 2-hydroxypropyl-β-cyclodextrin (HPCD), and polyethylene glycol α,ω-dipropargyl ether. Significantly, the HPCD acts as a sliding spacer threaded onto the polymer backbone in the resulting SR networks. The SR gels were identified by NMR study using a polyrotaxane model compound with the incorporation of HPCD controlled via its feed ratio. It was revealed that the introduction of sliding spacers between the sliding crosslinks afforded substantial improvement in terms of the mechanical properties of the SR gels, i.e. an increased storage modulus, and higher fracture stress

with constant extensibility, as shown via rheology and tensile measurements. Furthermore, we demonstrated that not only the elasticity but the swellability could also be tuned through the density of the sliding spacers. This synthetically simple strategy for SR gels incorporating sliding spacers enables a range of applications for these novel bio-compatible hydrogels while also allowing fundamental insight into our understanding of SR gels.

4.5 References

1. Hoffman, A. S. *Adv. Drug Deliv. Rev.* **2012**, *64*, 18-23.
2. Lee, K. Y.; Mooney, D. J. *Chem. Rev.* **2001**, *101*, 1869-1880.
3. Qiu, Y.; Park, K. *Adv. Drug Deliv. Rev.* **2012**, *64*, 49-60.
4. Tanaka, Y.; Gong, J. P.; Osada, Y. *Prog. Polym. Sci.* **2005**, *30*, 1-9.
5. Gong, J. P.; Katsuyama, Y.; Kurokawa, T.; Osada, Y. *Adv. Mater.* **2003**, *15*, 1155-1158.
6. Chen, Q.; Wei, D.; Chen, H.; Zhu, L.; Jiao, C.; Liu, G.; Huang, L.; Yang, J.; Wang, L.; Zheng, J. *Macromolecules* **2015**, *48*, 8003-8010.
7. Menyo, M. S.; Hawker, C. J.; Waite, J. H. *ACS Macro Lett.* **2015**, *4*, 1200-1204.
8. Murakami, T.; Brown, H. R.; Hawker, C. J. *J. Polym. Sci., Part A: Polym. Chem.* **2016**, 54, 1459-1467.
9. Wang, Q.; Mynar, J. L.; Yoshida, M.; Lee, E.; Lee, M.; Okuro, K.; Kinbara, K.; Aida, T. *Nature* **2010**, *463*, 339-343.
10. Tamesue, S.; Ohtani, M.; Yamada, K.; Ishida, Y.; Spruell, J. M.; Lynd, N. A.; Hawker, C. J.; Aida, T. *J. Am. Chem. Soc.* **2013**, *135*, 15650-15655.
11. Liu, M.; Ishida, Y.; Ebina, Y.; Sasaki, T.; Hikima, T.; Takata, M.; Aida, T. *Nature* **2015**, *517*, 68-72.
12. Bae, K. H.; Wang, L.-S.; Kurisawa, M. *J. Mater. Chem. B* **2013**, *1*, 5371-5388.
13. Guo, M.; Pitet, L. M.; Wyss, H. M.; Vos, M.; Dankers, P. Y.; Meijer, E. W. *J. Am. Chem. Soc.* **2014**, *136*, 6969-6977.
14. Cui, J.; del Campo, A. *Chem. Commun.* **2012**, *48*, 9302-9304.
15. Appel, E. A.; Biedermann, F.; Rauwald, U.; Jones, S. T.; Zayed, J. M.; Scherman, O. A. *J. Am. Chem. Soc.* **2010**, *132*, 14251-14260.

16. Xu, X.; Appel, E. A.; Liu, X.; Parker, R. M.; Scherman, O. A.; Abell, C. *Biomacromolecules* **2015**, *16*, 2743-2749.
17. Schmidt, B. V. K. J.; Hetzer, M.; Ritter, H.; Barner-Kowollik, C. *Prog. Polym. Sci.* **2014**, *39*, 235-249.
18. Tan, S.; Ladewig, K.; Fu, Q.; Blencowe, A.; Qiao, G. G. *Macromol. Rapid Commun.* **2014**, *35*, 1166-1184.
19. Hetzer, M.; Schmidt, B. V. K. J.; Barner-Kowollik, C.; Ritter, H. *Polym. Chem.* **2014**, *5*, 2142-2152.
20. Menyo, M. S.; Hawker, C. J.; Waite, J. H. *Soft Matter* **2013**, *9*, 10314-10323.
21. Fiore, G. L.; Klinkenberg, J. L.; Pfister, A.; Fraser, C. L. *Biomacromolecules* **2009**, *10*, 128-133.
22. Hunt, J. N.; Feldman, K. E.; Lynd, N. A.; Deek, J.; Campos, L. M.; Spruell, J. M.; Hernandez, B. M.; Kramer, E. J.; Hawker, C. J. *Adv. Mater.* **2011**, *23*, 2327-2331.
23. Ortony, J. H.; Choi, S.-H.; Spruell, J. M.; Hunt, J. N.; Lynd, N. A.; Krogstad, D. V.; Urban, V. S.; Hawker, C. J.; Kramer, E. J.; Han, S. *Chem. Sci.* **2014**, *5*, 58-67.
24. Nakahata, M.; Takashima, Y.; Yamaguchi, H.; Harada, A. *Nat. Commun.* **2011**, *2*, 511.
25. Harada, A.; Takashima, Y.; Nakahata, M. *Acc. Chem. Res.* **2014**, *47*, 2128-2140.
26. Harada, A.; Kobayashi, R.; Takashima, Y.; Hashidzume, A.; Yamaguchi, H. *Nat. Chem.* **2011**, *3*, 34-37.
27. Okumura, Y.; Ito, K. *Adv. Mater.* **2001**, *13*, 485-487.
28. de Gennes, P.-G. *Phys. A* **1999**, *271*, 231-237.
29. Arunachalam, M.; Gibson, H. W. *Prog. Polym. Sci.* **2014**, *39*, 1043-1073.
30. Ito, K. *Polym. J.* **2007**, *39*, 489-499.
31. Kato, K.; Okabe, Y.; Okazumi, Y.; Ito, K. *Chem. Commun.* **2015**, *51*, 16180-16183.
32. Kato, K.; Komatsu, H.; Ito, K. *Macromolecules* **2010**, *43*, 8799-8804.
33. Cai, T.; Yang, W. J.; Zhang, Z.; Zhu, X.; Neoh, K.-G.; Kang, E.-T. *Soft Matter* **2012**, *8*, 5612-5620.
34. Tan, S.; Blencowe, A.; Ladewig, K.; Qiao, G. G. *Soft Matter* **2013**, *9*, 5239-5250.
35. Kali, G.; Eisenbarth, H.; Wenz, G. *Macromol. Rapid Commun.* **2015**, *37*, 67-72.
36. Zhou, Y. X.; Fan, X. D.; Xue, D.; Xing, J. W.; Kong, J. *React. Funct. Polym.* **2013**, *73*, 508-517.

37. Murakami, T.; Schmidt, B. V. K. J.; Brown, H. R.; Hawker, C. J. *Macromolecules* **2015**, *48*, 7774-7781.
38. Ihara, T.; Uemura, A.; Futamura, A.; Shimizu, M.; Baba, N.; Nishizawa, S.; Teramae, N.; Jyo, A. *J. Am. Chem. Soc.* **2009**, *131*, 1386-1387.
39. Fujita, K.; Ueda, T.; Imoto, T.; Tabushi, I.; Toh, N.; Koga, T. *Bioorg. Chem.* **1982**, *11*, 72-84.
40. Lowe, A. B.; Hoyle, C. E.; Bowman, C. N. *J. Mater. Chem.* **2010**, *20*, 4745-4750.
41. Sprafke, J. K.; Spruell, J. M.; Mattson, K. M.; Montarnal, D.; McGrath, A. J.; Pötzsch, R.; Miyajima, D.; Hu, J.; Latimer, A. A.; Voit, B. I.; Aida, T.; Hawker, C. J. *J. Polym. Sci., Part A: Polym. Chem.* **2015**, *53*, 319-326.
42. Loftsson, T.; Duchêne, D. *Int. J. Pharm.* **2007**, *329*, 1-11.
43. Udachin, K. A.; Wilson, L. D.; Ripmeester, J. A. *J. Am. Chem. Soc.* **2000**, *122*, 12375-12376.
44. Mondjinou, Y. A.; McCauliff, L. A.; Kulkarni, A.; Paul, L.; Hyun, S. H.; Zhang, Z.; Wu, Z.; Wirth, M.; Storch, J.; Thompson, D. H. *Biomacromolecules* **2013**, *14*, 4189-4197.
45. Mondjinou, Y. A.; Hyun, S.-H.; Xiong, M.; Collins, C. J.; Thong, P. L.; Thompson, D. H. *ACS Appl. Mater. Interfaces* **2015**, *7*, 23831-23836.
46. Fleury, G.; Schlatter, G.; Brochon, C.; Travelet, C.; Lapp, A.; Lindner, P.; Hadziioannou, G. *Macromolecules* **2007**, *40*, 535-543.
47. Kato, K.; Yasuda, T.; Ito, K. *Macromolecules* **2013**, *46*, 310-316.
48. Kato, K.; Yasuda, T.; Ito, K. *Polymer* **2014**, *55*, 2614-2619.
49. Mayumi, K.; Tezuka, M.; Bando, A.; Ito, K. *Soft Matter* **2012**, *8*, 8179-8183.
50. Ito, K. *Polym. J.* **2012**, *44*, 38-41.
51. Bitoh, Y.; Akuzawa, N.; Urayama, K.; Takigawa, T.; Kidowaki, M.; Ito, K. *Macromolecules* **2011**, *44*, 8661-8667.

Chapter 5

Synthesis of PEO-based Physical Gels with Tunable Viscoelastic Properties

5.1 Introduction

Physical gels are association networks formed via non-covalent crosslinks. The physical crosslinks are based on reversible intermolecular interactions, e.g., hydrogen bonding, electrostatic, or hydrophobic interactions. In general, physical gels exhibit a liquid-to-solid transition derived from a glass transition or gelation, and behave as elastic solids and viscous liquids at short and long time periods, respectively.[1-2] These reversible crosslinks lead to unique rheological and mechanical properties and a number of tunable physical gels based on various kinds of polymers have been reported, e.g., polypeptides,[3] polysaccharides,[4] poly(vinyl alcohol),[5] polyacrylates,[6] and polyacrylamides.[7] Such physical gels have been extensively employed in a variety of biomedical applications, including drug delivery,[8-9] cell encapsulation,[10] tissue engineering,[11-12] and regenerative medicine.[13]

PEO-based physical hydrogels are often desirable for such biomedical applications because they exhibit excellent biocompatibility due to the non-toxic polyether backbone and are often stimuli responsive, injectable, and free from toxic crosslinking agents. Regarding the physical crosslinking mechanism, hydrophobic interactions are advantageous over hydrogen bonding or electrostatic interactions since they are not influenced by pH or ionic strength of the aqueous medium. To realize such materials formed through hydrophobic interactions, poly(ethylene oxide)-*b*-poly(propylene oxide)-*b*-poly(ethylene oxide) (PEO-*b*-PPO-*b*-PEO) triblock copolymers, a subset of which are called Pluronics®,[14] are widely used. These physical gels exhibit micelle and hydrogel formation through association of the hydrophobic PPO blocks. However, due to location of the hydrophobic segment in the middle of the block copolymer,

crosslinking occurs through intermicellar interactions above a critical concentration. As a result, materials derived from Pluronics® have several drawbacks, including weak mechanical properties and limited tunability, which stems from the high polymer concentrations required for gelation.[15] Therefore, hydrogels derived from Pluronics® can lose their mechanical integrity in the body due to dilution below their critical gelation concentrations. Regarding drug delivery applications, this can lead to rapid payload release, shorter relief time for patients and unwanted side effects.[16-17] In addition, Pluronic®-based gels lack tunability of viscoelastic properties in a wide range. Since this is crucial for mimicking natural extracellular matrices and regulating the differentiation of stem cells,[18] these materials are limited in their potential for synthetic cell culture scaffolds.

To overcome the high critical gelation concentration of Pluronic®-based gels, a variety of A-PEO-A triblock architectures have been reported. These PEO-based materials contain hydrophilic PEO as the mid-block and various hydrophobic blocks as end segments, e.g., polyesters (PLA)[19] or polyacrylates (PNIPAm).[20] The assembly of these copolymers leads to the bridging of individual flower-like micelles through triblock copolymers, thus differing considerably from the gelation mechanism of the Pluronic®-based gels, which is based on the packing of individual micelles.[21] As a result, the critical gelation concentration is dramatically lowered in the A-PEO-A gels. However, to the best of our knowledge, the development of similar gel architectures using hydrophobic interactions of *polyether end-blocks* is still in its infancy with only very few examples described in the literature.[21-23] In particular, the evaluation of A-PEO-A triblock-based physical gels with highly tunable stress relaxations has not been achieved in a systematic way. Therefore, the ability to tune and improve the properties of solely polyether-based A-PEO-A physical gels, especially while maintaining their unique properties at high dilution, would be advantageous.

To address this challenge, we aimed to tune the properties of A-PEO-A copolymer hydrogels by precisely controlling the assembly characteristics of the polyether end-blocks in the crosslinking domains.[24] For this, we aimed to vary the hydrophobicity of the end-blocks by tuning their molecular composition, i.e. varying the incorporation of hydrophobic and hydrophilic groups. To achieve this, we have used a modular

synthetic method using post-polymerization functionalization of the end-blocks with different functional groups of varying hydrophobicity. The main benefit of this strategy is that only one polymerization is required, which not only reduces the amount of work, but also ensures that the degree of polymerization is constant amongst the series, resulting in a true evaluation of crosslink modification.

Following this approach, we present a simple synthetic procedure to amphiphilic A-PEO-A triblock copolymers with well-controlled degrees of polymerization and compositions for the formation of physically crosslinked polyether-based hydrogels with a wide range of viscoelastic properties (Figure 5.1). Control over end-block hydrophobicity was achieved by a two-step process. First, starting from bifunctional hydroxyl-terminated PEO, anionic copolymerization of ethylene oxide (EO) with allyl glycidyl ether (AGE) as a reactive monomer was carried out to produce X-PEO-X triblock copolymers, which contained reactive allyl groups in the X end-blocks. Subsequent thiol-ene click coupling with different alkyl thiols was used to prepare a library of amphiphilic A-PEO-A triblock copolymers with A end-blocks of varying hydrophobicity. By systematically changing the length of the alkyl side-chains in the A blocks, control over sol-gel transitions and stress relaxations of the physical gels was achieved.

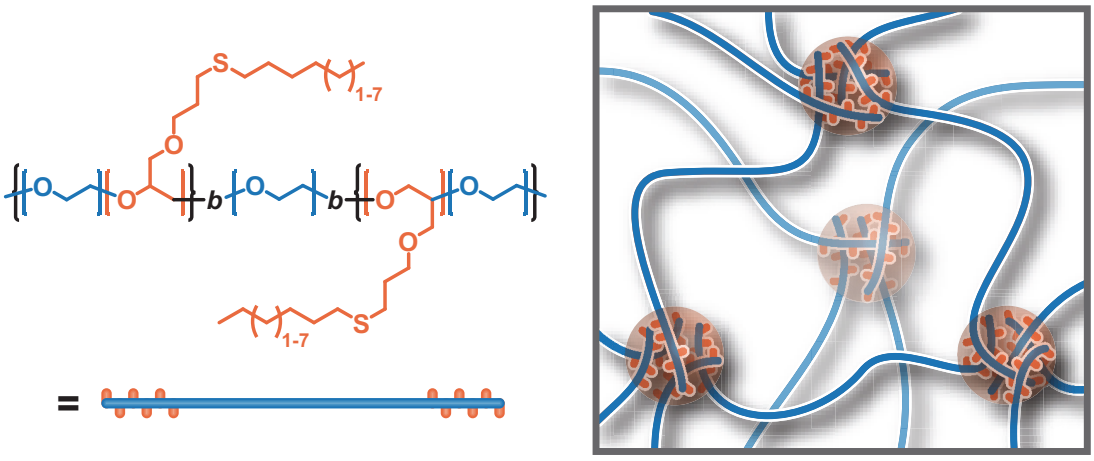

Figure 5.1. Schematic illustration of the chemical structure and the hydrogel formation of the PEO-based triblock copolymer with alkyl side-chains. The blue and red units represent hydrophilic and hydrophobic segments, respectively.

5.2 Experimental Section

Materials. Polyethylene oxide (PEO) and 2,2-dimethoxy-2-phenylacetopheone (DMPA) were purchased from Sigma-Aldrich. Ethylene oxide (EO) was purchased from Praxair. Allyl glycidyl ether (AGE) and 1-alkanethiols were purchased from Tokyo Chemical Industry. EO was distilled into a flame-dried buret, and kept at 0 °C in an ice-water bath until use. AGE was degassed through freeze-pump-thaw cycles, and distilled from *n*-butyl magnesium chloride into a flame-dried buret for storage. Tetrahydrofuran (THF) was collected from a dry solvent system equipped with two columns containing activated alumina and copper, and used immediately thereafter. Potassium naphthalenide (0.3 M in THF) was prepared from potassium metal (2.9 g) and naphthalene (9.6 g) in dry THF (250 mL), and stirred with a glass-coated stir-bar for 24 h at room temperature before use.

Characterization. ^{1}H and ^{13}C NMR spectra were recorded at 25 °C on a Varian VNMRS 600 spectrometer (600 and 150 MHz respectively). Chemical shifts are reported relative to residual solvent peaks in ^{1}H (δ 7.26 ppm for $CDCl_3$) and ^{13}C NMR (δ 77.16 ppm for $CDCl_3$). Gel permeation chromatography (GPC) was performed on a Waters 2695 separation module equipped with a Waters 2410 differential refractometer and a Waters 2998 photodiode array detector. Chloroform with 0.25% of triethylamine was used as an eluent at a flow rate of 1 mL/min. Molar mass and molar mass dispersity (Đ) were calculated relative to linear polystyrene standards. Rheological experiments were carried out at 25 °C on a TA Instruments ARES-LS1 rheometer equipped with a cone-and-plate geometry (25 mm diameter). Dynamic sweeps were performed at a frequency of 1 Hz or a strain of 1%. Stress relaxation was recorded after a strain of 5% was applied at 0 s. Swelling experiments were performed as follows. The pristine gels were roughly crushed and immersed in deionized water at room temperature for a week until an equilibrium swollen state was reached. The resulting swollen gels were collected by centrifuge, and dried in vacuo to calculate the equilibrium concentration of the swollen gels from the weight ratio of the swollen gels and the dried gels.

Synthesis of poly[(ethylene oxide)-*co*-(allyl glycidyl ether)]-*block*-poly(ethylene oxide)-*block*-poly[(ethylene oxide)-*co*-(allyl glycidyl ether)] PC_0. Anionic ring-

opening polymerization of epoxides was carried out according to the previously reported method.[25] A reactor and a Schlenk line were flame-dried under vacuum and purged with argon. PEO (M_n 20 kDa) was placed in the reactor, dried in vacuo, and dissolved in dry THF. Potassium naphthalenide (0.3 M in THF) was added dropwise by syringe until a light green color persisted in solution, indicating complete deprotonation of the macroinitiator. After adding EO (170 eq. to PEO) and AGE (20.7 eq. to PEO) to the reactor under an argon atmosphere, polymerization was carried out at 40 °C for 3 days. The polymerization was terminated with degassed methanol and poured into hexane. The resulting precipitate was filtered, washed with hexane, and dried in vacuo. The polymer was obtained as a white solid (yield 95%) and identified by ^{1}H, ^{13}C NMR and GPC.

[$EO_{75.4}$-*co*-$AGE_{10.3}$]-*b*-[EO_{454}]-*b*-[$EO_{75.4}$-*co*-$AGE_{10.3}$], **PC_0**. M_n 4.5k-20k-4.5k (^{1}H NMR). Đ 1.07 (GPC). ^{1}H NMR (600 MHz, $CDCl_3$): δ (ppm) 1.54 (d, *J*=8.4 Hz, -O-CH=CH-C$\underline{H}_3$), 3.47-3.75 (broad m, PEO main-chain), 3.98 (d, *J*=5.4 Hz, -O-C$\underline{H}_2$-CH=CH_2), 4.34 (quin, *J*=6.6 Hz, -O-CH=C$\underline{H}$-CH_3), 5.13-5.26 (m, -O-CH_2-CH=C$\underline{H}_2$), 5.84-5.90 (m, -O-CH_2-C$\underline{H}$=CH_2), 5.95 (d, *J*=4.2 Hz, -O-C$\underline{H}$=CH-CH_3). Each end-block contains 12 mol% of AGE units (including 1.2 mol% of the vinyl isomers).

Synthesis of poly[(ethylene oxide)-*co*-(3-alkylthiopropoxy glycidyl ether)]-*block*-poly(ethylene oxide)-*block*-poly[(ethylene oxide)-*co*-(3-alkylthiopropoxy glycidyl ether)] PC_x. General procedure for alkyl functionalization via thiol-ene click reaction is as follows.[26] Polyether PC_0 (M_n 29.0 kDa, 0.020 mmol) was placed in a Pyrex round bottom flask and dissolved in dry THF (10 mL). To the solution were added 1-alkanethiol (5.0 eq. to AGE units in PC_0, 2.0 mmol) and 2,2-dimethoxy-2-phenylacetophenone (0.5 mol% to AGE units in PC_0, 0.002 mmol). The solution was degassed through argon bubbling for 30 min, and subsequently irradiated by UV light (λ_{max} 365 nm, 15 W) at room temperature for 5 h while stirring. The reaction mixture was evaporated under reduced pressure, and precipitated from hexane. The resulting solid was filtered and washed with hexane several times. The polymer was obtained after drying as a white solid (conversion >93%) and identified by ^{1}H, ^{13}C NMR and GPC. Of the 20 AGE units in **PC_0,** a small percentage (10 mol%, 2 units) isomerized, which is common in these systems. Additionally, 17~21 mol% of the alkyl branches in

PC$_{6\text{-}12}$ are isomers derived from Markovnikov addition of thiols to the allyl groups and anti-Markovnikov addition of thiols to the vinyl isomers.

PC$_6$ (*n*-hexyl). M_n 5.7k-20k-5.7k (^{1}H NMR). Đ 1.10 (GPC). ^{1}H NMR (600 MHz, $CDCl_3$): δ (ppm) 0.86 (t, *J*=6.9 Hz, -S-$(CH_2)_5$-C$\underline{H}_3$), 1.23-1.30 (m, -S-$(CH_2)_3$-($C\underline{H}_2$)$_2$-CH_3), 1.35 (quin, *J*=7.7 Hz, -S-$(CH_2)_2$-$C\underline{H}_2$-$(CH_2)_2$-CH_3), 1.55 (quin, *J*=7.4 Hz, -S-CH_2-$C\underline{H}_2$-$(CH_2)_3$-CH_3), 1.80 (quin, *J*=6.8 Hz, -O-CH_2-$C\underline{H}_2$-CH_2-S-), 2.47 (t, *J*=7.2 Hz, -O-CH_2-CH_2-$C\underline{H}_2$-S-), 2.54 (t, *J*=7.2 Hz, -S-$C\underline{H}_2$-$(CH_2)_4$-CH_3), 3.44-3.74 (broad m, PEO main-chain). Degree of substitution 99%.

PC$_7$ (*n*-heptyl). M_n 31.8 kDa (^{1}H NMR). Đ 1.10 (GPC). ^{1}H NMR (600 MHz, $CDCl_3$): δ (ppm) 0.86 (t, *J*=6.9 Hz, -S-$(CH_2)_6$-C$\underline{H}_3$), 1.24-1.30 (m, -S-$(CH_2)_3$-($C\underline{H}_2$)$_3$-CH_3), 1.35 (quin, *J*=7.2 Hz, -S-$(CH_2)_2$-$C\underline{H}_2$-$(CH_2)_3$-CH_3), 1.55 (quin, *J*=7.5 Hz, -S-CH_2-$C\underline{H}_2$-$(CH_2)_4$-CH_3), 1.81 (quin, *J*=6.8 Hz, -O-CH_2-$C\underline{H}_2$-CH_2-S-), 2.47 (t, *J*=7.5 Hz, -O-CH_2-CH_2-$C\underline{H}_2$-S-), 2.54 (t, *J*=7.2 Hz, -S-$C\underline{H}_2$-$(CH_2)_5$-CH_3), 3.45-3.75 (broad m, PEO main-chain). Degree of substitution 100%.

PC$_8$ (*n*-octyl). M_n 32.0 kDa (^{1}H NMR). Đ 1.10 (GPC). ^{1}H NMR (600 MHz, $CDCl_3$): δ (ppm) 0.86 (t, *J*=6.9 Hz, -S-$(CH_2)_7$-C$\underline{H}_3$), 1.22-1.30 (m, -S-$(CH_2)_3$-($C\underline{H}_2$)$_4$-CH_3), 1.35 (m, -S-$(CH_2)_2$-$C\underline{H}_2$-$(CH_2)_4$-CH_3), 1.55 (quin, *J*=7.5 Hz, -S-CH_2-$C\underline{H}_2$-$(CH_2)_5$-CH_3), 1.81 (quin, *J*=6.8 Hz, -O-CH_2-$C\underline{H}_2$-CH_2-S-), 2.47 (t, *J*=7.5 Hz, -O-CH_2-CH_2-$C\underline{H}_2$-S-), 2.54 (t, *J*=7.2 Hz, -S-$C\underline{H}_2$-$(CH_2)_6$-CH_3), 3.45-3.75 (broad m, PEO main-chain). Degree of substitution 100%.

PC$_{10}$ (*n*-decyl). M_n 32.3 kDa (^{1}H NMR). Đ 1.10 (GPC). ^{1}H NMR (600 MHz, $CDCl_3$): δ (ppm) 0.86 (t, *J*=7.2 Hz, -S-$(CH_2)_9$-C$\underline{H}_3$), 1.21-1.30 (m, -S-$(CH_2)_3$-($C\underline{H}_2$)$_6$-CH_3), 1.35 (m, -S-$(CH_2)_2$-$C\underline{H}_2$-$(CH_2)_6$-CH_3), 1.55 (quin, *J*=7.4 Hz, -S-CH_2-$C\underline{H}_2$-$(CH_2)_7$-CH_3), 1.81 (quin, *J*=6.8 Hz, -O-CH_2-$C\underline{H}_2$-CH_2-S-), 2.47 (t, *J*=6.9 Hz, -O-CH_2-CH_2-$C\underline{H}_2$-S-), 2.54 (t, *J*=7.8 Hz, -S-$C\underline{H}_2$-$(CH_2)_8$-CH_3), 3.45-3.75 (broad m, PEO main-chain). Degree of substitution 93%.

PC$_{12}$ (*n*-dodecyl). M_n 33.2 kDa (^{1}H NMR). Đ 1.10 (GPC). ^{1}H NMR (600 MHz, $CDCl_3$): δ (ppm) 0.86 (t, *J*=7.2 Hz, -S-$(CH_2)_{11}$-C$\underline{H}_3$), 1.21-1.30 (m, -S-$(CH_2)_3$-($C\underline{H}_2$)$_8$-CH_3), 1.35 (m, -S-$(CH_2)_2$-$C\underline{H}_2$-$(CH_2)_8$-CH_3), 1.55 (quin, *J*=7.4 Hz, -S-CH_2-$C\underline{H}_2$-$(CH_2)_9$-CH_3), 1.81 (quin, *J*=6.8 Hz, -O-CH_2-$C\underline{H}_2$-CH_2-S-), 2.47 (t, *J*=7.5 Hz, -O-CH_2-CH_2-$C\underline{H}_2$-S-), 2.54 (t, *J*=7.5 Hz, -S-$C\underline{H}_2$-$(CH_2)_{10}$-CH_3), 3.44-3.75 (broad m, PEO main-chain). Degree of substitution

100%.

Preparation of the hydrogels. Polyethers **PC$_{6\text{-}12}$** were quickly mixed with deionized water and vigorously vortexed at room temperature to obtain aqueous mixtures. The mixtures were left a day, resulting in the complete dissolution of the polyethers. After this aging process, clear colorless hydrogels were collected by centrifugation.

5.3 Results and Discussion

Synthesis of triblock copolymers

The precursor triblock copolymer, containing pendant allyl functionalities in the end-blocks, was synthesized via statistical anionic ring-opening polymerization of ethylene oxide (EO) and allyl glycidyl ether (AGE) from a difunctional PEO macroinitiator, as shown in Scheme 1.[25] Although ABA-type triblock copolymers are common architectures for use in physical gels,[17] the presented polyethers have the specific combination of moderately hydrophilic end-blocks (EO$_{75}$-AGE$_{10}$) and a hydrophilic mid-block (EO$_{454}$). As a result, the backbone of the end-blocks, to a large extent, resembles PEO, with only ~12 mol% of repeat units being functionalized with allyl units (~3 mol% with respect to the triblock). This is in direct contrast to PPO-*b*-PEO-*b*-PPO,[22] where the mid-block is identical to that of this study but the end-blocks are wholly derived from propylene oxide, PO, repeat units, thus lacking tunability. The obtained P[EO-*co*-AGE]-*b*-PEO-*b*-P[EO-*co*-AGE] (**PC$_0$**) triblock was fully characterized by NMR and GPC, revealing a number-average molar mass (M_n) of 4500-20000-4500 with the end-blocks containing ~10 AGE units per A-block.

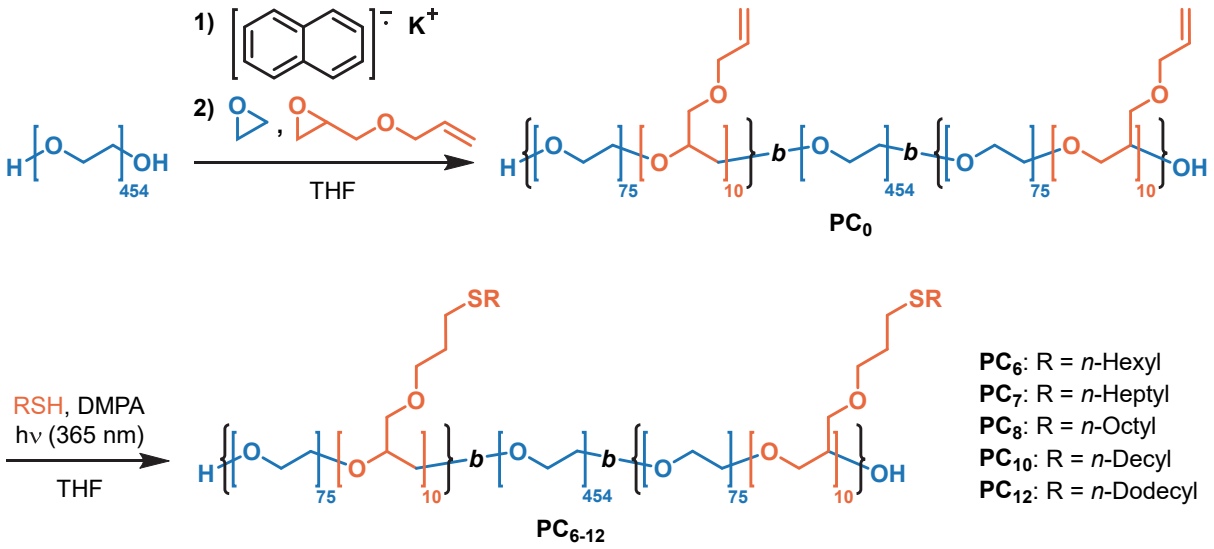

Scheme 5.1. Synthesis of alkyl-functionalized triblock copolymers **PC**$_{6\text{-}12}$.

A key feature of this synthetic design is the ability to use the same starting triblock copolymer, **PC**$_0$, for preparation of the target hydrogel library. Functionalization of **PC**$_0$ via thiol-ene click coupling with 1-alkanethiols,[26] where the number of carbons in the alkyl side-chains was varied between 6 and 12, yields a series of PEO-based triblocks: **PC**$_6$, **PC**$_7$, **PC**$_8$, **PC**$_{10}$, and **PC**$_{12}$ with *n*-hexyl, *n*-heptyl, *n*-octyl, *n*-decyl, and *n*-dodecyl groups, respectively. Near-quantitative functionalization of the starting triblock copolymer was demonstrated by ^{1}H NMR, with Figure 5.2 clearly showing the disappearance of resonances corresponding to the allyl units and the appearance of resonances for the alkyl chains. Importantly, GPC measurements revealed uniform, unimodal peaks with low molar mass dispersities (Đ ~ 1.1) for all functionalized copolymers, suggesting that the multiple thiol-ene functionalization reactions per backbone occur efficiently, with little to no side-reactions such as crosslinking. Based on the combination of controlled anionic ring-opening polymerization and a common starting material with quantitative thiol-ene click chemistry, well-defined functional triblock copolymers were obtained with precise tuning of polymer end-block hydrophobicity.

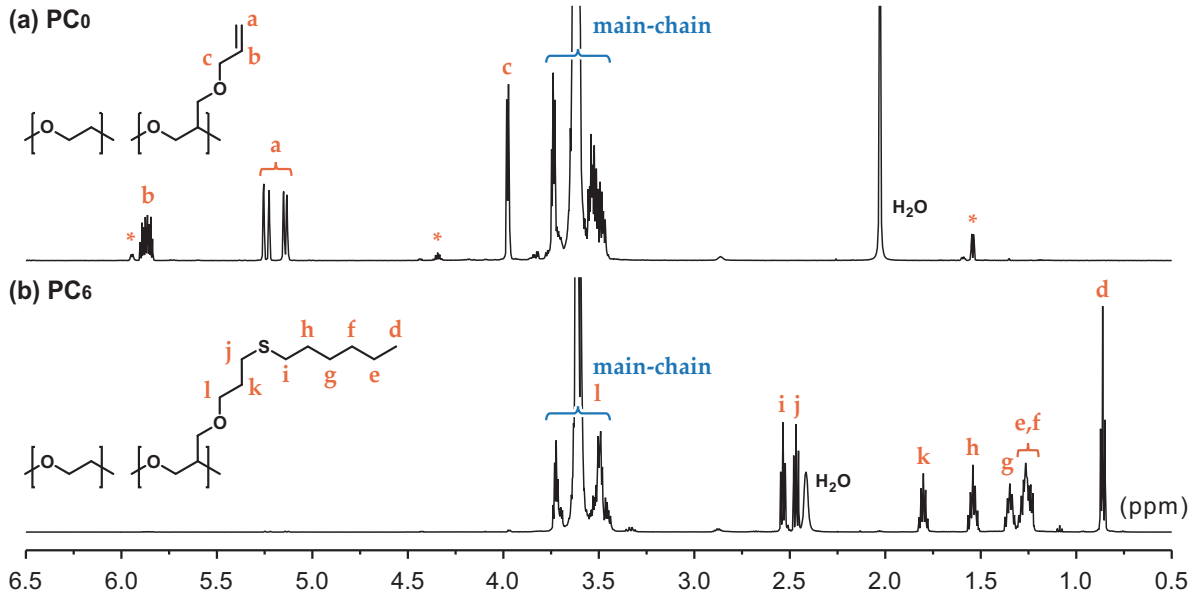

Figure 5.2. Comparison of ^{1}H NMR spectra between before (a, **PC$_0$**) and after (b, **PC$_6$**) functionalization. Asterisks denote protons derived from vinyl isomers. Chemical structures of the hydrophobic repeat units are shown in the insets.

Preparation of hydrogels

The physical gels were fabricated by first completely mixing the series of polyethers (**PC$_{6\text{-}12}$**) with deionized water. Upon swelling the polymers, the mixtures reached an equilibrium state after 24 hours, yielding homogeneous hydrogels at room temperature. Initial qualitative evaluation of hydrogel formation involved formation of a series of 5 wt% hydrogels that were then submitted to a vial inversion test (Figure 5.3). Interestingly, a well-defined trend for flow was observed across the samples: Hydrogels based on **PC$_6$** showed complete flow within 2 hours (liquid state), while samples prepared from **PC$_{10}$** and **PC$_{12}$** remained intact on this timescale (gel state). These preliminary experiments clearly indicate the influence of alkyl chain length on the viscoelastic properties of the corresponding triblock copolymer hydrogels, with the longer alkyl chains enhancing gel formation due to more stable hydrophobic associations. Additionally, it is also worth pointing out that the hydrogel of **PC$_{12}$** was slightly turbid, inferring that the end-blocks of **PC$_{12}$** may collapse and aggregate in water at room temperature. Temperature responsive behaviors and lower critical

solution temperatures of these hydrogels will be a matter for future investigation.

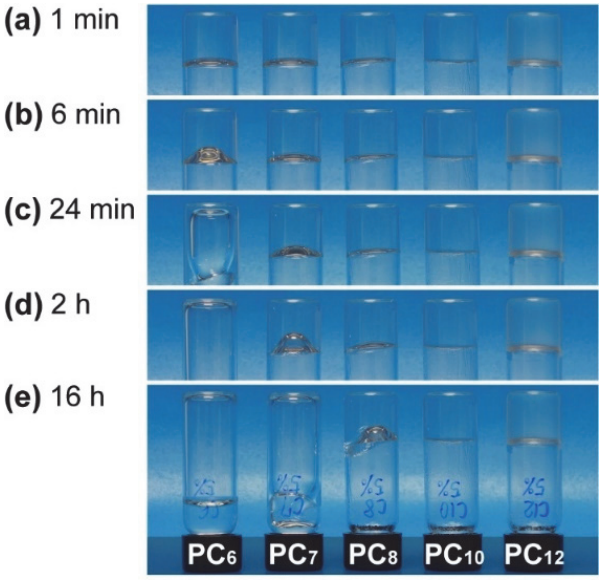

Figure 5.3. Photo images of the vial inversion test of 5 wt% aqueous solutions of **PC$_{6\text{-}12}$** from 1 min (a) to 16 h (e).

Rheological properties

Next, we evaluated the rheological properties of the physical gels in detail at room temperature (25 °C). Figure 5.4a-b shows dynamic frequency sweeps of the series of 5 wt% hydrogels containing **PC$_{6\text{-}12}$** at a strain of 1%. All hydrogels reached storage moduli of over 2 kPa at a low concentration. As the vial inversion test revealed, hydrogels containing polymers with shorter hydrophobic side-chains (e.g., **PC$_6$**) behaved more like viscous liquids (at low frequencies, 10^{-3} to 10^{-1} Hz) and those containing polymers with longer side-chains behaved like solids (over a range of frequencies, e.g., **PC$_{12}$**, 10^{-3} to 10 Hz). Figure 5.4c-d shows dynamic strain sweeps of 5 wt% hydrogels of **PC$_{6\text{-}12}$** at a frequency of 1 Hz. Notably, all the hydrogels except for **PC$_{12}$** yielded above a strain of 10% and exhibited shear thinning effects at high shear rates, which can be favorable for injectable gel applications.[27]

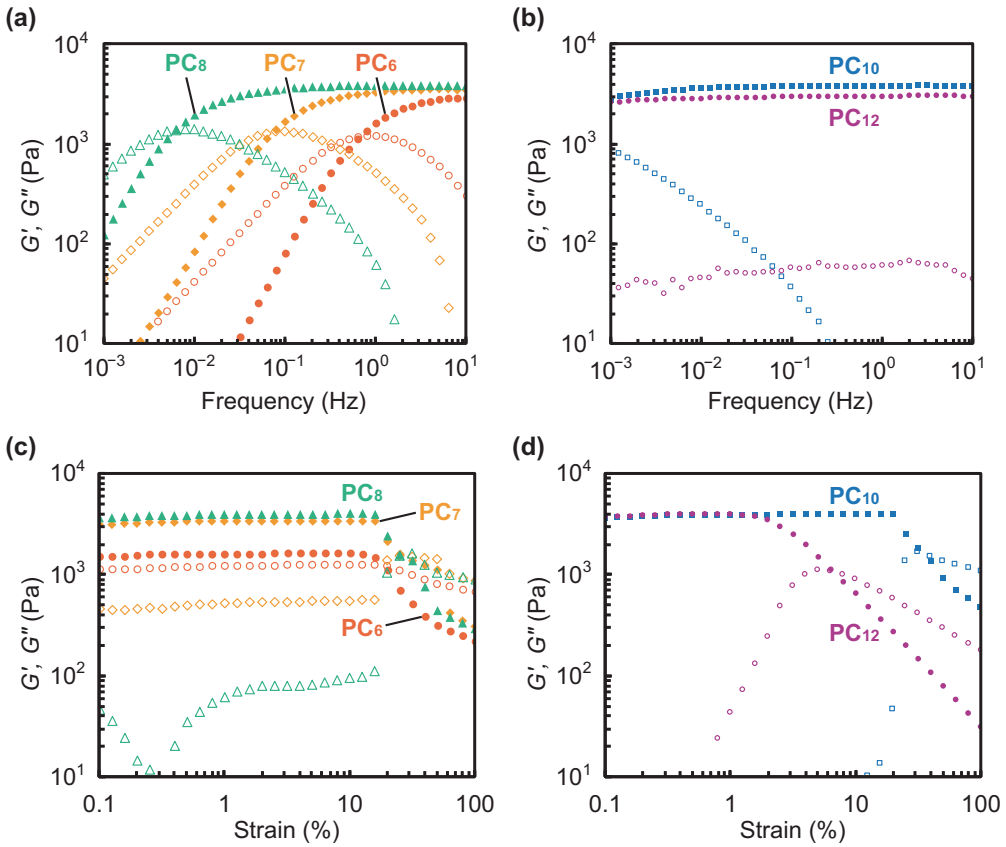

Figure 5.4. Dynamic frequency (a, b) and strain (c, d) sweeps of 5 wt% hydrogels of **PC**$_{6\text{-}12}$. Filled symbols denote G' and open symbols denote G''.

We performed stress relaxation experiments to clarify the relaxation behaviors more thoroughly. Relaxation moduli ($G(t)$) of **PC**$_{6\text{-}12}$ were recorded after a strain of 5% was applied at 0 s, as shown in Figure 5.5a. **PC**$_{6\text{-}10}$ have simple exponential relaxations, while **PC**$_{12}$ has a two-step relaxation; we predict the faster one is derived from relaxation at macro scales regarding aggregated microgels, and the slower one is derived from relaxation at micro scales occurring inside the microgels.[28] Relaxation time (τ) were determined from these experiments under the assumption that the relaxation has a single component for **PC**$_{6\text{-}10}$ or a double component for **PC**$_{12}$, calculated by curve fitting with exponential decay, using a generalized Maxwell model, and plotted against the length of the alkyl side-chains (Figure 5.5b). In addition, relaxation times from frequency sweeps were also determined to be $\tau = \omega^{-1}$, where ω is the angular frequency where G' crossed G''. These two results are highly consistent with each other

and show that the relaxation times of **PC$_{6\text{-}12}$** depend exponentially on the length of the alkyl side-chains ($\tau \propto \exp(n)$ or $\log\tau \propto n$). In the present systems, the hydrophobic side-chains likely associated to form multiple-chain junction domains. Consequently, by making small changes to the length of the hydrophobic side-chains in the end-blocks, the chain mobilities in the junction domains were dramatically changed. Accordingly, the viscoelastic properties of the resultant hydrogels are highly tunable (relaxation times range from 10^{-1} to 10^{5} s). Having a highly tunable hydrogel system is especially advantageous for optimizing cell culture scaffolds for applications such as regulating the fate of stem cells.[18]

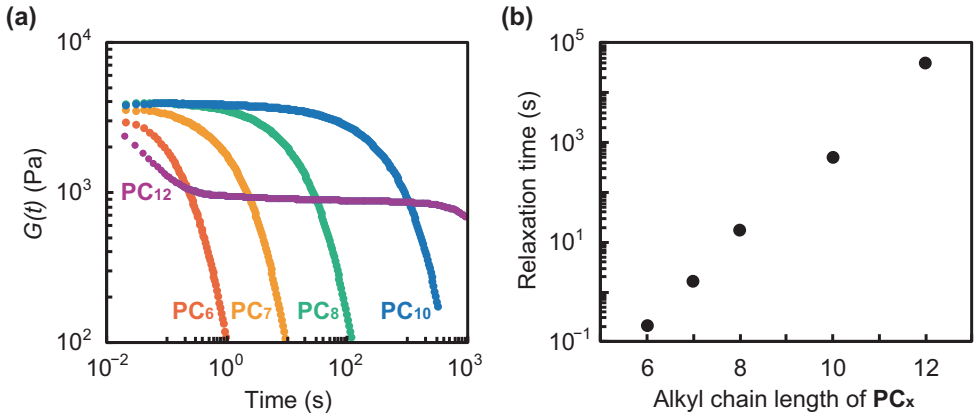

Figure 5.5. (a) Stress relaxation curves of 5 wt% hydrogels of **PC$_{6\text{-}12}$**. (b) Relaxation times of 5 wt% hydrogels of **PC$_{6\text{-}12}$** plotted against the length of the alkyl side-chains.

Swelling properties

To further understand hydrogel formation within this series of triblock copolymers, equilibrium swelling of the physical gels was also examined to provide information about the polymer network. Initially, the hydrogels were immersed in excess deionized water for a week. The resulting swollen hydrogels were centrifuged, weighed, dried and weighed again to calculate the concentrations of the hydrogels at their equilibrium swollen states (wt% of polymers to water at equilibrium swollen states). The equilibrium concentrations of **PC$_{6\text{-}12}$** were approximately 3 wt% (Table 5.1), indicating efficient formation of random polymer networks via intermolecular interactions between hydrophobic end-blocks. On the contrary, our previously

reported PPO-*b*-PEO-*b*-PPO (M_n 4.0k-20k-4.0k) were extremely brittle especially in an atactic counterpart, and their equilibrium concentrations were 17-19 wt% and significantly higher than the present materials.[22] From these results, physical gels derived from the presented ABA-type amphiphilic triblock copolymers are more likely to retain their mechanical integrity after injected into the body; this characteristic makes them promising candidates for drug delivery systems.

Table 5.1. Summary of the characterization of **PC$_{6\text{-}12}$**.

Polymer	R group	M_n (NMR)	Đ (GPC)	G' (Pa) [1,4]	τ (s) [2,4]	C (wt%) [3]
PC$_0$	-	4.5k-20k-4.5k	1.07	-	-	-
PC$_6$	*n*-Hexyl	5.7k-20k-5.7k	1.10	2880	0.209±0.004	2.5
PC$_7$	*n*-Heptyl	5.9k-20k-5.9k	1.10	3300	1.63±0.03	2.8
PC$_8$	*n*-Octyl	6.0k-20k-6.0k	1.10	3610	16.9±0.3	3.2
PC$_{10}$	*n*-Decyl	6.2k-20k-6.2k	1.10	3500	506±12	3.1
PC$_{12}$	*n*-Dodecyl	6.6k-20k-6.6k	1.10	2950	39100±300	2.7

[1] Storage moduli recorded at a frequency of 50 Hz and a strain of 1%. [2] Relaxation times calculated from stress relaxation. [3] Polymer concentrations at an equilibrium swollen state in deionized water. [4] Based on 5 wt% hydrogels of **PC$_{6\text{-}12}$** as prepared.

5.4 Conclusions

A P[EO-*co*-AGE]-*b*-PEO-*b*-P[EO-*co*-AGE] triblock copolymer, coupled with highly reliable thiol-ene click chemistry was used to synthesize a series of PEO-based polymers with alkyl side-chains of different lengths located in the end-blocks. Physically crosslinked hydrogels of these polymers were formed due to the intermolecular hydrophobic interactions of the alkyl side-chains. Their sol-gel transitions and rates of stress relaxation were precisely tuned over a wide range based on the length of the alkyl side-chains. We believe that this approach can push the

limitations of PEO-based hydrogels and enable us to tailor hydrogels to exhibit desired properties. The physical gels fabricated through this approach may be a candidate for the next generation polyether platform for drug delivery systems and cell culture scaffolds.

5.5 References

1. Peppas, N. A.; Hilt, J. Z.; Khademhosseini, A.; Langer, R. *Adv. Mater.* **2006**, *18*, 1345-1360.
2. Winter, H. H. *Macromolecules* **2013**, *46*, 2425-2432.
3. Yan, C.; Pochan, D. J. *Chem. Soc. Rev.* **2010,** *39*, 3528-3540.
4. Fitzgerald, M. M.; Bootsma, K.; Berberich, J. A.; Sparks, J. L. *Biomacromolecules* **2015**, *16*, 1497-1505.
5. Alves, M.-H.; Jensen, B. E. B.; Smith, A. A. A.; Zelikin, A. N. *Macromol. Biosci.* **2011**, *11*, 1293-1313.
6. Miquelard-Garnier, G.; Demoures, S.; Creton, C.; Hourdet, D. *Macromolecules* **2006**, *39*, 8128-8139.
7. Tuncaboylu, D. C.; Sari, M.; Oppermann, W.; Okay, O. *Macromolecules* **2011**, *44*, 4997-5005.
8. Hoare, T. R.; Kohane, D. S. *Polymer* **2008**, *49*, 1993-2007.
9. Qiu, Y.; Park, K. *Adv. Drug Deliv. Rev.* **2001**, *53*, 321-39.
10. Wang, C.; Varshney, R. R.; Wang, D.-A. *Adv. Drug Deliv. Rev.* **2010**, *62*, 699-710.
11. Zhu, J.; Marchant, R. E. *Expert Rev. Med. Devices* **2011,** *8*, 607-626.
12. Tibbitt, M. W.; Anseth, K. S. *Biotechnol. Bioeng.* **2009**, *103*, 655-63.
13. Annabi, N.; Tamayol, A.; Uquillas, J. A.; Akbari, M.; Bertassoni, L. E.; Cha, C.; Camci-Unal, G.; Dokmeci, M. R.; Peppas, N. A.; Khademhosseini, A. *Adv. Mater.* **2014**, *26*, 85-124.
14. Alexandridis, P.; Alan Hatton, T. *Colloids Surf. A Physicochem. Eng. Asp.* **1995**, *96*, 1-46.
15. Roy, D.; Brooks, W. L. A.; Sumerlin, B. S. *Chem. Soc. Rev.* **2013**, *42*, 7214-7243.
16. Li, Y.; Rodrigues, J.; Tomás, H. *Chem. Soc. Rev.* **2012**, *41*, 2193-2221.
17. Huynh, C. T.; Nguyen, M. K.; Lee, D. S. *Macromolecules* **2011**, *44*, 6629-6636.

18. Chaudhuri, O.; Gu, L.; Klumpers, D.; Darnell, M.; Bencherif, S. A.; Weaver, J. C.; Huebsch, N.; Lee, H.-p.; Lippens, E.; Duda, G. N.; Mooney, D. J. *Nat. Mater.* **2016**, *15*, 326-334.
19. Kissel, T.; Li, Y.; Unger, F. *Adv. Drug Deliv. Rev.* **2002**, *54*, 99-134.
20. Filippov, S. K.; Bogomolova, A.; Kaberov, L.; Velychkivska, N.; Starovoytova, L.; Cernochova, Z.; Rogers, S. E.; Lau, W. M.; Khutoryanskiy, V. V.; Cook, M. T. *Langmuir* **2016**, *32*, 5314-5323.
21. Mortensen, K.; Brown, W.; Jorgensen, E. *Macromolecules* **1994**, *27*, 5654-5666.
22. McGrath, A. J.; Shi, W.; Rodriguez, C. G.; Kramer, E. J.; Hawker, C. J.; Lynd, N. A. *Polym. Chem.* **2015**, *6*, 1465-1473.
23. Mihajlovic, M.; Staropoli, M.; Appavou, M.-S.; Wyss, H. M.; Pyckhout-Hintzen, W.; Sijbesma, R. P. *Macromolecules* **2017**, *50*, 3333-3346.
24. Anseth, K. S.; Bowman, C. N.; Brannon-Peppas, L. *Biomaterials* **1996**, *17*, 1647-1657.
25. Lee, B. F.; Kade, M. J.; Chute, J. A.; Gupta, N.; Campos, L. M.; Fredrickson, G. H.; Kramer, E. J.; Lynd, N. A.; Hawker, C. J. *J. Polym. Sci., Part A: Polym. Chem.* **2011**, *49*, 4498-4504.
26. Dimitriou, M. D.; Zhou, Z.; Yoo, H. S.; Killops, K. L.; Finlay, J. A.; Cone, G.; Sundaram, H. S.; Lynd, N. A.; Barteau, K. P.; Campos, L. M.; Fischer, D. A.; Callow, M. E.; Callow, J. A.; Ober, C. K.; Hawker, C. J.; Kramer, E. J. *Langmuir* **2011**, *27*, 13762-13772.
27. Guvendiren, M.; Lu, H. D.; Burdick, J. A. *Soft Matter* **2012**, *8*, 260-272.
28. Mohan, L.; Cloitre, M.; Bonnecaze, R. T. *J. Rheol.* **2014**, *59*, 63-84.

Chapter 6

Thermoresponsive Ionic Coacervate Gels with Hydrophobic Cores

6.1 Introduction

Hydrogels constructed via ionic bonding have attracted many researchers thanks to their facile preparations, mechanical toughness, and self-healing properties. These features are derived from reversible but relatively strong non-covalent crosslinking between positively and negatively charged moieties. Alginate and hyaluronate hydrogels are among the most studied natural compounds of this class for various bio-applications, exhibiting mechanical toughness when crosslinked together with cationic compounds. Recently, Gong et al. reported synthetic hydrogels with superior mechanical properties, prepared utilizing electrostatic interactions.[1] In recent years, we have developed hydrogels prepared via ionic coacervation of polyelectrolytes, which typically consist of a pair of an ABA-type triblock copolymer with sulfonate-moieties in both of the "A" end-blocks and an analog with guanidinium-moieties instead of sulfonates.[2] The coacervate hydrogels have turned out to form regularly ordered structures of coacervate domains and show high storage modulus values, and are hopeful candidates for various biomedical applications such as carriers for drug delivery system (DDS).

Controlled drug release in response to external stimuli, e.g. temperature, pH, and light, has been strongly desired for practical applications of DDS. For example, an amphiphilic triblock polyether poly(ethylene oxide)-*b*-poly(propylene oxide)-*b*-poly(ethylene oxide) (PEO-PPO-PEO) called Pluronic is widely used as drug carriers due to their temperature responsive properties. On the other hand, there has been no report about temperature responsive coacervate gels.

Herein, we report novel coacervate hydrogels with a hydrophobic core in each of

the coacervate domains which shows temperature responsive properties. An amphiphilic ABA-type triblock copolymer (ionic-hydrophobic-ionic) with a PPO mid-block ("B") and sulfonated "A" end-blocks is prepared, where PPO is utilized to form hydrophobic cores in the coacervate hydrogels. The triblock copolymer is combined with a series of another-type ABA triblock copolymers (B = PEO, A = guanidinium-functionalized block) to form temperature responsive coacervate hydrogels. Their rheological, swelling, and temperature responsive properties are evaluated and compared to the regular coacervate hydrogels without hydrophobic cores. Drug releasing experiments are also performed to study the difference between the coacervate hydrogels with and without the hydrophobic cores. We believe that the temperature responsive coacervate hydrogel is a hopeful candidate as a carrier with a controlled drug release capacity.

6.2 Experimental Section

Materials. Chemicals were purchased from Sigma-Aldrich and used as received unless otherwise specified. Allyl glycidyl ether (AGE) and sodium 3-mercapto-1-propanesulfonate were purchased from Tokyo Chemical Industry. AGE was degassed through freeze-pump-thaw cycles, and distilled from butyl magnesium chloride into a flame-dried buret for storage. Tetrahydrofuran (THF) was collected from a dry solvent system equipped with two columns containing activated alumina and copper, and used immediately thereafter. Potassium naphthalenide (0.3 M in THF) was prepared from potassium metal (2.9 g) and naphthalene (9.6 g) in dry THF (250 mL), and stirred with a glass-coated stir-bar for 24 h at room temperature before use.[9]

Characterization. ^{1}H NMR spectra were recorded at 25 °C on a Varian VNMRS 600 spectrometer (600 MHz). Chemical shifts are reported relative to residual solvent peaks in ^{1}H NMR (δ 7.26 ppm for $CDCl_3$ and 4.79 ppm for D_2O). Gel permeation chromatography (GPC) was performed on a Waters 2695 separation module equipped with a Waters 2410 differential refractometer and a Waters 2998 photodiode array detector. Chloroform with 0.25% of triethylamine was used as an eluent at a flow rate of 1 mL/min. Molar mass and molar mass dispersity (Đ) were calculated relative to

linear polystyrene standards.

Rheological experiments were carried out at 25 °C on a TA Instruments ARES-LS1 rheometer equipped with a cone-and-plate geometry (25 mm diameter). Dynamic sweeps were performed at a frequency of 1 Hz or a strain of 1%. Stress relaxation was recorded after a strain of 5% was applied at 0 s.

Swelling experiments were performed as follows. The pristine gels were roughly crushed and immersed in deionized water at room temperature for a week until an equilibrium swollen state was reached. The resulting swollen gels were collected by centrifuge, and dried in vacuo to calculate the equilibrium concentration of the swollen gels from the weight ratio of the swollen gels and the dried gels.

Dynamic light scattering (DLS) analysis was performed on a Wyatt Technology DynaPro NanoStar instrument. The refractive index increment (dn/dc) was assumed to be 0.136 mL/g for PEG in water. Reported values are averages of 100 acquisitions.

Small angle x-ray scattering (SAXS) was performed on a custom-built instrument with a GeniX Cu low divergence micro-focus x-ray source (λ = 0.154 nm), a two-slit scatter-less collimator (beam size = 0.8×0.8 mm^2, beam flux = 3×10^7 ph/s), and a Pilatus100K detector. Samples were injected into 1.5 mm boron enriched quartz capillary tubes. Both ends of the capillary were sealed by wax. The incident and diffracted x-ray beam path were held under vacuum with a distance of 1.4 m from the sample to the detector. 2D SAXS patterns were azimuthally integrated to produce 1D profiles.

Synthesis of poly(allyl glycidyl ether)-*block*-poly(propylene oxide)-*block*-poly(allyl glycidyl ether)] (PAGE-PPO-PAGE). Anionic ring-opening polymerization of epoxides was carried out according to the reported method.[10-11] A reactor and a Schlenk line were flame-dried under vacuum and purged with argon several times. Poly(propylene glycol) (PPG, M_n 4 kDa) was dried in vacuo and dissolved in dry THF. Potassium naphthalenide (0.3 M in THF) was added dropwise by syringe until a light green color persisted in solution, indicating complete deprotonation of the initiator. After adding AGE, polymerization was carried out at room temperature for 3 days.

The polymerization was terminated with degassed methanol. The reaction mixture was filtered through a short silica gel column, evaporated and dried in vacuo. The polymer was obtained as colorless viscous liquid and identified by ^{1}H NMR and GPC.

AGE$_{12}$-*b*-PO$_{69}$-*b*-AGE$_{12}$. M_n 6.7 kDa (^{1}H NMR). Đ 1.36 (GPC). ^{1}H NMR (600 MHz, $CDCl_3$): δ (ppm) 1.11 (t, *J*=5.7 Hz, -O-CH$_2$CH(C<u>H</u>$_3$)-O-), 3.3-3.7 (broad m, main-chain), 3.96 (d, *J*=5.4 Hz, -O-C<u>H</u>$_2$CH=CH$_2$), 5.13 (d, *J*=10.2 Hz, -O-CH$_2$CH=C<u>H</u>$_2$), 5.23 (d, *J*=16.8 Hz, -O-CH$_2$CH=C<u>H</u>$_2$), 5.86 (m, -O-CH$_2$C<u>H</u>=CH$_2$).

Synthesis of sulfonate-functionalized triblock copolymer 1a. Polymer **1a** was synthesized via a typical thiol-ene click reaction. PAGE-PPO-PAGE (M_n 6.7 kDa, 0.50 mmol), sodium 3-mercaptopropane-1-sulfonate (5.0 eq. to AGE units, 60 mmol), and 2-hydroxy-4'-(2-hydroxyethoxy)-2-methylpropiophenone (5.0 mol% to AGE units, 0.60 mmol) were dissolved in a 4:1 THF/water mixture (200 mL) in a Pyrex round bottom flask in the dark. The obtained mixture was degassed through argon bubbling for 20 min, and subsequently irradiated by UV light (λ_{max} 365 nm, 15 W) with stirring at room temperature for 3 h. The resulting mixture was dialyzed against deionized water using rehydrated cellulose membranes (MWCO: 3.5k) for three days. The obtained solution was concentrated and lyophilized. The polymer was yielded as white solid and identified by ^{1}H NMR.

fAGE$_{12}$-*b*-PO$_{69}$-*b*-fAGE$_{12}$ **1a**. M_n 10.9 kDa (^{1}H NMR). ^{1}H NMR (600 MHz, D_2O): δ (ppm) 1.04 (s, -O-CH$_2$-CH(C<u>H</u>$_3$)-O-), 1.19 (s, -O-CH$_2$CH(C<u>H</u>$_3$)-S-, cis isomer), 1.77 (s, -O-CH$_2$C<u>H</u>$_2$CH$_2$-S-), 1.91 (s, -S-CH$_2$C<u>H</u>$_2$CH$_2$-SO$_3$Na), 2.54 (s, -O-CH$_2$CH$_2$C<u>H</u>$_2$-S-), 2.58 (s, -S-C<u>H</u>$_2$CH$_2$CH$_2$-SO$_3$Na), 2.64 (s, -S-C<u>H</u>$_2$CH$_2$CH$_2$-SO$_3$Na, cis isomer), 2.89 (s, -S-CH$_2$CH$_2$C<u>H</u>$_2$-SO$_3$Na), 2.97 (s, -O-CH$_2$C<u>H</u>(CH$_3$)-S-, cis isomer), 3.3-3.9 (broad m, main-chain). The content of sulfonate groups was 2.16 mmol/g. The degree of substitution was 98%.

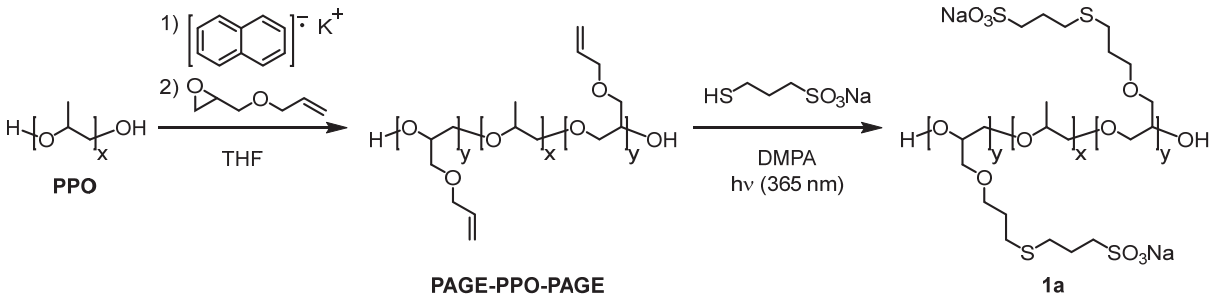

Scheme 6.1. Synthesis of polymer **1a**.

Synthesis of sulfonate and guanidinium-functionalized triblock copolymers 2b,c and 3b,c. Polymers **2b,c** and **3b,c** were synthesized from PAGE-PEO-PAGE according to the literature,[1] and identified by ^{1}H NMR.

Preparation of ionic coacervate hydrogels. Sulfonate- and guanidinium-functionalized triblock copolymers were dissolved separately in deionized water. Resulting solutions were combined to achieve an equimolar mixture of positive and negative charges, and immediately mixed until homogeneous with a vortex mixer or a pair of syringes connected together via a Luer connection.

Drug releasing experiments. Doxorubicin hydrochloride (DOX) loaded hydrogels were prepared by mixing aqueous solutions of the polymers and the drug at room temperature, resulting three samples of 500 mg hydrogels. The concentrations of the polymers and the drug were fixed at 20 wt% and 0.4 wt%, respectively. Each sample was placed in a vial and centrifuged to level the surface and make the specific surface area uniform across all the samples. Next, drug releasing experiments were carried out using the prepared samples. Phosphate buffered saline (PBS, pH 7.4 at 25 °C) solution containing 137 mM NaCl, 2.7 mM KCl, and 10 mM phosphate buffer was used as a release medium. 75 mL PBS solutions were poured onto the top of the samples, and the vials were gently shaken for 2 days at 37 °C, collecting 300 μL aliquots to measure release. The concentrations of released drug in each aliquot were determined by measuring absorbance at 480 nm (λ_{max}) based on the calibration curve ranging from 0.1 to 50 μg/mL of DOX in PBS. The cumulative released amounts of DOX were calculated from the integration of all the aliquots, and expressed as a percentage of the loaded

amount.

6.3 Results and Discussion

Preparation of triblock copolymers

According to the previous literatures, we used the established ionic coacervation (IC) system; a negatively charged triblock copolymers with anionic end-blocks was combined with a positively charged one with cationic end-blocks. Sulfonate and guanidinium groups in this system give strong electrostatic interactions due to a large ΔpK_a of 15.1.[2] In this study, we designed and synthesized an amphiphilic triblock copolymer with a hydrophobic mid-block in order to impart temperature responsive properties to IC hydrogels (Figure 6.1A). PPO was chosen as the hydrophobic mid-block, because it is a representative hydrophobic polyether and provides good comparison to the previously used hydrophilic mid-block, PEO. Moreover, it is well-known that PPO and PPO-containing poloxamers exhibit phase transition behaviors at lower critical solution temperatures (LCST),[6] which is probably a good characteristic to introduce the temperature responsive properties to the hydrogels.

Precursor triblock copolymers with pendant allyl groups in the end-blocks were synthesized by anionic ring-opening polymerization, and subjected to ionic functionalization via thiol-ene reaction. From PAGE-*b*-PPO-*b*-PAGE was prepared a sulfonate-functionalized triblock copolymer (**1a**), and from PAGE-*b*-PEO-*b*-PAGE were prepared sulfonate-functionalized triblock copolymers (**2b** and **2c**) and guanidinium-functionalized ones (**3b** and **3c**). The obtained polymers were characterized by NMR and GPC, and the data were summarized in Table 6.1.

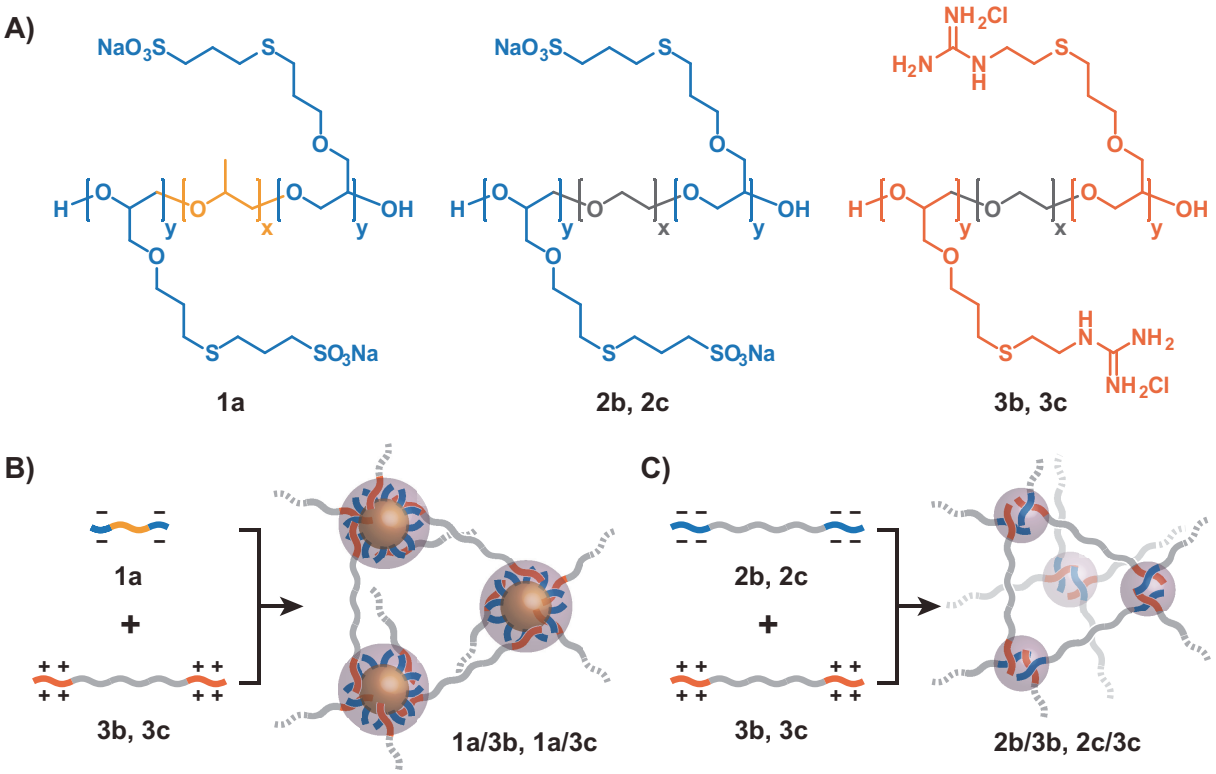

Figure 6.1. (A) Chemical structures of the triblock copolymers. (B and C) Schematic illustrations of the formation of ionic coacervate hydrogels hypothesized based on DLS and SAXS. Blue and red lines denote the negatively and positively charged end-blocks, and yellow and gray lines denote the hydrophobic and hydrophilic neutral mid-blocks, respectively. Yellow and purple spheres denote the hydrophobic and ionic coacervate domains, respectively.

Table 6.1. Summary of characterization of the triblock copolymers.

Polymer	Functionality	Degree of polymerization	M_n (kDa)	Content of ionic groups (mmol/g)
1a	Sulfonate	fAGE$_{12}$-PO$_{69}$-fAGE$_{12}$	3.4-4.0-3.4	2.16
2b		fAGE$_{47}$-EO$_{227}$-fAGE$_{47}$	13.6-10-13.6	2.50
2c		fAGE$_{42}$-EO$_{454}$-fAGE$_{42}$	12.3-20-12.3	1.88
3b	Guanidinium	fAGE$_{44}$-EO$_{227}$-fAGE$_{44}$	10.3-10-10.3	2.88
3c		fAGE$_{42}$-EO$_{454}$-fAGE$_{42}$	9.5-20-9.5	2.02

Preparation of ionic coacervate hydrogels

IC hydrogels with the hydrophobic PPO mid-block were successfully prepared in the same manner as those with hydrophilic PEO mid-blocks (Figure 6.1B and C). The preparation only required mixing two aqueous solutions of oppositely charged polyelectrolytes at an equimolar ratio of ionic groups. All the samples were equilibrated for a day to ensure consistency.[7] A series of hydrogels was obtained by varying the structure of polyether mid-block (PPO or PEO) and the length of the mid-block (PPO mid-block: 4 kDa, PEO mid-block: 10 or 20 kDa). Hydrogels with PPO mid-block (**1a/3b** and **1a/3c**) were prepared by combining **1a** with **3b** or **3c**, and those with PEO mid-block (**2b/3b**, **2b/3c**, **2c/3b**, and **2c/3c**) were prepared by combining **2b** or **2c** with **3b** or **3c**.

The intermolecular electrostatic interaction between the oppositely charged end-blocks plays an important role in the formation of the heterogeneous three-dimensional networks, where the end-blocks were segregated from the neutral mid-blocks to form IC domains bridged with spacers (Figure 6.1B and C). As discussed below in detail, the triblock copolymer with the hydrophobic PPO mid-block forms a micelle in water, and the hydrophobic core which should be encapsulated in each of IC domains is likely originated from the micelle. We can tune the domain spacing and the core size by changing the lengths of PEO and PPO mid-blocks, respectively.

Rheological investigations

First, the dependence of the polymer concentration on rheological properties of the coacervate hydrogels was investigated. Storage and loss moduli of the hydrogels were plotted against the polymer concentration. The storage modulus values increased with increasing the concentration and reached over 10^3 Pa at 20 wt% for all the samples except for **1a/3b** and at 30 wt% for **1a/3b**, indicating that the polymer complex **1a/3b** with PPO blocks and shorter PEO blocks required higher concentrations (30 wt%) for gelation due to less effective formation of polymer networks at low concentrations. Additionally, vial inversion tests showed that aqueous solutions of **1a/3c**, **2b/3b**, and **2c/3c** turned to gel at 10 or 20 wt%, and that of **1a/3b** turned to gel at 30 wt%. Thus, the polymer concentrations to prepare the hydrogels to study about more detailed

properties described below were fixed at 20 wt% for **1a/3c**, **2b/3b**, and **2c/3c** and at 30 wt% for **1a/3b** unless otherwise specified.

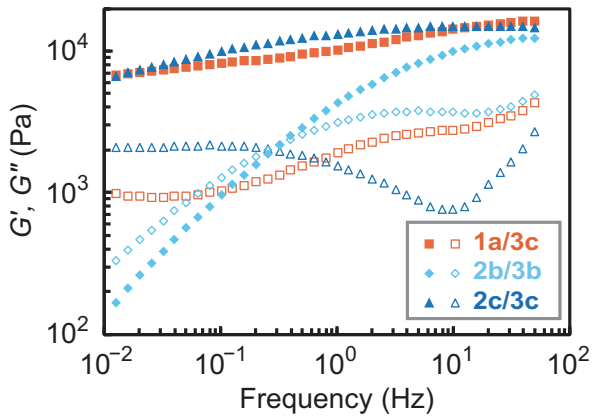

Figure 6.2. Dynamic frequency sweeps of the hydrogels at a concentration of 20 wt% at a strain of 1%. Filled symbols denote *G′* and open symbols denote *G″*.

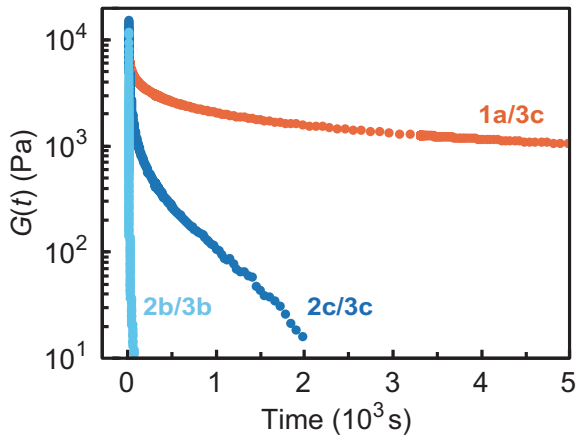

Figure 6.3. Stress relaxation curves of the coacervate hydrogels at a concentration of 20 wt%. A strain of 5% was applied at 0 s.

Next, the rheological properties of the coacervate hydrogels were investigated in more detail. Dynamic frequency sweeps were carried out at the polymer concentration of 20 wt% and at 1% strain (Figure 6.2). The hydrogel **1a/3c** with 4 kDa PPO and 20 kDa PEO mid-blocks exhibited nearly the same modulus as the hydrogel **2c/3c** with 20 kDa PEO mid-blocks. *G′* crossed over *G″* at a frequency of 0.3 Hz for **2b/3b** with 10

kDa PEO mid-blocks, while *G'* was higher than *G"* over a wide range of frequency for the others. Moreover, stress relaxation experiments were also performed to evaluate viscoelasticity of the hydrogels (Figure 6.3). A single step strain of 5% was applied at time zero, and the shear stress was recorded as a function of time. The hydrogels with PPO mid-block behaved more like elastic solid rather than viscous liquid compared to the hydrogels without PPO mid-block. Relaxation times were estimated by curve fitting of the decays at the plateau region where the rate becomes constant (upper limit). Relaxation time of **1a/3c** (9800±70 s) was one order of magnitude larger than that of **2c/3c** (560±16 s), indicating the combination of the hydrophobic interaction and the electrostatic one provides robust IC networks. The stress relaxation is supposed to occur mainly through collapse and subsequent reformation of ionic bonds in the coacervate domains, following initial rapid drops related to slippage and flow of microgels or defects. Thus, it can be considered that the presence of the hydrophobic core in each of the coacervate domains causes the improvement of rheological properties of the coacervate hydrogels.

Swelling behaviors

Equilibrium swelling test was carried out to reveal durability of the hydrogels in water. The prepared gels were crushed and immersed into water for five days. The swollen gels were collected by centrifugation and dried by lyophilization. The polymer concentrations at an equilibrium swollen state were calculated by weight ratios of swollen gels to dried gels. Surprisingly, the **2b/3b** gel completely dissolved into water, which can be attributed to the shorter PEO mid-block and higher contents of ionic groups, while the other gels were swollen but insoluble in water. It is noteworthy that **1a/3b** and **1a/3c** gels resisted swelling much more significantly than the others. The polymer concentrations of **1a/3b** and **1a/3c** at an equilibrium swollen state were 36.7% and 14.0%, respectively. The **2c/3c** gel swelled much more and the polymer concentration reached 4.1%. Naturally, the hydrogels with PPO swell less than those without it because the hydrophobic PPO mid-blocks in the former contribute to higher degree of non-covalent crosslinking in water, compared to those of the latter with electrostatic interactions only.

This result is consistent with the fact that the PEO segment plays an important role in the network formation. The combination of the negatively charged end-block segments with the positively charged ones results in the formation of IC domains, while the PEO mid-block segments are located outside the domains and connect them. Below the critical gelation concentration (CGC), the coacervate domains are not sufficiently connected to each other due to a lack of PEO bridging. CGC of the gels was highly dependent on the length of the PEO mid-block segment.

Structural characterization

We carried out small angle X-ray scattering (SAXS) experiments to investigate the structures of the hydrogels. SAXS profiles are shown in Figure 6.4. The profiles of **1a/3b** and **1a/3c** gels indicate two different periodic structures. First, the peaks corresponding to 30.5 nm (q 0.0206) and 33.7 nm (q 0.0186) spacing should be derived from the ordered structure of IC domains, considering the reported values of the bcc structure of the previous gels.[2] The domain spacing values in the IC gels with PPO turned out to be slightly larger than those without it, i.e., 2b/3b (q 0.0305, 20.6 nm) and 2c/3c (q 0.0260, 24.1 nm), which is attributable to larger domain sizes in the former, considering the formation of the PPO-based hydrophobic core in each of the domains. The mixture of the negatively charged triblock copolymers and the positively charged ones in this study also formed regularly ordered IC domains acting as non-covalent crosslinks.

Second, each of **1a/3b** and **1a/3c** has an additional peak corresponding to 12.2 nm (q 0.0517) and 11.4 nm (q 0.0551) spacing, respectively, which was uniquely observed to the IC gels with PPO cores. The additional broad peak must indicate the different domain structure of the IC gels with PPO cores with another characteristic length that is smaller than the hydrodynamic radius of the PPO block-based micelle. The SAXS profiles inferred core-shell structure of the IC domains in the IC gels with PPO cores. It is probable that the presence of two peaks is derived from the core-shell structure. Further investigation is needed to determine the detailed structure.

The samples were disordered with no higher order lattice reflections; however, there was a well-defined first-order peak which indicated that coacervate domains were still formed and had a preferential spacing.[8]

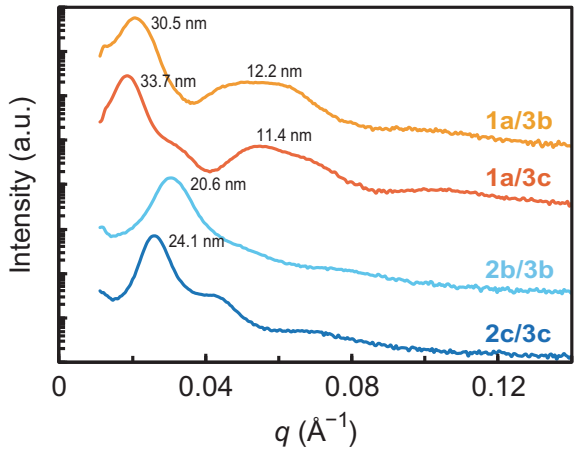

Figure 6.4. SAXS profiles of the coacervate hydrogels at a concentration of 20 wt% (**1a/3c**, **2b/3b**, **2c/3c**) or 30 wt% (**1a/3b**).

Temperature responsive behaviors

Dynamic light scattering (DLS) analysis was carried out to clarify the temperature responsive behaviors of the amphiphilic copolymer **1a** in water. Figure 6.5 shows the temperature dependence of hydrodynamic radius of an aqueous solution of **1a**. The hydrodynamic radius is related to the size of a PPO segment-based micelle in water. Interestingly, with an increase in temperature, the hydrodynamic radius gradually decreased in the temperature range from 25 °C to 45 °C and became nearly half at temperatures over 45 °C. This indicates that the PPO-based micelles gradually collapse (and shrink) with an increase in temperature from 25 °C to 45 °C. This is probably related to hydrophobic PPO's LCST-type phase separation behavior, that is, PPO decreases its solubility in water at higher temperature. It is noted that the aqueous solution of the polymer **1a** did not exhibit any LCST-type phase transition in the temperature range, because of the poly(sulfonate) segment's strong affinity to water. As a result, it can be reasonably expected that the PPO cores in the coacervate gels also show such the temperature responsive behavior; that is, shrinkage at higher temperatures based on PPO's temperature-dependent water solubility.

Figure 6.6 shows temperature sweeps of moduli of **1a/3c** and **2c/3c** gels. Interestingly, storage modulus of **1a/3c** showed a rapid decrease around 40 °C. It

indicates that above the temperature, the gel lost its strength likely due to water's exuding from the gel, because the strength of the gel immediately recovered at room temperature. This result corresponds to the PPO micelle's collapse behavior observed through DLS analysis mentioned above.

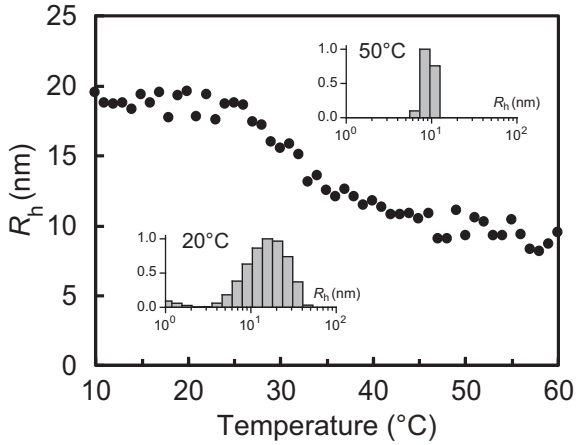

Figure 6.5. Temperature dependence of hydrodynamic radius (R_h) of polymer **1a** via DLS analysis at a concentration of 1 mg/mL in water. The inset shows the size distributions at temperatures of 20 (left) and 50 °C (right).

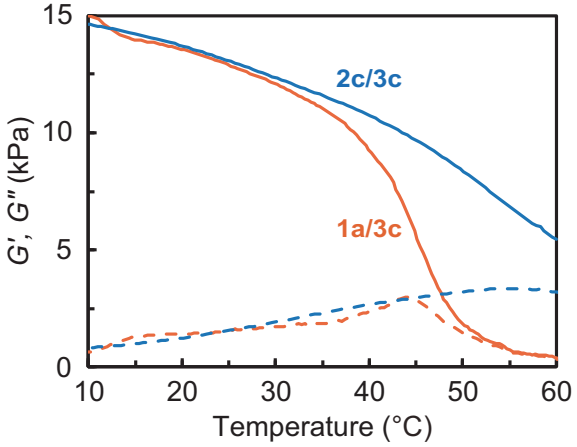

Figure 6.6. Temperature sweeps of the coacervate hydrogels at a concentration of 20 wt%, a frequency of 1 Hz, a strain of 1%, and a ramp rate of 2 °C/min. Solid lines denote *G'* and dashed lines denote *G"*.

Drug releasing experiments

We performed the drug releasing experiments to demonstrate drug releasing behaviors of the IC gels. We previously reported anionic dye-releasing behaviors from coacervate microgel particles. The release profiles were affected by affinity between cargo and carrier, specific surface area of hydrogel, and ionic strength of release medium.[9] In the present study, doxorubicin hydrochloride (DOX) was chosen as a model drug, which is a well-known anticancer drug and widely used for drug delivery system, e.g. PEGylated liposome. The anthracycline moiety can intercalate between base pairs of a DNA/RNA duplex. The intercalation prevents the replication of rapidly growing cancer cells.

First, DOX was loaded in the 20 wt% hydrogels at a concentration of 0.4 wt%. Flat disk-shaped samples were fabricated on the bottom of vials by centrifugation, because the specific surface area needs to be uniform across the samples. Next, the release of DOX from the samples was performed in a large excess of phosphate buffered saline (PBS) solution at 37 °C. The cumulative released amount of DOX was traced by absorbance at 480 nm based on a calibration curve, and plotted as a function of time in Figure 6.7.

Overall, the hydrogel with PPO cores (**1a/3c**) released the drug much faster than the hydrogel without them (**2c/3c**). The release rate of **1a/3c** was several times as fast as that of **2c/3c**. Surprisingly, **2c/3c** released only 10% of DOX in 2 days in spite of its low swelling resistance, indicating that DOX in the coacervate domain was strongly trapped by the electrostatic interaction between a positively charged ammonium group of DOX and negatively charged sulfonate-functionalized polymers. On the other hand, **1a/3c** can release the payloads more effectively at the body temperature thanks to the temperature responsive behavior derived from the PPO cores that the hydrogel shrinks above the transition temperature.

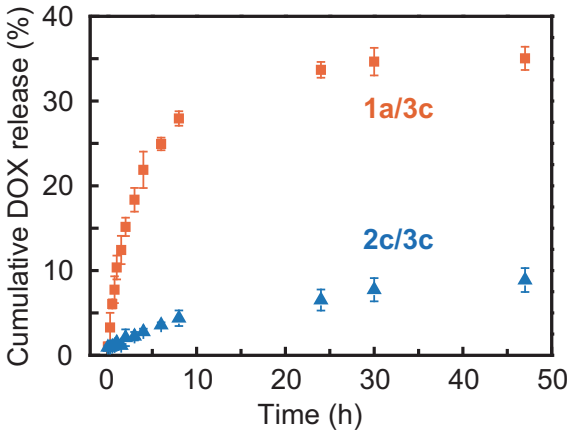

Figure 6.7. The cumulative release of DOX from the coacervate hydrogels **1a/3c** and **2c/3c** at 37 °C in PBS solution (pH 7.4). The error bars denote the standard error based on n = 3 samples.

6.4 Conclusions

Here, we have shown that the combination of ionic coacervation by electrostatic interactions between amphiphilic triblock copolymer chains and hydrophobic core association inside the ionic domains brought novel IC gels with core-shell structure. Temperature responsive IC hydrogels were successfully prepared via anionic ring-opening polymerization and thiol-ene reactions. The yielded hydrogels showed relatively high storage modulus (up to 2 kPa at 20 wt% concentration). The PPO core brought stiffness and robustness in mechanical properties to the IC gels. DLS revealed the micelle formation of the amphiphilic copolymer **1a** with a hydrophobic PPO segment and sulfonated end-segments and its temperature-responsive behavior. SAXS profiles strongly indicated the presence of the core-shell structure derived from the PPO-based micelle for the core and the IC domains for the shells. The IC gels with PPO showed rheological properties' change with an increase in temperature, indicating that the hydrophobic PPO segment's temperature-responsive property in water was reflected to the IC gel's temperature-responsive behavior. Finally, drug releasing behavior of the IC hydrogels was traced using DOX as a model drug, and the IC gel **1a/3c** showed rapid and efficient releasing at 37 °C. The temperature-responsive

hydrogels developed in this study are hopeful candidates for biomedical applications such as drug delivery and cell culture scaffolds.

6.5 References

1. Luo, F.; Sun, T. L.; Nakajima, T.; Kurokawa, T.; Zhao, Y.; Sato, K.; Ihsan, A. B.; Li, X.; Guo, H.; Gong, J. P. *Adv. Mater.* **2015**, *27*, 2722-2727.
2. Hunt, J. N.; Feldman, K. E.; Lynd, N. A.; Deek, J.; Campos, L. M.; Spruell, J. M.; Hernandez, B. M.; Kramer, E. J.; Hawker, C. J. *Adv. Mater.* **2011**, *23*, 2327-2331.
3. Kazanskii, K. S.; Solovyanov, A. A.; Entelis, S. G. *Eur. Polym. J.* **1971**, *7*, 1421-1433.
4. Lee, B. F.; Kade, M. J.; Chute, J. A.; Gupta, N.; Campos, L. M.; Fredrickson, G. H.; Kramer, E. J.; Lynd, N. A.; Hawker, C. J. *J. Polym. Sci., Part A: Polym. Chem.* **2011**, *49*, 4498-4504.
5. Lee, B. F.; Wolffs, M.; Delaney, K. T.; Sprafke, J. K.; Leibfarth, F. A.; Hawker, C. J.; Lynd, N. A. *Macromolecules* **2012**, *45*, 3722-3731.
6. Alexandridis, P.; Alan Hatton, T. *Colloids Surf. A Physicochem. Eng. Asp.* **1995**, *96*, 1-46.
7. Krogstad, D. V.; Lynd, N. A.; Miyajima, D.; Gopez, J.; Hawker, C. J.; Kramer, E. J.; Tirrell, M. V. *Macromolecules* **2014**, *47*, 8026-8032.
8. Krogstad, D. V.; Lynd, N. A.; Choi, S.-H.; Spruell, J. M.; Hawker, C. J.; Kramer, E. J.; Tirrell, M. V. *Macromolecules* **2013**, *46*, 1512-1518.
9. Wang, C. X.; Utech, S.; Gopez, J. D.; Mabesoone, M. F. J.; Hawker, C. J.; Klinger, D. *ACS Appl. Mater. Interfaces* **2016**, *8*, 16914-16921.

Chapter 7

Conclusion

We synthesized the novel hydrogels with various network architecture through efficient modular strategies utilizing the concept of click chemistry and evaluated their properties thoroughly, which demonstrated that the architecture in hydrogel systems plays an important role in their functions and properties.

First, chemical hydrogels with the topologically interlocked architecture have been studied; interpenetrating network (IPN) gels formed via simultaneous double click reactions and slide-ring (SR) gels formed via crosslinking of supramolecular polyrotaxanes. Next, physical hydrogels with reversible and dynamic architecture have been studied; PEO-based physical gels of random polymer networks formed via hydrophobic effects and thermoresponsive ionic coacervate gels with hydrophobic cores formed via ionic bonding of polyion complexes.

In Chapter 2, the rapid, one-pot fabrication of robust IPN gels via orthogonal double click reactions was presented. The tight and loose networks were synthesized simultaneously from tetra/bi-functional PEO-based macromonomers with epoxy, amine, azide, and alkyne groups by orthogonal double click reactions: epoxy-amine reaction and copper catalyzed azide-alkyne cycloaddition. The network architecture was precisely tuned via the topologies and the molecular weights of the macromonomers. Compared to corresponding single network gels, the IPN gels containing both tightly and loosely crosslinked networks exhibited superior mechanical properties with shear moduli and fracture stresses. The synthetic versatility of this one-pot approach will further establish design principles for the next generation of robust hydrogel materials.

In Chapter 3, a modular and robust one-pot "click" fabrication of SR gels with little or no unwanted covalent crosslinking was demonstrated. Initial complexation of monothiolated β-cyclodextrin with poly(allyl glycidyl ether)-*block*-poly(ethylene

glycol)-*block*-poly(allyl glycidyl ether) could be carried out in water by simple sonication. Network formation and end-capping were simultaneously accomplished by photo thiol-ene reaction. The resulting one-pot process leads to strong and stretchable SR gels that do not contain covalent crosslinks in an efficient way, greatly expanding future applications of SR gels.

In Chapter 4, a one-pot strategy for the fabrication of novel SR gels with cyclodextrin-derived crosslinks and additional free cyclodextrin ring spacers co-threaded onto the polymer backbones was developed as a successive study to understand the effects of threaded macrocycles in SR networks. The sliding crosslinks and free spacers were introduced into the networks with the product ratio controlled by the feed ratio. This structural tuning leads to dramatic changes in the rheological properties, mechanical properties, and swelling behavior for the SR gels. In addition, the coupling of simple synthetic procedures with enhanced properties offers a versatile approach to novel elastomeric materials.

In Chapter 5, a library of physical hydrogels with highly tunable viscoelastic properties based on PEO-based triblock copolymers was described. Aqueous solutions of the triblock copolymers formed durable physical hydrogels at low concentrations with stress relaxation and sol-gel transition being systematically controlled depending on the length of the side-chains (*n*-hexyl to *n*-dodecyl). The synthetic accessibility of these PEO derivatives from commercially available starting materials, combined with the inert nature of the polyether backbone, illustrates a versatile route to next generation biomaterials.

In Chapter 6, ionic coacervate gels with hydrophobic cores derived from polyelectrolyte having a poly(propylene oxide) segment were demonstrated. We synthesized triblock polyelectrolytes with hydrophilic and hydrophobic segments in the mid-block using established functional polyethers and thiol-ene chemistry, prepared hydrogels from the polyelectrolytes, and characterized them via DLS and SAXS. The present novel coacervate gels with hydrophobic cores brought significant changes in thermoresponsive and drug releasing properties as well as mechanical and swelling properties compared to those without hydrophobic cores.

The control over the network architecture in hydrogels leads to a variety of novel properties, e.g. mechanical reinforcement, self-healing, and stimuli response, and opens up new opportunities regarding architectural diversity and applications. We believe these efficient approaches for hydrogels with various network architecture will expand and facilitate future applications of not only PEO-based biocompatible hydrogels but also advanced soft materials.

List of Publications

Chapter 2

1. One-Pot Fabrication of Robust Interpenetrating Hydrogels via Orthogonal Click Reactions.
   Murakami, T.; Brown, H. R.; Hawker, C. J.
   J. Polym. Sci., Part A: Polym. Chem. **2016**, *54*, 1459-1467.

Chapter 3

2. One-Pot "Click" Fabrication of Slide-Ring Gels.
   Murakami, T.; Schmidt, B. V. K. J.; Brown, H. R.; Hawker, C. J.
   Macromolecules **2015**, *48*, 7774-7781.

Chapter 4

3. Structural Versatility in Slide-Ring Gels: Influence of Co-threaded Cyclodextrin Spacers.
   Murakami, T.; Schmidt, B. V. K. J.; Brown, H. R.; Hawker, C. J.
   J. Polym. Sci., Part A: Polym. Chem. **2017**, *55*, 1156-1165.

Chapter 5

4. Synthesis of PEO-based Physical Gels with Tunable Viscoelastic Properties.
   Murakami, T.; Kawamori, T.; Gopez, J. D.; McGrath, A. J.; Klinger, D.; Saito, K.
   J. Polym. Sci., Part A: Polym. Chem. in press. Article DOI: 10.1002/pola.28992.

Chapter 6

5. Temperature Responsive Ionic Coacervate Hydrogels with Hydrophobic Cores.
   Murakami, T.; Gopez, J. D.; Mabesoone, M. F. J.; Maeda, T.; Saito, K.; Hawker, C. J.
   To be submitted.

Other Publications

6. Synthesis and properties of [2.2] paracyclophane-layered polymers.
   Morisaki, Y.; Murakami, T.; Chujo, Y.
   Macromolecules **2008**, *41*, 5960-5963.
7. [2.2] Paracyclophane-layered polymers end-capped with fluorescence quenchers.
   Morisaki, Y.; Murakami, T.; Sawamura, T.; Chujo, Y.
   Macromolecules **2009**, *42*, 3656-3660.
8. Synthesis and Photostability of Poly (p-phenylenevinylene-borane) s.
   Nagai, A.; Murakami, T.; Nagata, Y.; Kokado, K.; Chujo, Y.
   Macromolecules **2009**, *42*, 7217-7220.
9. Synthesis, structure, and properties of aromatic ring-layered polymers containing ferrocene as a terminal unit.
   Morisaki, Y.; Murakami, T.; Chujo, Y.
   J. Inorg. Organomet. Polym. Mater. **2009**, *19*, 104-112.
10. Synthesis of anthracene-stacked oligomers and polymer.
    Morisaki, Y.; Sawamura, T.; Murakami, T.; Chujo, Y.
    Org. Lett. **2010**, *12*, 3188-3191.
11. Thermoresponsive Properties of PEO Derivatives with Sparsely Grafted Alkyl Side-chains.
    Murakami, T.; Kawamori, T.; Gopez, J. D.; McGrath, A. J.; Klinger, D.; Saito, K.
    To be submitted.

Patents

12. Aromatic copolymer having proton conductive group and application thereof.
    Murakami, T.; Kadota, T.; Yamakawa, Y. JP5854046 (B2) 2016.2.9, WO2013018677 (A1) 2013.2.7, US2014154610 (A1) 2014.6.5.
13. Polyarylene block copolymer having sulfonic acid group and use thereof.
    Yamakawa, Y.; Kadota, T.; Murakami, T.; Tsunoda, Y. JP5692226 (B2) 2015.4.1, US8729219 (B2) 2014.5.20, WO2011155520 (A1) 2011.12.15.
14. Electrode electrolyte for polymer electrolyte fuel cell and electrode varnish using

the same, electrode paste, and membrane-electrode assembly.
Kadota, T.; Yamakawa, Y.; Murakami, T.; Iguchi, M.; Ishimaru, R. JP5611761 (B2) 2014.10.22, JP2011108642 (A) 2011.6.2.

15. Aromatic copolymer and its use.
Yamakawa, Y.; Kadota, T.; Murakami, T. JP5581937 (B2) 2014.9.3, JP2012067216 (A) 2012.4.5.
16. Electrode electrolyte for solid polymer fuel cell, and electrode varnish, electrode paste and membrane-electrode assembly using the same.
Yamakawa, Y.; Kadota, T.; Murakami, T.; Tsunoda, Y.; Iguchi, M. JP5455800 (B2) 2014.3.26, JP2011258461 (A) 2011.12.22.
17. Polyarylene block copolymer having sulfonic acid group, and its application.
Yamakawa, Y.; Kadota, T.; Murakami, T.; Tsunoda, Y.; Iguchi, M.; Fukuda, K. JP5181004 (B2) 2013.4.10, JP2012046655 (A) 2012.3.8, US2012052412 (A1) 2012.3.1.

Patent Application Publications

18. Liquid crystal alignment agent, liquid crystal alignment film and method for producing the same, liquid crystal element, polymer and compound.
Murakami, T.; Suguri, T.; Suhara, R.; Yasuike, N.; Kashishita, K.; Okada, T. JP2017200991 (A) 2017.11.9.
19. Liquid crystal alignment agent, liquid crystal alignment film and method for manufacturing the same, and liquid crystal device.
Okada, T.; Murakami, T.; Kashishita, K. JP2017156438 (A) 2017.9.7.
20. Liquid crystal alignment agent, liquid crystal alignment film and method for manufacturing the same, and liquid crystal device.
Okada, T.; Kashishita, K.; Murakami, T. JP2017156436 (A) 2017.9.7.
21. Copolymer, composition, polymer electrolyte membrane, membrane-electrode assembly, and solid polymer fuel cell.
Kadota, T.; Murakami, T.; Fujishita, S.; Higami, M. WO2013183386 (A1) 2013.12.12.
22. Aromatic copolymer with sulfonic acid groups and uses thereof.
Yamakawa, Y.; Kadota, T.; Murakami, T.; Rozhanskii, I. WO2012017965 (A1)

2012.2.9.

23. Polyarylene copolymer having, in side chain thereof, aromatic ring containing phosphonate group.
Kadota, T.; Yamakawa, Y.; Murakami, T. WO2011049211 (A1) 2011.4.28.